Experimental and Numerical Analysis of Transient Natural Convection in a Cylindrical Enclosure

by

Nathan John Blair

A thesis submitted in partial fulfillment

of the requirements for the degree of

MASTER OF SCIENCE

(Mechanical Engineering)

at the

UNIVERSITY OF WISCONSIN - MADISON

1993

ABSTRACT

The transient heat transfer response is examined for a heat source within a fluid filled enclosure. The specific geometry studied is a toroid centered within a cylinder filled with water. This geometry has application to in-tank heat exchangers common in many thermal storage strategies. The geometry is studied both numerically and experimentally. In both studies, the initial condition is an isothermal, quiescent fluid with a step change in coil wall temperature. The transient heat transfer response can be divided into three regimes: pure conduction, quasi-steady, and decay.

The numerical study was conducted using a finite difference fluid dynamics package to examine the effect on transient heat transfer of the height of the toroid within the enclosure, the effect of five geometric modifications with the intent of improving thermal stratification, and the effect of three lengths of vertical shrouds. The relative coil height to enclosure height ratio (R) was varied at 0.5, 0.3, and 0.175. The height ratio of 0.3 heated the enclosure fluid most quickly. None of the five geometric modifications studied improved the thermal stratification or heated the enclosure fluid more quickly. All three vertical shroud lengths improved the transient heat transfer by lengthening the quasi-steady period and heating the enclosure fluid more quickly than the unshrouded case.

The transient heat transfer for this geometry was studied experimentally by pumping heated fluid through the toroid. The experimental response compares well to the

previous numerical study done of this geometry. The duration of both the conduction period and the quasi-steady period compared very well to the numerical study. The effect of coil height within the enclosure was studied for height ratio values (R) of 0.7, 0.4, 0.3, 0.2, 0.1, and 0.029. It was found that an R value of 0.029 produced the best heat transfer in that it heated the enclosure fluid most quickly. The effectiveness of the toroid heat exchanger was determined experimentally. The effectiveness increases linearly with an increasing temperature difference between the coil and the fluid temperature. As the toroid is moved lower within the enclosure, the effectiveness becomes constant with respect to the temperature difference.

ACKNOWLEDGMENTS

The three people that I need to thank the most for help in completing this project are Dr. Doug Reindl, Prof. Beckman, and Prof. Mitchell. The three of them were always there to answer my questions (including when I asked for a clarification of what exactly a Nusselt number was in my third weekly meeting). They were very understanding of my lack of engineering background which I really appreciated. Special thanks go to Doug who went out of his way to help me and without whom I would probably still be trying to figure out the experimental equipment. I would also like to thank Sandy Klein and Jack Duffie for their advice and excellent lectures.

I would also like to express my appreciation for the help and friendship of the other people in the lab. First, I would like to thank Jeff Thornton for all of his help with the computers, for coming to pick me up in Milwaukee when I crashed my car, and for organizing some fun activities like water-skiing. Second, the people that I am graduating with; Kevin Warren (and Jen), Mike Skolnick, Tim McDowell and Gerold Furler. I am proud to count them all as my friends. Next, the people that graduated before us; Oystein, Steve, Bob, Dick, Jurgen, Matthias, Colin, Jorge, Svein (and whoever I am forgetting at this late hour). Finally, there are the current people in the lab; Todd, Martin, Al, Barrett, Keary, John A., Jon G., Eric, Kevin C., Claus, Gunnar, Laurie, Sherri, and of course, Shirley. Thanks for the laughs and bearing the moods of a thesis writer.

Outside of the lab, my greatest thanks must go to my roommate and best friend, Matt Sullivan. Just as at Gustavus, we helped each other along through Thermo, Fluids, and everything else that they forgot to explain to us in physics. I would also like to thank my other great roommate, Jeff Nelson.

As with everything I accomplish in my life, I must thank my family. Without their lifelong support, encouragement, and love, I would not have the confidence to attempt anything. While at Madison, the weekly phone calls from Mom and Dad were a great source of insight, laughter, and a listening ear.

I would like to thank all the friends I made at the Lutheran Campus Center. That group includes Emily whom I would like to especially thank for the Silly Putty.

Lately, I have been thinking about my experience in Madison. The lab, the Terrace, the Sailing Club, biking to Picnic Point, going to the Market Square budget theater just for the air conditioning, playing poker at Tim's, State Street, etc. All great times. Despite considerable frustration and an overwhelming urge to see if my experimental apparatus could fly, I have truly enjoyed many parts of the research experience. I also have learned more in the last 18 months about engineering, plumbing, Macintosh applications and Wisconsin than I thought there was to know. Most importantly, I have learned a great deal about myself. I will carry the fond memories of Madison and the Solar Lab with me wherever I go.

LIST OF FIGURES

LIST OF TABLES

NOMENCLATURE

A	External Surface Area of the Heat Exchanger Coil (m^2)
A_o	External Area of the Insulated Enclosure (m^2)
Cp	Thermal Specific Heat Capacity (kJ/kg-C)
D	Heat Exchanger Coil Cross-sectional Diameter (m)
D_o	Enclosure Diameter (m)
$d\bar{T}/dt$	Instantaneous Time Rate of Change of Bulk Fluid Temperature (C/sec)
g	Gravitational Acceleration Constant (9.81 m/s^2)
h	Static Enthalpy in FLUENT
H_{hx}	Height of the Heat Exchanger Coil (m)
$\bar{h}_L$	Surface Average Heat Loss Coefficient (W/m^2-C)
H_o	Enclosure Height (m)
k	Thermal Conductivity (W / m-C)
k_{air}	Conductivity of Air (W / m-C)
L	Length of Vertical Plate (m)
LMTD	Log Mean Temperature Difference (C)
$\dot{m}$	Fluid Flowrate within the Heat Exchanger (m^3/sec)
$(mc)_{tank}$	Composite Mass-Capacitance of the Enclosure (J/C)
$m_0 ... m_5$	Bulk Temperature Curve Fit Coefficients

Nu	Nusselt Number = hD/k
Nu_ε	Nusselt Number used in Effectiveness Equation
Pr	Prandtl Number (ν/α)
Q_{in}	Heat Flow into the Enclosure (W)
Q_{out}	Heat Flow out of the Enclosure (W)
Q_{max}	Maximum possible Heat Transfer from Heat Exchanger (W)
q_L	Heat Loss from the Enclosure (W)
Rc	Cylindrical Heat Exchanger Radius (m)
Ra_D	Rayleigh Number ($g\beta D^3\Delta T/\nu\alpha$)
Ra_H	Rayleigh Number based on Enclosure Height
Sm	Mass Source Term in FLUENT (kg/sec)
t	Time (sec)
$\overline{T}$	Bulk Temperature of Fluid within the Enclosure (C)
$\overline{T_o}$	Initial Bulk Temperature of Enclosure Fluid (C)
$T_{HX,i}$	Fluid Temperature at Heat Exchanger Inlet (C)
$T_{HX,o}$	Fluid Temperature at Heat Exchanger Outlet (C)
T_s	Average Bulk Temperature of Enclosure Fluid (C)
T_{wall}	Instantaneous Coil Wall Temperature (C)
T_∞	Ambient Air Temperature (C)
u_i	Velocity Components in FLUENT (m/s^2)

Greek Symbols

α	Thermal Diffusivity (m^2/sec)
β	Volume Expansion Coefficient (1/C)
ε	Heat Exchanger Effectiveness

Actual Heat Transfer / Maximum Heat Transfer

Δma	Change in Capacitance Probe Output (ma)
Δt_c	Duration of the Conduction Dominated Regime (sec)
$\Delta T_{in\text{-}out}$	Difference between Fluid Inlet Temperature and Fluid Outlet Temperature (C)
Δt_{qs}	Duration of the Quasi-Steady Regime (sec)
η	Relative Tube Exchanger Radius (m)
ϕ	Relative Tube Radius (m)
ρ	Density (kg/m^3)
τ_{ij}	Stress Tensor used in FLUENT

TABLE OF CONTENTS

CHAPTER
ONE

INTRODUCTION

The study of convection examines energy transfer from a surface to a fluid in motion. The driving potentials are temperature differences and/or concentration differences. Convection involves both molecular conduction and large scale fluid motion. Convective heat transfer is subdivided into three areas based on the fluid flow: forced, natural and mixed. If the fluid is mechanically forced over the surface (such as a fluid pumped through a pipe) or the surface is pushed through the fluid (such as an airfoil through air), forced convection occurs. Natural convection occurs when the fluid motion is driven by body forces including gravitational, Coriolis, or centrifugal forces. Density (or concentration) gradients within the fluid create different amounts of force from the body forces. These force differences create fluid motion and, thereby, energy transfer. The forces that produce natural convection are also present in forced convection, but are negligible compared to the inertial forces. Mixed convection occurs when both the inertial and body forces are of the same magnitude and neither is negligible.

Prior study of natural convection systems is extensive. A majority of this research deals with flow over external surfaces. These configurations have many applications. Because the surface is external the conditions outside the boundary layer are usually known and are often constant. This simplifies the governing equations and makes the

analysis easier. Natural convection within an enclosure is more difficult to study because the boundary conditions are affected by the flow. The boundary conditions change with time due to energy storage within the enclosure.

Natural convection plays a major role in many thermal systems. In nature, these include atmospheric and oceanic circulation systems. Technologically, natural convection is used in domestic heating systems, computer chip cooling, electric engines, and thermal energy storage systems. Active solar energy thermal storage systems often use water tanks to store the energy provided by the solar energy. Many of these systems use an in-tank heat exchanger to transfer the energy from the solar collector fluid (which is often a different material than the storage fluid) to the storage fluid.

This research will explore transient natural convection in enclosures both experimentally and to a lesser degree numerically. The main thrust will consist of an experimental analysis of a coiled tube, toroid, within a cylinder. This has applications to the in-tank heat exchangers mentioned above. It is also interesting from a theoretical convection standpoint because few studies have used this geometry.

1.1 Literature Survey

In this section, some of the previous natural convection investigations that deal specifically with the geometry that will be studied in this research are discussed. Fundamental background research and research specific to in-tank heat exchangers are included as is the research of Reindl (1992) which forms the main motivation for the current research.

1.1.1 Steady State Infinite Cylinder

A large body of research is available on natural convection from horizontal cylinders in an infinite medium. Morgan (1975) attempted to compare and consolidate the vast experimental results and correlations and found a wide dispersion within both the experimental results and correlations. The experimental results had a percent coefficient of deviation (100 x std dev./mean) that varied from 3% to 35% depending on the Rayleigh number. Correlations given in the literature had a deviation of 5% up to 26%, again depending on the Rayleigh number. Many reasons were given to account for this variation in results. These include "heat conduction to the supports and the temperature measurement locations; distortion of the temperature and velocity fields by bulk fluid movements, the use of undersized containing chambers or the presence of the temperature measurement system and supports".

Morgan proposed a correlation of the heat transfer based on previous experimental results and correlations. The maximum uncertainty is reported at 5%. The Morgan correlation, Eq. 1.1, is dependent only on the Rayleigh number and not the Prandtl number.

$$Nu_{D,f} = B_1 \, Ra_{D,f}^{m_1} \tag{1.1}$$

B_1 and m_1 are constants that vary over the range of Rayleigh numbers as shown in Table 1.1. The D and f subscripts indicates that the Rayleigh number and Nusselt number are based on the cylinder diameter and the film temperature.

Table 1.1 Values for Morgan Natural Convection from a Cylinder Correlation

Range of $Ra_{d,f}$	B_1	m_1
10^{-10} to 10^{-2}	0.675	0.058
10^{-2} to 10^{2}	1.02	0.148
10^{2} to 10^{4}	0.850	0.188
10^{4} to 10^{7}	0.480	0.250
10^{7} to 10^{12}	0.125	0.333

These values lead to the steady state Nusselt number values for the specified Rayleigh numbers shown in Figure 1.1.

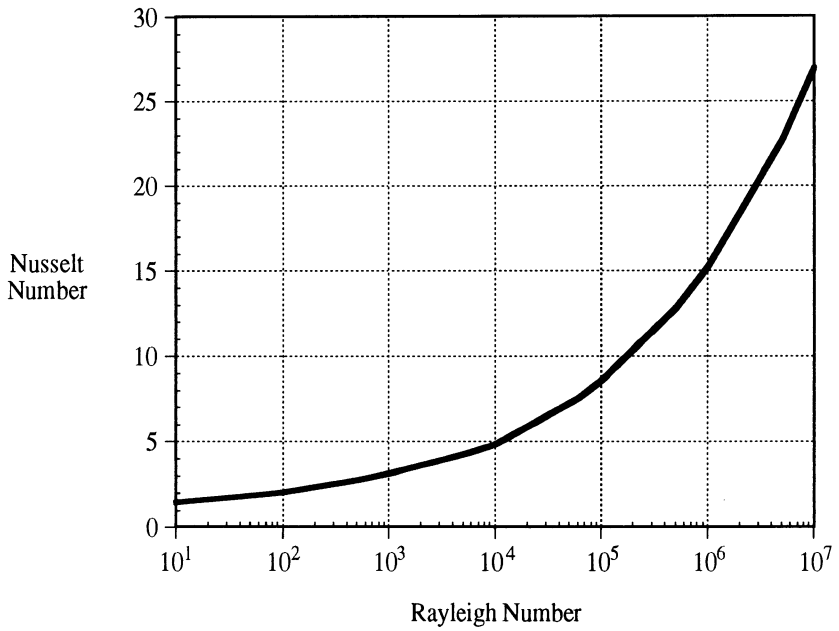

Figure 1.1 Specific Values of Nusselt Numbers Using Morgan's Correlation

Churchill and Chu (1975) also examined the same experimental results as Morgan. They produced another correlation of the following form.

$$Nu^{1/2} = 0.60 + 0.387\left(\frac{Ra}{\left[1 + (0.559/Pr)^{9/16}\right]^{16/9}}\right)^{1/6} \qquad (1.2)$$

The constant at the beginning is added due to experimental data which suggests that there is a significant influence of pure conduction at very small Rayleigh numbers.

Finally, Fand, Morris and Lum (1977) proposed a correlation that incorporated the Prandtl number dependence. It was found that Morgan's correlation was adequate for air and water but deviated from experimental results for larger Prandtl numbers. The range used in this study is $2.5 \times 10^2 < Ra < 1.8 \times 10^7$ and $0.7 < Pr < 3090$. The proposed correlation is

$$Nu_j = 0.478 Ra_j^{0.25} Pr_j^{0.050} \qquad (1.3)$$

where the fluid properties are evaluated at $t_j = t_b + 0.32(t_s - t_b)$. This equation correlates the data of all fluids combined [air, water, several oils] with zero mean error and a mean deviation of 1.5%.

Figure 1.2 illustrates the differences between the three correlations mentioned above. The Prandtl number used was that of water at 305K, 5.20. The variation among the three correlations is greatest at large Rayleigh numbers.

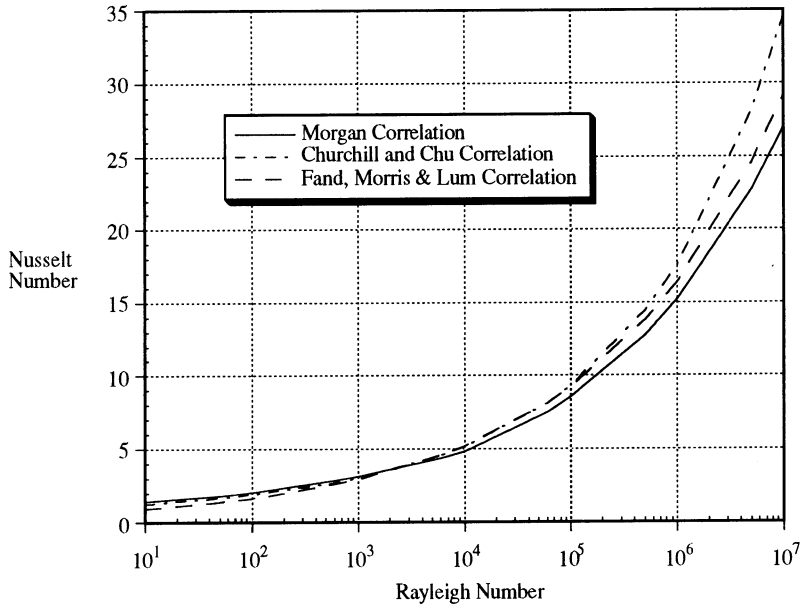

Figure 1.2 Comparison of Three Horizontal Cylinder Natural Convection Correlations

1.1.2 Enclosure Studies

The geometry under study is that of a single coiled tube within a cylinder that is closed at both ends and filled with fluid. The transient heat transfer will be studied because, as the cylinder forms an enclosure around the coil, the internal fluid properties will change. The two most notable being temperature and density causing convection currents that build up over time. This research also seeks to understand how the relative size of the enclosure affects the heat transfer.

The results of the following studies are relevant to this end. Sparrow and Charmchi (1983) studied natural convection from a cylinder placed within a larger cylinder as shown in Figure 1.3. They varied both the height of the inner cylinder and also its

axial position within the larger cylinder. They varied the inner cylinder position vertically while it was concentrically centered within the larger cylinder. At height ratios of 0.1375 to 0.8625, it was found that there is only a weak dependence of the steady state Nusselt number on the elevation of the inner cylinder. In fact, for $Ra > 10^4$, the Nusselt number is virtually independent of the elevation. This is probably due to the fact that within the narrow gap between the bottom of the inner cylinder and the bottom of the outer cylinder, that occurs at a relative inner cylinder elevation of 0.1375, direct heat conduction between the cylinders would be very high and there would be little natural convection. Then, as the cylinder is raised higher in the tank, the convection would increase while the conduction would decrease. In this experiment, the outer cylinder was made of aluminum which would enable high conduction along the surface of the outer cylinder at these elevations.

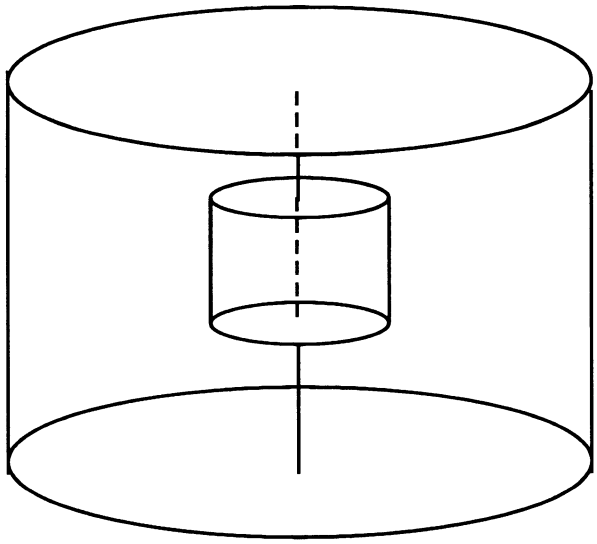

Figure 1.3 Approximate Geometrical Setup Studied by Sparrow and Charmchi

The eccentricity of the inner cylinder was also varied. The results showed that the steady state Nusselt number was also not affected by the eccentricity of the inner cylinder. It was concluded that the Nusselt number was independent of the position of the inner

cylinder. However, it was noted that the overall flow fields within the outer cylinder for different inner cylinder positions appear, from numerical analysis, to be quite different. A conclusion can be drawn from this work and applied to this research. Although the position of the internal source may be irrelevent in the steady state case, the difference in convective flow patterns for different positions suggests that the transient heat transfer may differ depending on the position of the inner source.

Sparrow and Pfeil (1984) studied the heat transfer from a horizontal cylinder within a vertical channel. The vertical channel was imposed by the presence of two vertical plates placed symmetrically on both sides of the cylinder. The plates form an opening both above and below the cylinder. These vertical plates form a vertical shroud around the cylinder. They varied the width and depth of the vertical channel as well as the conductivity of the shroud material. The heat transfer was greatly increased by the presence of a shroud. The heat transfer increased as the vertical shroud became narrower and as the schroud became taller. When the shroud is 1.5 times as wide as the cylinder diameter and is 20 times as high as the cylinder diameter, there is a 40% increase in heat transfer. Also, the Nusselt numbers are remarkably insensitive to the thermal characterisitics of the shroud. This research suggests that placing a shroud around the coil within the cylinder may dramatically increase the heat transfer in a steady state situation. However, the effect of the shroud on heat transfer during the entire transient may be different than the increase seen in the steady state case.

1.1.3 Previous In-Tank Heat Exchanger Experiments

Feiereisen (1984) studied several in-tank heat exchangers experimentally. Several existing heat exchanger geometries (mostly horizontal, bayonet type) were used in a full sized domestic storage system. The effect of varying the height of the heat exchanger was

studied. It was found that, at the two possible heights (0.2 m and 0.4 m from the bottom), there was no difference between the heat transfer rate for similar log mean temperature differences. However, it was observed that the temperature of the tank fluid below the heat exchanger remained relatively constant and played little part in the convection flow. Therefore, the lower heat exchanger utilized a larger portion of the tank for thermal energy storage.

Feiereisen found that there was minimal thermal stratification above the location of the heat exchanger coil in the absence of a draw (load) on the storage tank. It was concluded that "the convection currents produced by the heat exchange process are sufficient to thoroughly mix the water at all points above the immersed coil."

Additionally, Feiereisen placed a vertical single pass heat exchanger within a chimney in the center of the cylinder. The chimney, a plastic tube, extended to the bottom of the tank and fluid was able to enter it at the bottom of the tank and exit at the top of the tank. The purpose of the plastic tube is to act as a chimney in an attempt to extend the convective currents to the bottom of the tank and thereby incorporate the fluid below the heat exchanger. Unfortunately, the heat transfer rate actually decreased. It was proposed that the openings at the bottom of the chimney were too small and, in fact, water was observed entering the edge of the chimney top and exiting the center of chimney top.

Farrington and Bingham (1986) tested four types of immersed coil heat exchangers in a similar manner to Feiereisen. These included a multi-turn smooth coil, a finned spiral, a single-wall bayonet, and a double-wall bayonet. It was found that the performance was dependent on the flow rate and that the temperature difference between the heat exchanger inlet and the storage tank can strongly affect heat exchanger performance. They defined the heat exchanger effectiveness as

$$\varepsilon = \frac{A\,(LMTD)}{(\dot{m}C_P)_{Hx}(T_{Hx,i} - T_S)} \frac{k}{D} \overline{Nu} \qquad (1.4)$$

where

A is the surface area of the heat exchanger coil

LMTD is the log mean temperature difference $LMTD = \frac{(T_{Hx,i} - T_{Hx,o})}{\ln\left[\frac{(T_{Hx,i} - T_S)}{(T_{Hx,o} - T_S)}\right]}$

$\overline{Nu}$ represents the heat transfer from the tube and is approximated as laminar flow around a horizontal tube, $\overline{Nu} = C(\overline{Ra})^{0.25}$

$T_{Hx,i}(t)$ is the fluid temperature within the heat exchanger at the storage tank inlet

$T_{Hx,o}(t)$ is the fluid temperature within the heat exchanger at the storage tank outlet

$T_S(t)$ is the average bulk temperature of the fluid within the storage tank

k is the conductivity of the fluid within the storage tank

D is the diameter of the heat exchanger coil

$(\dot{m}C_P)_{Hx}$ is the capacitance rate of the fluid within the heat exchanger

Figure 1.4 shows the effectiveness plotted against $T_{HX,i} - T_S$ for several different flow rates for the geometry of a multi-turn coil heat exchanger. The effectiveness rapidly approaches an asymptotic value with temperature differences greater than about 10 C. Lower flow rates produce a higher efficiency. Flow visualization showed that the expected independence of azimuthal angle did not occur. Although difficult to discern, convection currents were unstable and three dimensional. The smooth coil had the highest effectiveness followed, in order, by the finned spiral, the single-wall bayonet and the double-walled bayonet.

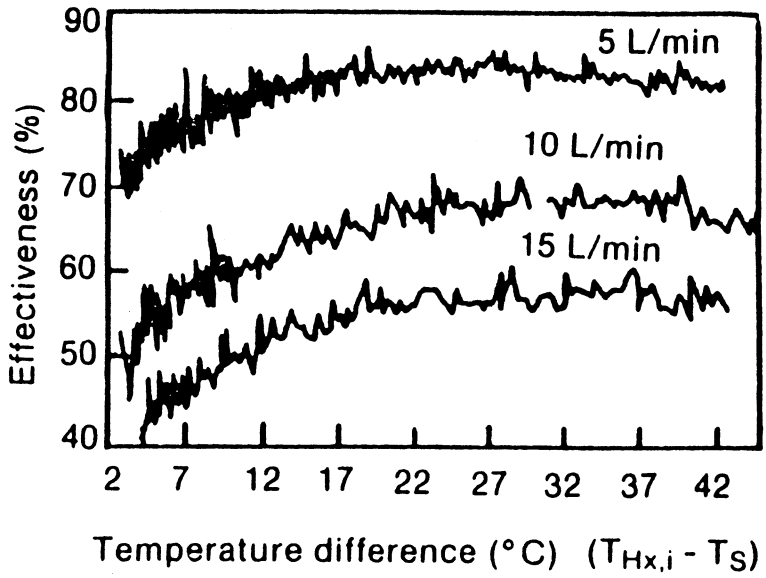

Figure 1.4 Effectiveness plots for a multi-turn smooth coil heat exchanger

1.2 Precedent Research

The work of Reindl (1992) will be explained in greater detail because the current research has developed directly from it. In an effort to complete and extend previous numerical and experimental studies of natural convection in enclosures, Reindl studied transient natural convection in enclosures using two basic geometries. The first geometry, examined numerically, was that of a vertical flat plate located in the center of a rectangular cavity. The second geometry, examined both numerically and experimentally, consisted of a single-turn coiled tube within a cylinder.

1.2.1 Numerical Results

These geometries were examined numerically, by Reindl, using a finite element computer program called FIDAP, which has the ability to model a variety of fluid flow problems including those considered in his research. Several symmetrical reductions were used to reduce the domain size. In the first geometry (vertical plate within a rectangle), only half the rectangle was used so that it appears that the heated plate is on one side of the enclosure. In the three dimensional geometry of the coiled tube within the cylinder, the axisymmetry is exploited to reduce the problem to a two dimensional cross-section. Half of this cross-section is used resulting in the computational domain shown in Figure 1.5.

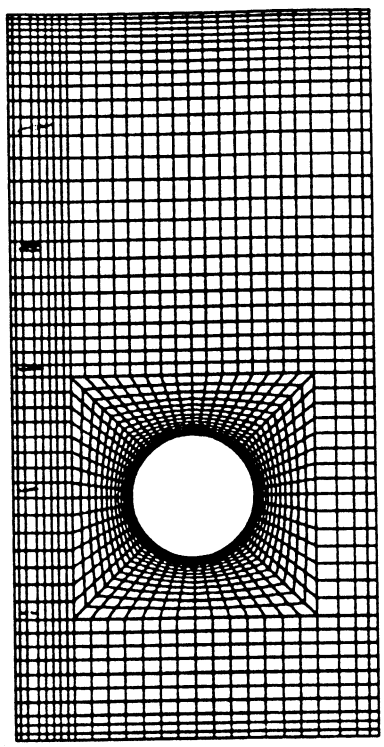

Figure 1.5 FIDAP computational domain for the coil within a cylinder geometry

Several parameters were varied in the first geometry including the relative plate size to enclosure size, vertical position of the plate and the Rayleigh number. Initially, the fluid was at rest and uniform temperature. At time = 0, a step change in temperature was imposed on the vertical plate. Figure 1.6 illustrates the heat transfer response of this geometry for various Rayleigh numbers.

Figure 1.6 illustrates several aspects of the transient response. First, the transient response can be divided into three distinct regimes. The initial regime, known as the conduction regime, lasts for a few seconds and is characterized, on the graph, by a rapidly dropping value of Nusselt number. The conduction regime continues from the start until buoyancy forces within the conduction regime overcome the viscous forces and significant

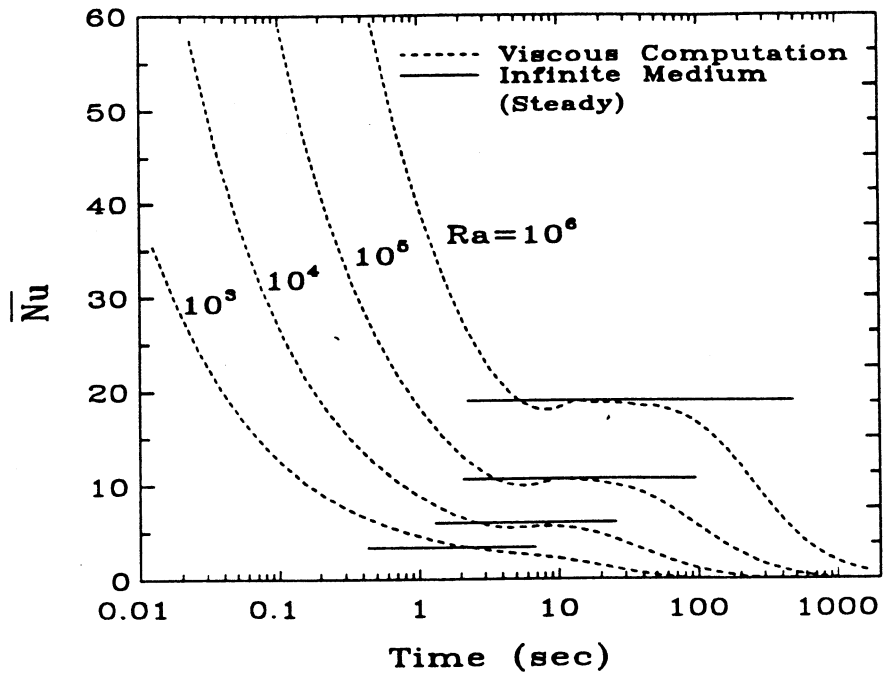

Figure 1.6 Transient Nusselt number for vertical plate geometry using FIDAP

fluid motion begins. Using scale analysis based on work by Patterson and Imberger (1980), Reindl was able to accurately estimate the duration of the conduction regime with the following equation.

$$\Delta t_c \sim \frac{L^2}{\alpha Ra^{1/2}} \tag{1.5}$$

The second regime begins when there is significant fluid motion and is characterized by the fact that the heat transfer can be approximated accurately by the infinite medium steady state solution for a vertical plate. This is especially true for higher Rayleigh number solutions as illustrated in Figure 1.6. During this quasi-steady regime, there has not been significant bulk temperature increase within the enclosure and the water entrained in the convection flow is approximately at the initial temperature and so an infinite medium is a valid approximation. The quasi-steady regime ends when the bulk temperature begins to increase significantly. A scale analysis estimate of the duration of this regime, Equation 1.6, was obtained using the estimate that significant heating will occur after fluid equal to the volume above the vertical plate has passed through the boundary layer.

$$\Delta t_{qs} \sim \frac{L^2}{\alpha \phi Ra^{1/4}}\left[1-\left(\eta+\phi/2\right)\right] \tag{1.6}$$

The decrease in temperature difference that occurs after this volume of fluid has passed through the boundary layer causes a subsequent decrease in heat transfer rate and the onset of the third regime known as the decay regime. The Nusselt number decays to zero as time increases to infinity. Scale analysis also enables an estimate of the Nusselt number during the decay regime as follows.

$$\overline{Nu} \sim \left[1+\frac{\alpha Ra^{1/4}_t}{2HW}\right]^{-5} Ra^{1/4} \qquad (1.7)$$

When the relative plate length within the enclosure was increased, the quasi-steady regime became shorter in duration. It appears that the enclosure must be at least 1.5 times larger than the plate in order for the quasi-steady infinite medium value to be reached although the duration of the quasi-steady period is extremely short. Additionally, the vertical position of the plate within the enclosure has a definite effect on the heat transfer response. The conduction regime response is identical but the quasi-steady period lasts longer if the plate is lower in the tank. For a plate placed high within the enclosure, the enclosure top impedes the flow of the boundary layer. Also, due to some degree of stratification within the enclosure, the driving force at the top of the tank decreases faster than at the enclosure bottom.

The second geometry, a coil within a cylindrical enclosure, was studied using the same boundary conditions of an initially quiescent fluid with an initial step change in temperature of the coil surface. Figure 1.7 shows the transient heat transfer response for this geometry with varying Rayleigh numbers. This transient response shows the same three distinct regimes that were obvious with the vertical plate geometry.

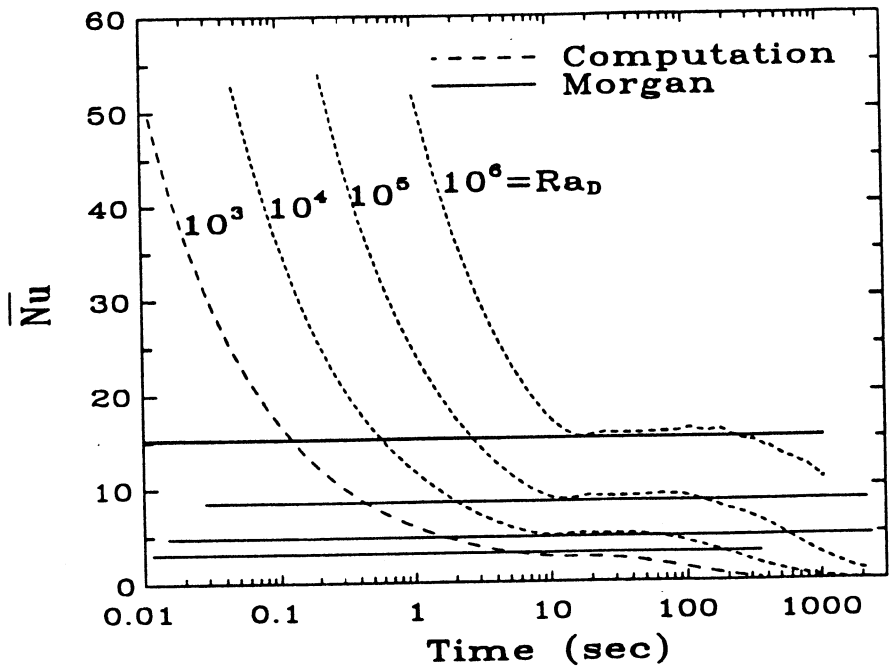

Figure 1.7 Transient Nusselt number for coil in cylinder geometry using FIDAP

As before, the initial heat transfer is conduction dominated and ends when significant fluid flow begins. Again using scale analysis, the duration of the conduction regime can be determined from

$$\Delta t_c \sim \frac{D^2}{\alpha Ra_D^{1/2}} \tag{1.8}$$

As stated earlier, the infinite medium, steady state results for a horizontal cylinder have considerable variance among them. Figure 1.7 includes the results of Morgan's infinite medium correlation. This shows that there is excellent correlation between the steady state infinite medium results of Morgan and the quasi-steady values of Reindl's numerical

results. Scale analysis accurately estimates the duration of the quasi-steady period as

$$\Delta t_{qs} \sim \frac{r_x^{1/2}\gamma[1-(\eta+\phi)]}{2\alpha\phi^2 Ra_D^{1/4}} \tag{1.9}$$

where $r_x = D/2$, $\gamma = R_T/H_T$, $\phi = r_x/H_T$. Finally, the decay regime can be characterized using scale analysis and using an overall energy balance on the enclosure to get the following estimate.

$$\overline{Nu} \sim 0.5686\left[1+\frac{\alpha\kappa\phi^2 Ra_D^{1/4} t}{\gamma^2 D^2}\right]^{-5} Ra_D^{1/4} \tag{1.10}$$

where α is the thermal diffusivity, $\kappa = R_c/H_T$, $\phi = r_x/H_T$, $\gamma = R_T/H_T$ and Ra_D is defined based on the initial temperature difference. The coefficient was determined from a least squares fit of the decay period at all orders of Rayleigh number.

The flow field for the second, coil configuration consists mainly of a plume rising above the coil. This plume forms at the start of the quasi-steady period as bouyancy forces overcome viscous forces and large scale fluid motion begins. The plume "waves" back and forth for the duration of the transient. There was significant stratification within the retangular geometry which is destroyed in the coil geometry due to the mixing action of eddies that form above the coil.

1.2.2 Experimental Results

Reindl experimentally examined the second geometry of the coiled tube in a cylinder with the goal of validating the above numerical solutions. He intended to measure

both the bulk temperature and the Nusselt number of the heat exchanger. He originally selected a cylinder of acrylic but switched to borosilicate glass to avoid undue thermal expansion. The coil was constructed of a single resistive heating element wound five times within 0.5 in (12.7 mm) copper tubing. The coil temperature was controlled by a PID controller with an analog proportioning output coupled with a phase angle fired solid state relay.

The bulk temperature was ingeniously measured using the thermal expansion characteristics of water. As the water is heated within the cylinder by the coil, the density decreases causing natural convection and a volume expansion. There is a small hole in the top of the cylinder through which the interior fluid can expand into a vertical tube. The height of the water within the tube, once calibrated, was a measure of the bulk temperature within the tank. Also, additional calibration had to be done to account for the thermal expansion of the tank.

The Nusselt number was calculated two ways during this experiment. The first way incorporates the power used by the heater within the coil. An energy balance on the enclosure, including the heat loss term,is given by Equation 1.11. The left hand side represents the convective heat transfer from the coil surface. The convective heat transfer is equal to the sum of the power supplied to the coil ($I(t)^2R$) and the heat lost from the enclosure.

$$\overline{h_x}\, A\,(T_w - T_o) = I(t)^2R + \overline{h_L}\, A_o\left(\overline{T}(t) - T_o\right) \qquad (1.11)$$

In Equation 1.11,

$\overline{h_x}$ is the surface average heat transfer coefficient from the heat exchanger

A is the external area of the heat exchanger

T_W is the instantaneous temperature of the coil wall

T_O is the initial temperature of the transient

I(t) is the current used by the coil

R is the measured resistance of the coil heater

$\overline{h_L}$ is the average heat loss from the insulated enclosure

A_o is the total exterior area of the insulated enclosure

$\overline{T}(t)$ is the volume average bulk temperature of the fluid

Equation 1.11 can be solved for the convective heat transfer coefficient and thereby the Nusselt number which results in Equation 1.12.

$$\overline{Nu}(t) = \frac{I(t)^2 R}{2\pi^2 k_w R_c (T_w - T_o)} + \frac{\overline{h_L} A_o (\overline{T}(t) - T_o)}{2\pi^2 k_w R_c (T_w - T_o)} \tag{1.12}$$

In addition to the variables of Equation 1.11, R_c is the cylindrical coil radius and k_w is the conductivity of the fluid (water).

The second method of determining the Nusselt number is based solely on the bulk temperature and has the following form.

$$\overline{Nu}(t) = \frac{(mc)_{tank}}{2\pi^2 k_w R_c (T_w - T_o)} \frac{d\overline{T}(t)}{dt} + \frac{\overline{h_L} A_o (\overline{T}(t) - T_o)}{2\pi^2 k_w R_c (T_w - T_o)} \tag{1.13}$$

where $(mc)_{tank}$ is the composite mass-capacitance of the enclosure.

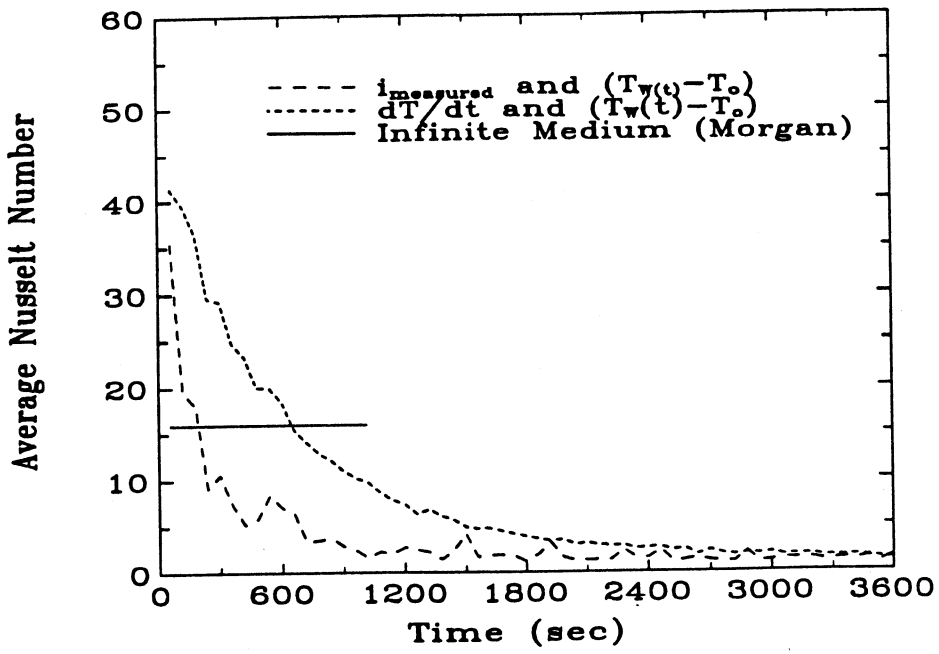

Figure 1.6 Experimental transient Nusselt number for coil in cylinder geometry

Figure 1.6 gives the initial experimental results, found by Reindl, using both of these Nusselt number calculations and also shows the magnitude and expected duration of the quasi-steady period. The lower curve was found using the Nusselt formulation that incorporates the heater power consumption. The higher curve was calculated using the bulk temperature Nusselt formulation. Obviously, the expected results were not obtained. The primary reason for these results is that the boundary conditions are different. Flow visualization showed that the coil heater controller "pulsed" the resistive heater in an effort to maintain the constant coil temperature. This meant that the coil temperature resulting in a reformation of the convective plume at roughly 15 second intervals. This oscillation created a great deal of additional mixing which was not present in the numerical model. The scale analysis equation used to correlate the decay period in the numerical modeling actually can be used, with excellent results, to describe the experimental transient response.

The final correlation takes the following form where the constant has been found from a least squares fit on the experimental data.

$$\overline{Nu} \sim 1.407\left[1 + \frac{\pi^2 k R_c Ra_D^{1/4} t}{4\ (mc)_{tank}}\right]^{-5} Ra_D^{1/4} \qquad (1.14)$$

1.3 Research Objective

This project will continue the experimental examination of a toroidal heat exchanger in a cylindrical tank. The first step will be to develop experimental techniques to more closely approximate the boundary condition of a constant temperature coil by using a forced fluid flow within the coil instead of a resistive heater. Validation of the previous numerical work will be attempted. Additionally, several parameters, including the effect of the height of the coil within the enclosure, will be varied to ascertain the effect of the enclosure on the heat transfer including the effect of the height of the coil within the enclosure. The free convection will be observed by measuring the bulk temperature of the fluid in conjunction with the coil surface temperature and by flow visualization.

Several methods of increasing the thermal stratification within the tank have been suggested including a porous media above the coil to slow the convective plume and various geometric structures. Several of these ideas will be examined numerically using a finite difference computational fluid dynamics package, FLUENT.

Finally, there is some disagreement about the use of a vertical shroud. Although it increases the steady-state heat transfer rate, its overall affect on the transient heat transfer is unknown. This will be studied numerically.

CHAPTER
TWO

NUMERICAL ANALYSIS OF A COILED TUBE WITHIN A CYLINDER

A large number of methods for promoting thermal stratification using the coil within a cylinder geometry have been explored numerically. An attempt has been made to optimize the vertical position of the coil within the enclosure. In addition, the effects of adding a vertical shroud, or chimney, around the coil have been studied numerically. This method is useful for ruling out possible design ideas prior to experimental construction.

2.1 FLUENT

A numerical technique was found that allowed for approximate results without an exorbitant amount of computation time. A fluid dynamics computation package called FLUENT was chosen because of availability. FLUENT is a commercial computational fluid dynamics package. This program is run on a SPARCStation IPC computer at the University of Wisconsin Computer Aided Engineering Center.

Three main conservation equations govern the flow experienced in this experiment. The first of these is the conservation of mass that is expressed in FLUENT in the following equation where the subscript i indicates an individual Cartesian direction.

$$\frac{\partial \rho}{\partial t} + \sum_i \frac{\partial}{\partial x_i}(\rho u_i) = S_m \tag{2.1}$$

In this experiment, S_m, which is a mass source term, is zero because no mass is generated within the enclosure.

The conservation of momentum equation is represented in FLUENT by

$$\frac{\partial}{\partial t}(\rho u_i) + \sum_j \frac{\partial}{\partial x_j}(\rho u_i u_j) = \frac{\partial p}{\partial x_i} + \frac{\partial \tau_{ij}}{\partial x_i} + \rho g_i + F_i \tag{2.2}$$

In the FLUENT nomenclature, p is the static pressure, τ_{ij} is the stress tensor, and g_i and F_i represent gravitational acceleration and external body forces.

The energy equation is solved in terms of the conservation of the static enthalpy h defined as:

$$h = m\, C_p\, dT \tag{2.3}$$

C_p is the specific heat at a constant pressure. The energy equation cast in terms of h can be written as

$$\frac{\partial}{\partial t}(\rho h) + \sum_i \frac{\partial}{\partial x_i}(\rho u_i h) = \sum_i \frac{\partial}{\partial x_i}\left(k \frac{\partial T}{\partial x_i}\right) - \sum_i \frac{\partial}{\partial x_i}(hJ) + \frac{\partial p}{\partial t} + \sum_i u_i \frac{\partial p}{\partial x_i} \tag{2.4}$$

In this equation,

T is the temperature

J is the momentum flux, $\rho u_i u_j$

and k is the thermal conductivity.

According to the FLUENT manual[1], FLUENT first converts these governing partial differential equations to their finite-difference analogs. This is done by fully implicit integration over the computational cells into which the domain is divided. The resulting algebraic equations are solved by a semi-implicit interactive scheme that starts from arbitrary initial conditions and iterates to converge on the solution. A power law differencing scheme is used to interpolate between grid points and to calculate the derivatives of the flow variables.

2.2 General Numerical Approach

The enclosure consists of a cylinder with a unit aspect ratio (the height equals the diameter). The cylinder walls are adiabatic. The heat exchanger is a toroid with a radius equal to half the tank radius. The width of the toroid cross-section is one quarter of the cylinder diameter. The height of the cylinder is 0.018 m while the cylinder radius is 0.009 m that results in a cross-sectional toroid diameter of 0.0045 m. The geometry was posed in cylindrical coordinates.

At this point, certain geometric assumptions were made to reduce the size of the grid. The geometry was assumed to be axisymmetric. This assumption allows the use of a two dimensional slice through the cylinder. Additionally, only half of this slice was used because of the axisymmetry assumption. The resulting situation is shown in Figure 2.1. The left side, the top, and the bottom are standard walls with zero heat flux and an imposed no slip condition. The right side, which runs along the vertical centerline of the cylinder, is a wall of symmetry as defined by FLUENT and assumed to have a zero flux of all quantities across the boundary. There is no convective flux across a symmetry

---

[1]FLUENT Users Guide; Fluent Incorporated, 10 Cavendish Court Lebanon NH 03766

plane. The normal velocity components at the symmetry wall are zero. There is also no diffusion flux across a symmetry plane. The normal gradients of all flow variables are thus zero at the symmetry plane. The FLUENT finite difference grid was set up with 40 divisions vertically and 20 divisions horizontally as shown in Figure 2.2.

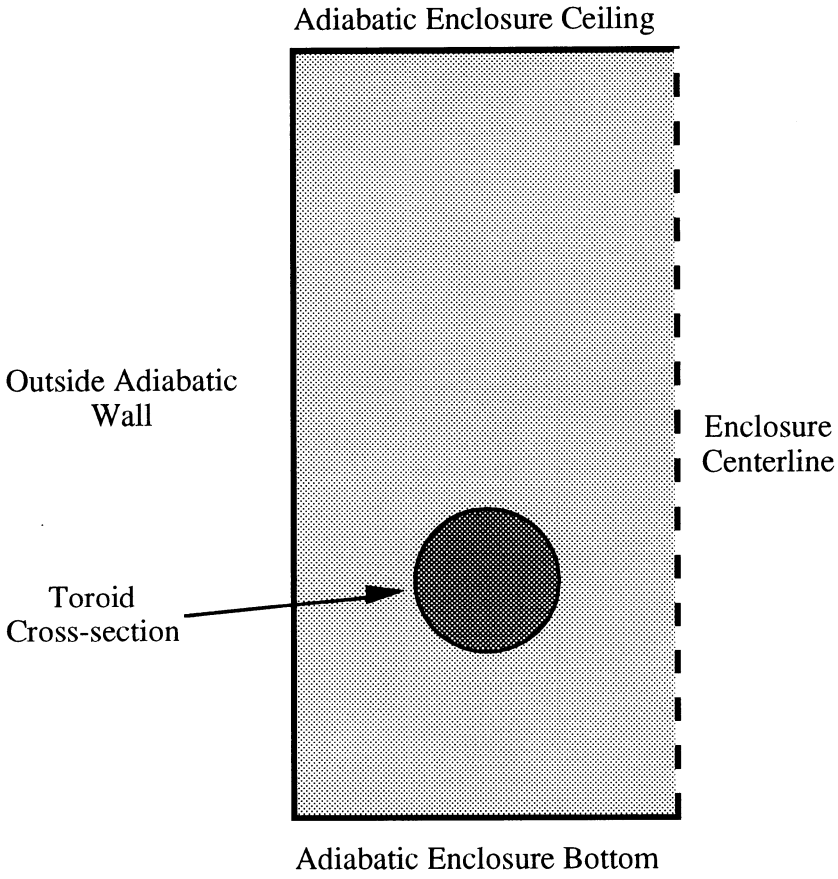

Figure 2.1 Reduced Geometry for Numerical Experiments

The temperature of the coil is held constant throughout the transient at 305 K. The temperature of the water within the cylinder is set, at the beginning of the transient, to a constant 300 K. The density of the water is entered as a three factor polynomial from a curve fit to water density values for this temperature range, from Incropera and Dewitt

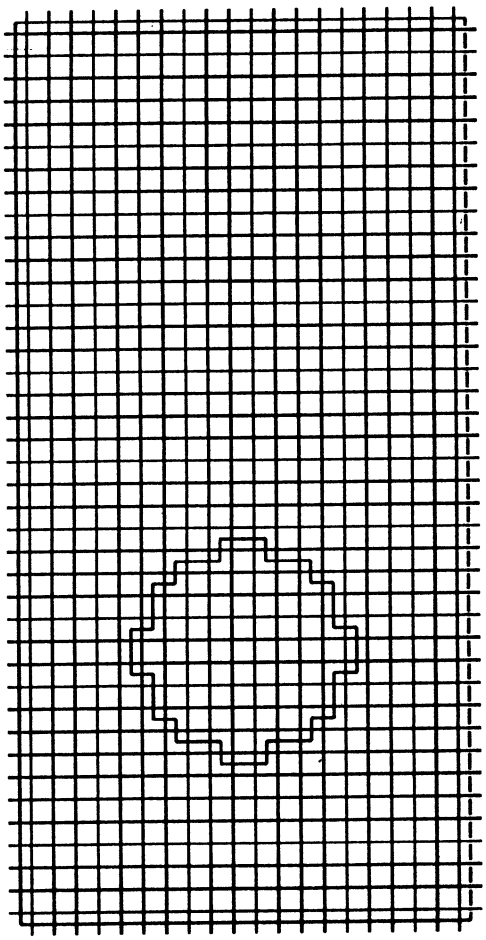

Figure 2.2 Basic FLUENT Grid Layout

(1990), as shown in Figure 2.3. FLUENT does not use the Boussinesq approximation (unlike FIDAP used by Reindl which does). The curve extends far past the 300 to 305 K temperature range because the original temperature difference was to be 30 degrees. Properties, other than density, are entered as constants appropriate for this temperature range (300 K to 305 K).

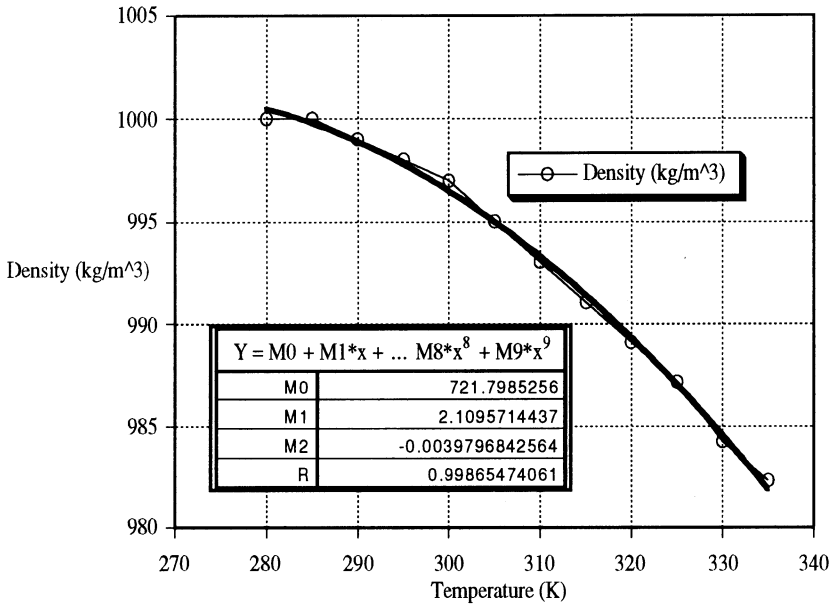

Figure 2.3 Polynomial Curve fit of Density for use in FLUENT

The problem is time dependent. The time step is one second. The maximum number of iterations per time step is 300 and the minimum enthalpy residual is 1 x 10^{-5} J/kg.

2.3 Numerical Difficulties

The original design of the grid was an enclosure 18 cm high, instead of 1.8 cm high. The intended temperature difference was 30 C, not 5 C. In addition, the intended,

relative coil diameter was to be smaller. However, after 300 seconds (300 time steps) and 24 hours of computing time, the bulk temperature within the enclosure had only risen around 1 degree. The transient heat transfer was still well within the quasi-steady regime. In an effort to decrease the Rayleigh number and thereby the charging time, the geometry was changed to that discussed above.

Each of these runs took over 24 hours to complete. With additional time or a faster computing system, a finer grid could be used to see if there is a significant effect on the results. The coil, as represented in the FLUENT grid, is only approximately round and is not smooth. This rough grid is expected to have a minimal effect on the qualitative results of the plume size, thermal stratification, the charging rate, etc.

2.4 Coil Height Optimization

As stated before, the heat transfer from the coil surface is natural convection and driven by the difference in temperature between the coil and the water in the tank. As the water around the coil (toroid) is heated, the buoyancy force causes it to rise and it then entrains cooler water from around and under the heat exchanger. This warmer water rises until it reaches the top of the enclosure. The heating creates a warmer layer of water at the top of the enclosure that "grows" downward into the enclosure as additional warm water is added to it. This developing stratification assumes that the mixing in the tank is minimal and that there is almost total thermal stratification. When this layer reaches the heat exchanger, the heat transfer rate drops off as the temperature difference between the heat exchanger and surrounding fluid decreases and there is less driving potential for heat transfer. This theory would imply that the heat exchanger should be put on the bottom of the enclosure where the water will be cooler for longest period of time. However, if the heat exchanger is placed too close to the bottom of the enclosure, the flow will be

restricted and the heat transfer rate will drop as viscous forces imposed by the tank floor oppose the buoyancy force. Hence, there is an optimum height from the floor at which the heat transfer is maximized.

To examine the effect of coil height on heat transfer, the height of the coil within the enclosure was set at three different positions. The lowest height had one grid point between the bottom of the coil and the tank floor resulting in a coil height to tank height ratio (R) of 0.175. The second height has R = 0.3 while the last position is centered in the tank with R = 0.5. According to the above theory, the middle height (R=0.3) should produce the highest transient heat transfer.

Several figures have been included to give an idea of the development of the heat transfer through the transient. The early transient, at a time of 5 seconds, can be visualized from Figure 2.4 and Figure 2.5 which show the velocity vectors and temperature contours at each grid point. The convective flow is already developing after the first five seconds. As can be seen from the temperature contours in Figure 2.5, there is a warm body of water being convected above the coil. Figures 2.6, 2.7, and 2.8 demonstrate the velocity profile, temperature contours, and stream function respectively during the decay region. The water within the cavity moves in a counterclockwise direction driven by the diminished temperature difference. This counterclockwise motion shows a preference to rise in the center due to the vertical line of symmetry which is on the right side of the grid. Figures 2.9 and 2.10 demonstrate the slight thermal stratification that develops toward the end of the decay region. In Figure 2.9, this is evident along the outside of the enclosure but is absent in the center of the enclosure. In Figure 2.10, the water above the coil is basically at a constant temperature while the fluid beneath the coil is almost perfectly stratified. Again, this occurs as the water beneath the coil is heated primarily by conduction.

FLUENT reports the average heat flux for the entire surface of the coil at each time

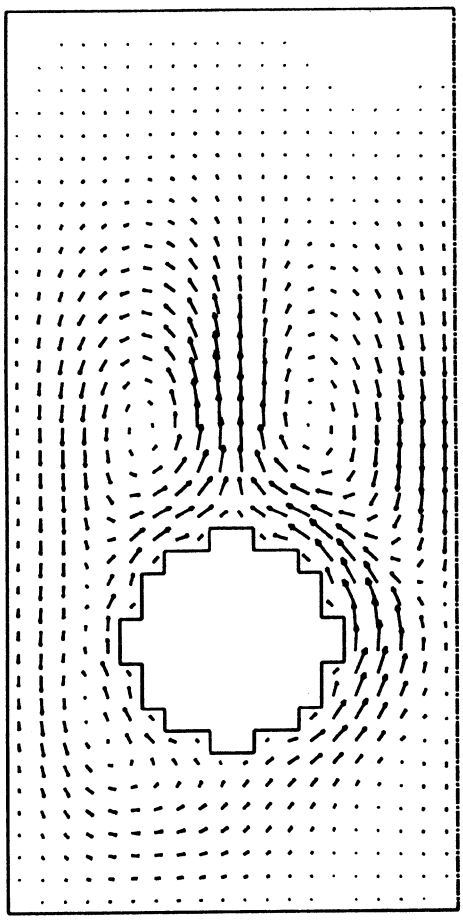

Figure 2.4 Velocity Vectors at Time of 5 seconds for R = 0.3

Max. Velocity = 2.30 x 10^{-3} m/s

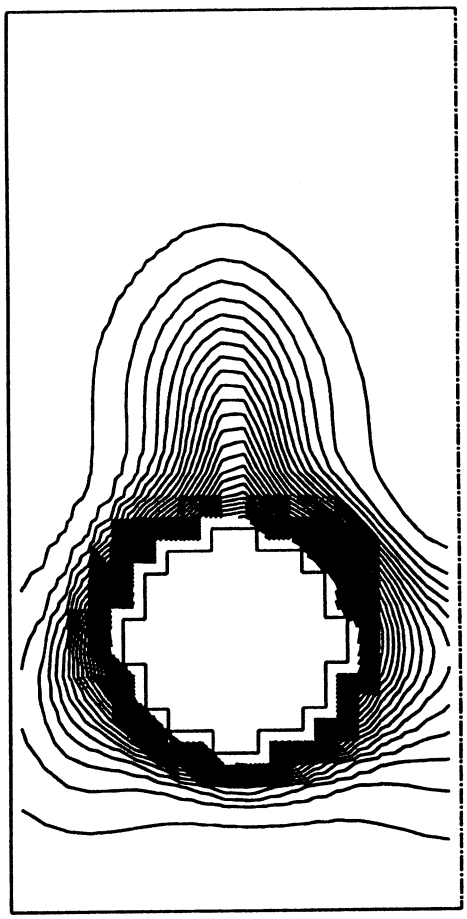

Figure 2.5 Temperature Contours at Time of 5 seconds for R = 0.3

Max. Temp.= 305 K Min. Temp.= 300 K

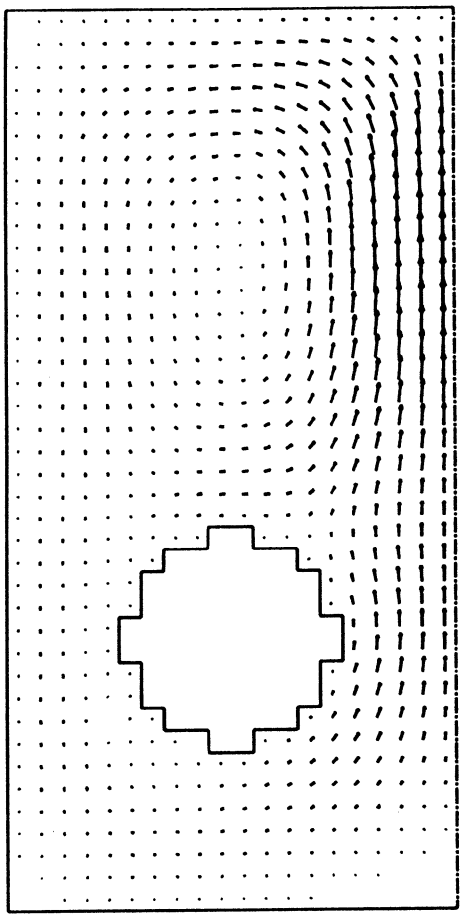

Figure 2.6 Velocity Vectors at Time of 200 seconds for R = 0.3

Max. Velocity = 1.95×10^{-3} m/s

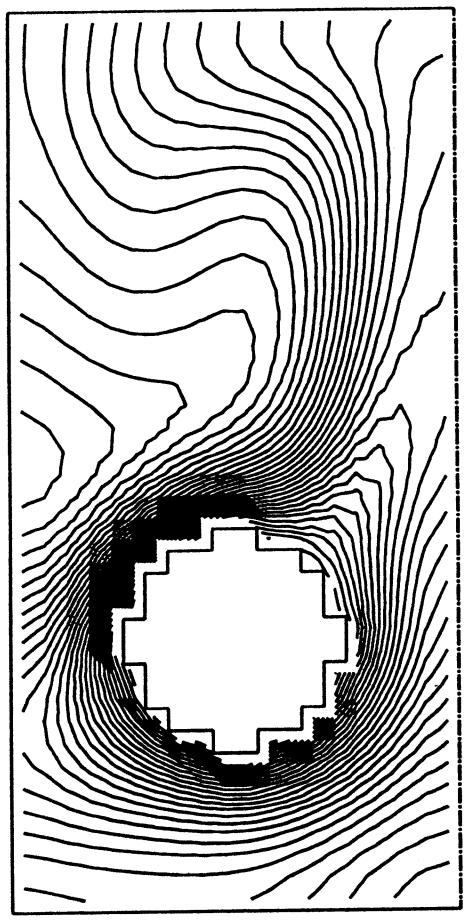

Figure 2.7 Temperature Contours at Time of 200 seconds for R = 0.3

Max. Temp.= 305 K Min. Temp.= 304.4 K

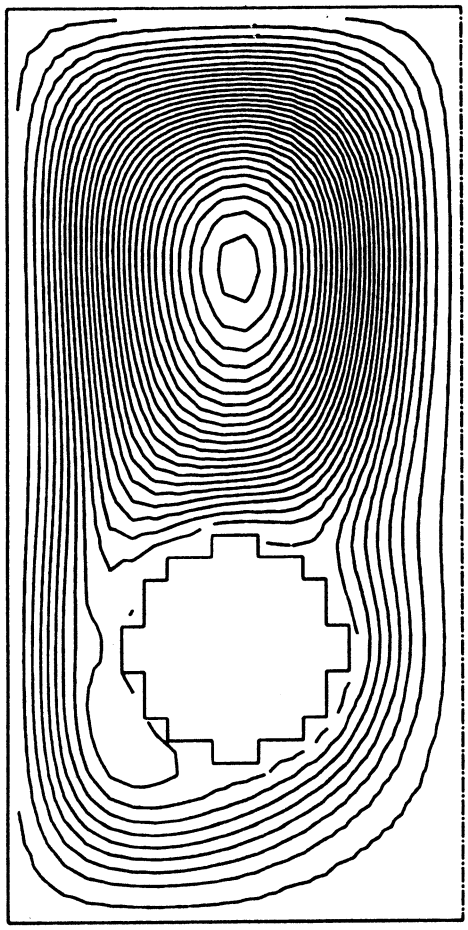

Figure 2.8 Stream Function Contours at Time of 200 seconds for R = 0.3

Maximum = 8.1 x 10-9 m^2/s Minimum = -1.74 x 10-12 m^2/s

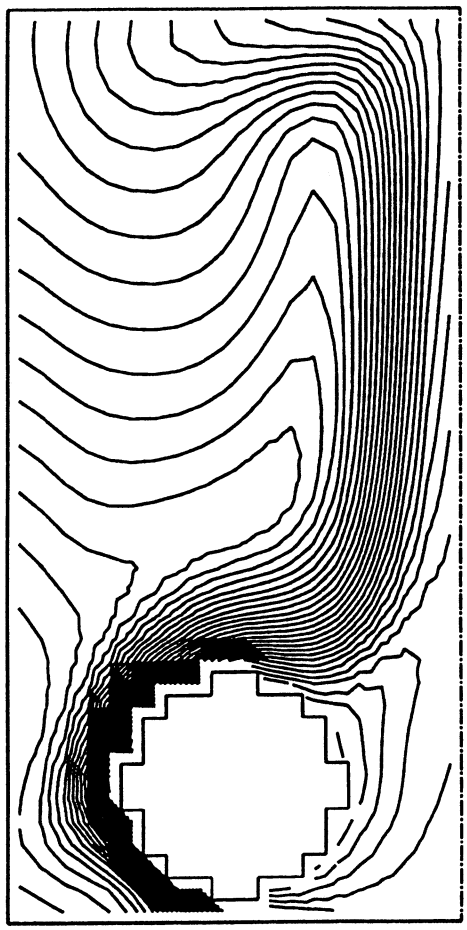

Figure 2.9 Temperature Contours at Time of 50 seconds at R = 0.175

Max. Temp.= 305 K Min. Temp.= 301.5 K

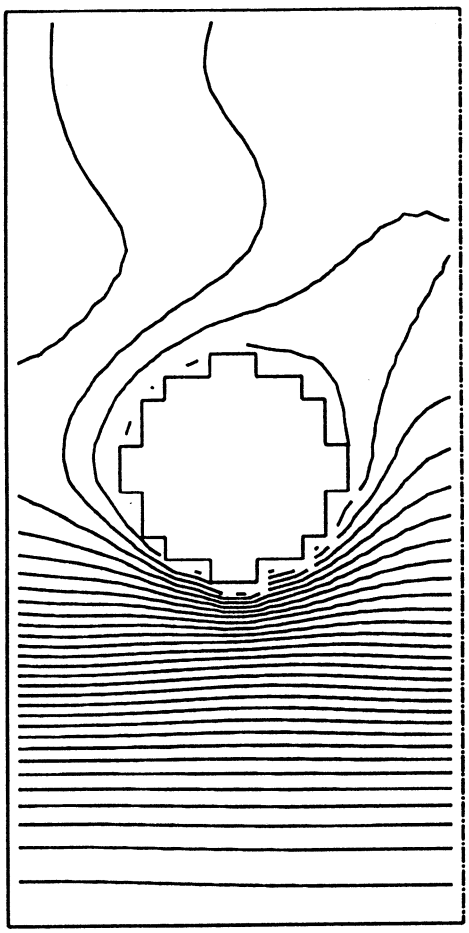

Figure 2.10 Temperature Contours at Time of 200 seconds at R = 0.5

Max. Temp.= 305 K Min. Temp.= 302.5 K

step. The Nusselt number is based on this heat flux and not the heat transfer coefficient that is reported by FLUENT. Based on the results of FLUENT on other projects, it was concluded that the heat flux result was more robust than the heat transfer coefficient. The Nusselt number is found using Equation 2.5. The heat flux was divided by the initial temperature difference to obtain the heat transfer coefficient.

$$Nu = \frac{\text{Coil Heat Flux}\left[W/m^2\right]}{T_{coil} - T_{bulk,\ initial}}\left(\frac{D_{coil}}{k_w}\right) \tag{2.5}$$

Figure 2.11 shows the transient Nusselt number response for all three coil heights. R is the ratio of height of the center of the coil above the cylinder bottom to the total height of the cylinder. The general trend of all three curves is similar. Initially, there is a pure conduction period during which the heat transfer drops off quickly as the heated conduction zone around the coil thickens and the driving force decreases. The conduction period is followed by the quasi-steady period during which the Nusselt number flattens out. The quasi-steady period can be modeled as a coil in an infinite medium. However, the Nusselt number does not become constant during this period. The probable reason for the decreasing Nusselt value during the quasi-steady period is the relatively large coil size. The larger coil means that the walls and floor of the enclosure affect the heat transfer to a greater degree than in previous numerical experiments. This greater effect causes the quasi-steady period to start dropping off almost immediately.

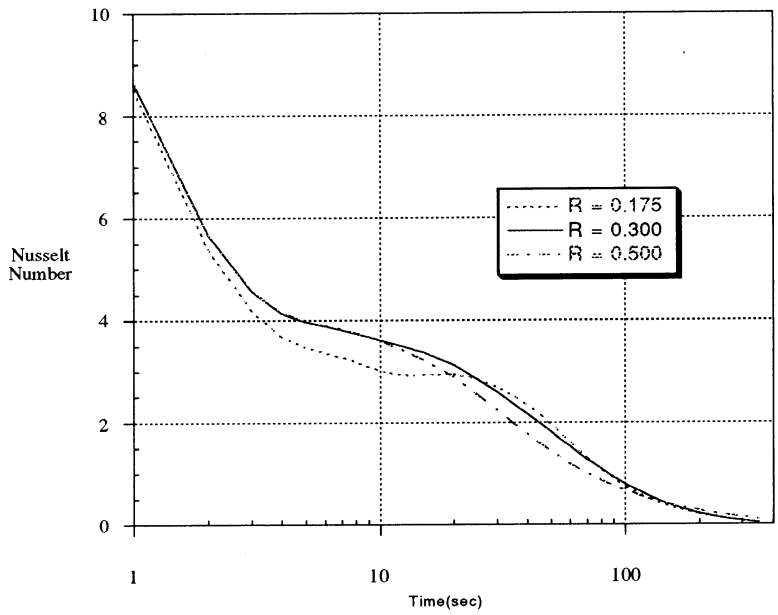

Figure 2.11 Transient Nusselt number response at three different coil height to cylinder height ratios with Ra = $9.8x10^3$, found using FLUENT .

The variation of coil height seems to have the expected effect on the Nusselt number response. The middle (R= 0.3) and upper (R= 0.5) coil height positions follow closely during the initial pure conduction period and early quasi-steady period but then the upper coil height response has a shorter quasi-steady period as the temperature rises in the fluid at that height more quickly than at the middle coil height position. The lowest coil position has a lower Nusselt number during the quasi-steady period because the presence of the cylinder floor impedes the flow from below. The lowest coil position also has the longest quasi-steady period. These results validate the above stated theory but is contradictory to the results of Sparrow and Charmchi (1983).

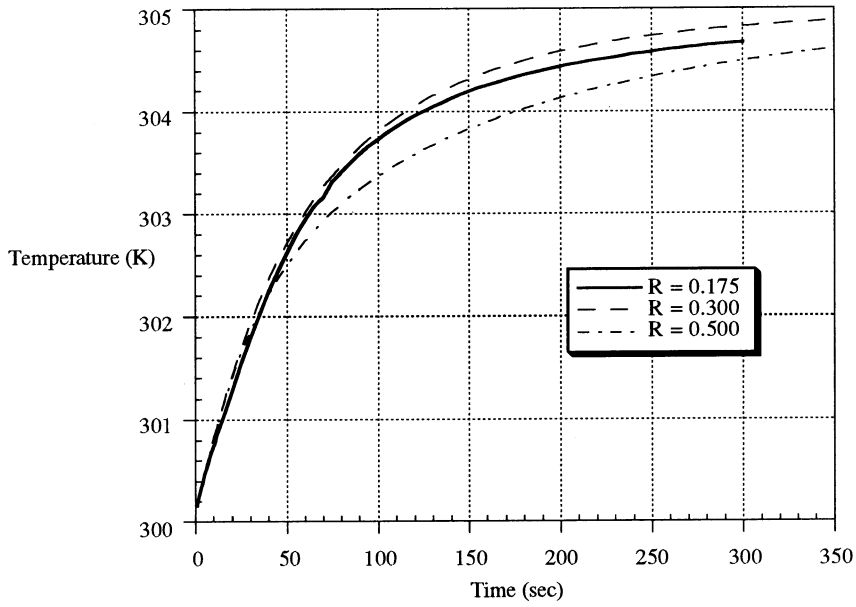

Figure 2.12 Bulk Temperature Response at three different coil height to cylinder height ratios at Ra = 9.8×10^3 found using FLUENT

The charging time is the time necessary to increase the average bulk temperature of the fluid within the enclosure the desired temperature. Figure 2.12 contains the bulk temperature response for the three coil height positions examined in this research. The figure illustrates the effect that a higher overall heat transfer rate has upon the charging time of the enclosure. The R = 0.500 case initially heats the enclosure fluid quickest. However, as the heat transfer drops off for the R = 0.500 case, the charging rate also decreases and the bulk temperature falls below the values for the other coil height cases.

These results were compared to prior results in two ways. First, as the quasi-steady period can be treated as a coil within an infinite medium, the Nusselt number was compared with the steady state, infinite medium results of Morgan (1975) and Churchill

and Chu (1975). These results are plotted on Figure 2.13. Obviously, these results are significantly on the low side of the infinite medium results.

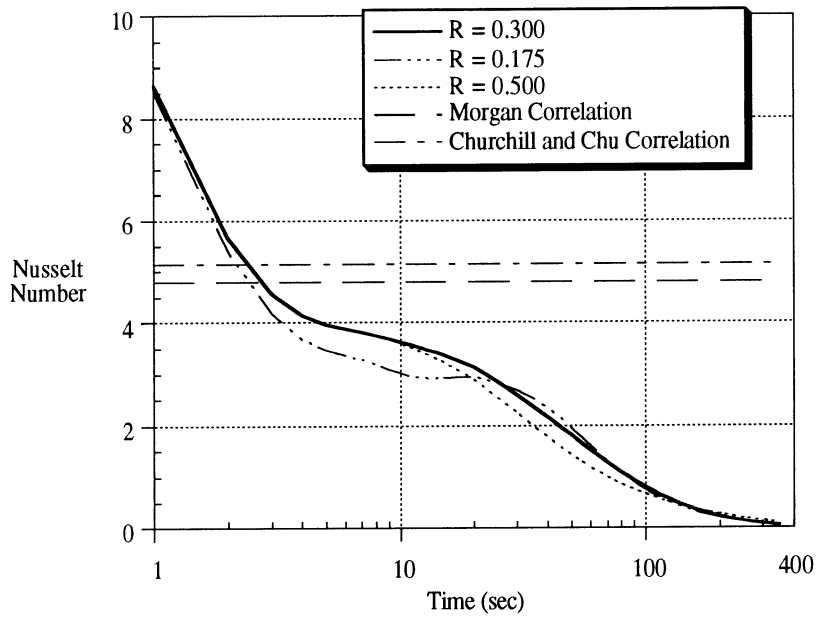

Figure 2.13 Comparison of FLUENT Nusselt Number Results at Ra = 9.8 x10^3 to Literature Correlations for Infinite Medium Case

Secondly, these results were compared to the numerical results of Reindl (1992). Figure 2.14 contains the numerical results of Reindl for Ra = 1x10^4. Again, the FLUENT results underpredicted the results of Reindl in both Nusselt value and the duration of the quasi-steady period. The probable reason for this is that, in the present study, the coil radius to cylinder radius is much larger than in Reindl's numerical study. All of his numerical experiments were conducted with the same ratio with coil radius/cylinder height = 1/12. As discussed in Section 2.3, Reindl's numerical geometry was not replicated due to time and computer access constraints.

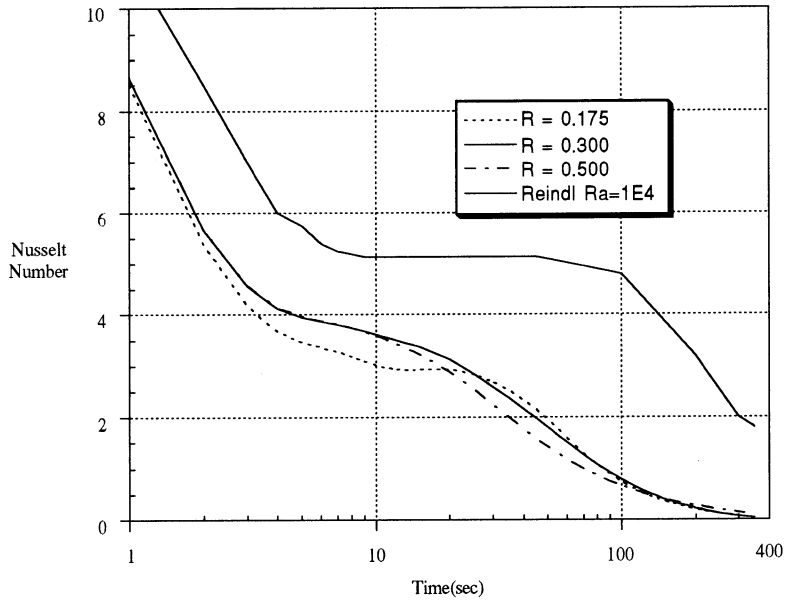

Figure 2.14 Transient Nusselt response for different heights at Ra = 9.8 x 10^3 with FLUENT and Results using FIDAP done by Reindl (1992)

The results of the current study do not compare well with the results of Reindl's numerical work or other literature correlations. This comparison points to the conclusion that the quantitative results of this study are not reliable. This conclusion was not unexpected because of the rough grid and small enclosure size used in the study. However, the qualitative results of this study should not be affected by this inaccuracy. All the geometric configurations are affected by the grid inaccuracies in the same way. The conclusions drawn about coil height optimization, stratification enhancement, and vertical shroud heat transfer enhancement are trustworthy because they are based solely on comparisons between runs within this study and not to results from outside this study.

2.5 Thermal Stratification Enhancement

Several attempts were made to improve the stratification within the cylinder. They included using a FLUENT subroutine that imposes a momentum sink, imposing a horizontal wall grid above the coil, and several variations of vertical and horizontal plates within the cylinder. Incidentally, from the height optimization it is obvious that the transient would be well into the decay region after 200 seconds and so these runs were only 200 seconds long. Also, due to an oversight by the author, these runs were done using Cartesian coordinates and not cylindrical coordinates. However, this fact is found to have little effect on comparisons between different flow impediment geometries.

2.5.1 Geometric Explanation and Flow Field Results

The first attempt was to use the porous media option supplied with FLUENT. The goal was to slow the convective plume as it rises above the coil. Theoretically, this would promote thermal stratification within the cavity. As can be seen by comparing Figure 2.15.a and 2.15.b, the porous media barrier above the coil seemed to have no significant effect on the flow. In the porous media model, the standard momentum equations are augmented by a general momentum sink.

$$\frac{\mu}{\alpha}V + C_2\left(\frac{1}{2}\rho v|v|\right) \tag{2.6}$$

where α and C2 are empirical inputs the user provides. This term creates a pressure drop proportional to the fluid velocity in the cell. The porous media was set up following the example tutorial in the FLUENT manual for a half open mesh. Following an initial, ineffective run, the constants governing the inertial dampening of the porous media were

increased by a factor of ten. This still had no significant effect. The author thinks that the porous media subroutine was not intended for low velocity natural convection flows.

Next, an approximate 50% mesh was created by placing a short vertical wall at every other grid point. This was imposed to slow the convective plume again as with the porous media model. Figure 2.16 shows this setup and the velocity profiles at 5 seconds into the transient. This flow impediment geometry has the opposite effect of the porous media model. The water rises up from the coil, spreads out across the bottom of the mesh and is pulled back down the sides. As the temperature plot shows in Figure 2.17, there is minimal heating of the fluid above the mesh, the opposite of the desired effect. Obviously, this is too dramatic of a flow impediment.

The next geometry attempted is a less obtrusive flow impediment and is shown in Figure 2.18. A small flat plate is placed above the coil at a slightly higher level than the mesh. The idea behind this flow impediment is still to slow the convective plume by forcing it to rise up and around this horizontal plate. As the velocity profiles show in Figure 2.18, a similar effect to that of the 50% mesh occurred although not as severely. Instead of merely slowing the flow on its way to the top of the cylinder, the flow takes a right turn to the side wall and back down to be entrained in the flow around the coil. In fact, this plate is totally ineffective later in the transient as a counterclockwise flow pattern develops as shown in Figure 2.19 .

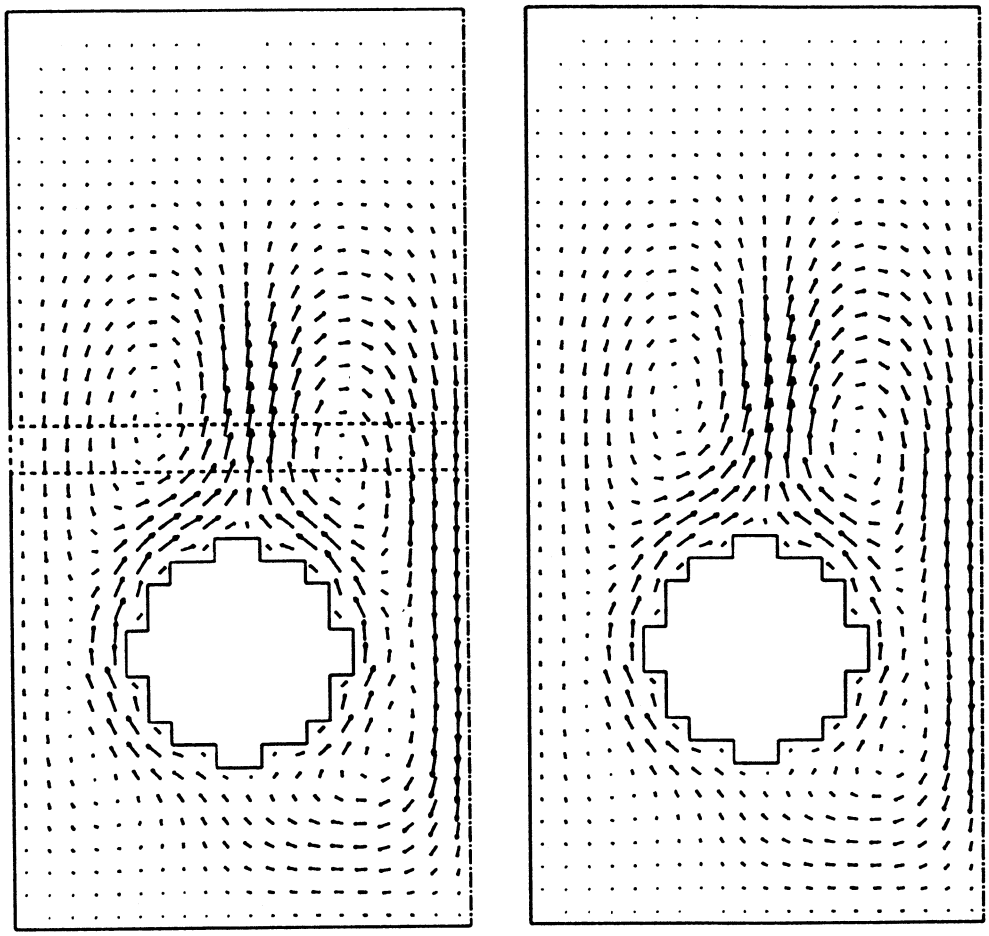

a) Porous Media Model

Max. Velocity = 1.92 x 10^{-3} m/s

b) No Impediment Case

Max. Velocity =2.3 x 10^{-3} m/s

Figure 2.15 Velocity Vectors at Time of 5 seconds with (a) and without (b) the FLUENT Porous Media Model

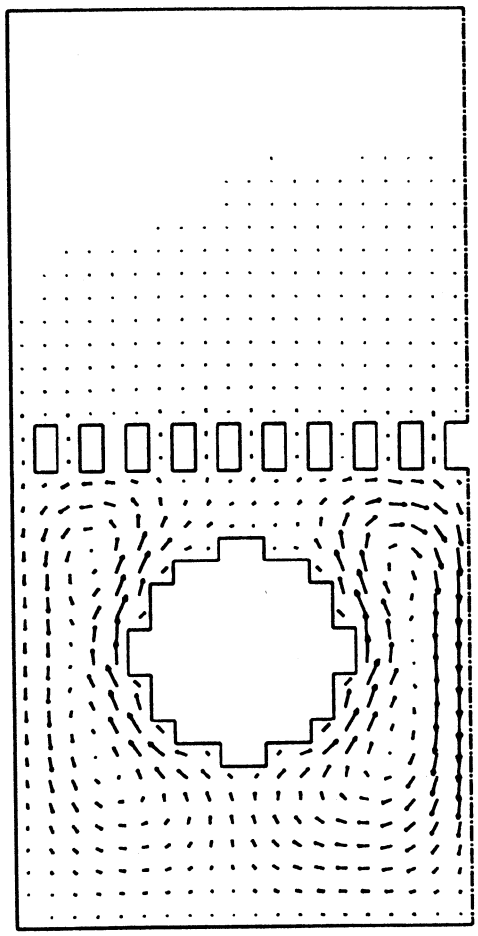

Figure 2.16 Velocity Vectors at Time of 5 Seconds for 50% Physical Mesh Geometry

Max. Velocity = 1.55×10^{-3} m/s

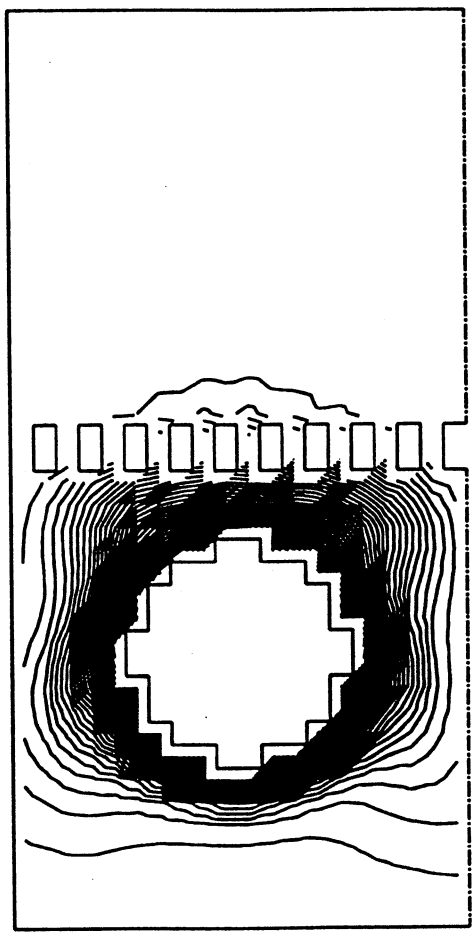

Figure 2.17 Temperature Contours at Time of 5 Seconds for 50% Physical Mesh Geometry, Max. Temp.=305 K Min. Temp.= 300 K

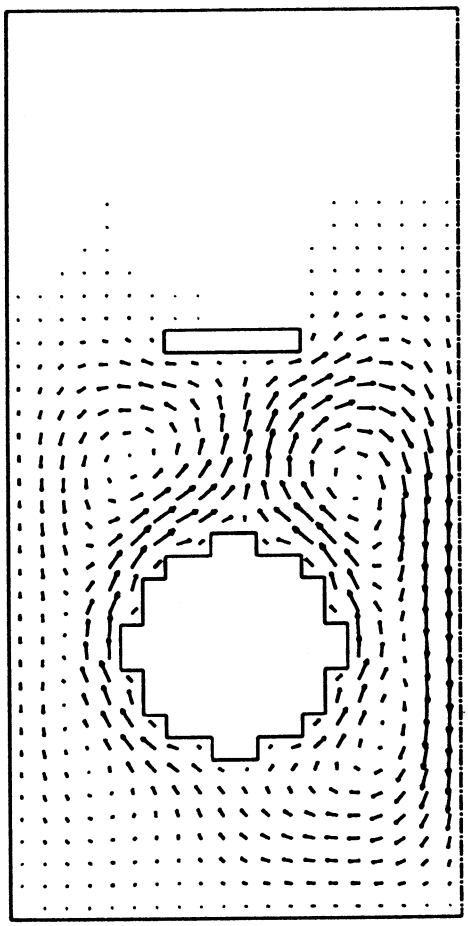

Figure 2.18 Velocity Vectors at Time of 5 seconds for Single Flat Plate Geometry

Max. Velocity = 1.89×10^{-3} m/s

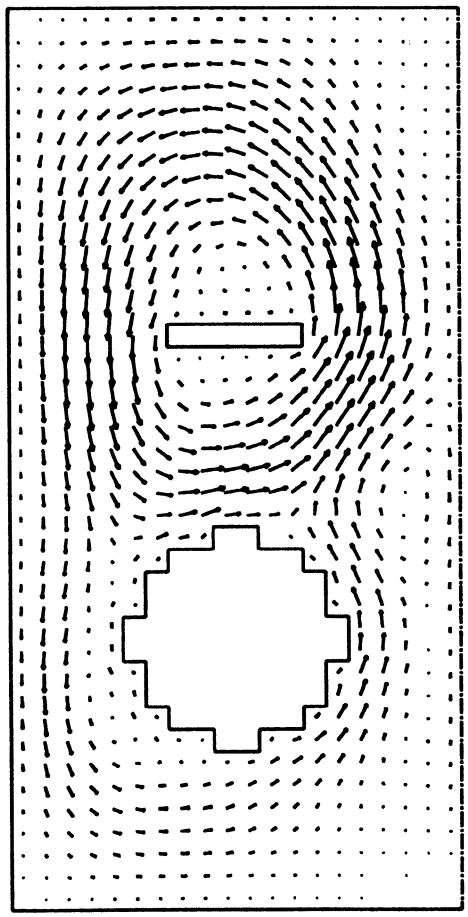

Figure 2.19 Velocity Vectors at Time of 10 seconds for Single Flat Plate Geometry

Max. Velocity = 3.00×10^{-3} m/s

Another configuration was examined and is displayed in Figure 2.20. Two small plates are placed above the coil with open space directly above the coil for the plume to rise and space along the side for downward flow. This method should not directly block the plume but restrict its upward flow to a specific opening. The returning, descending fluid would also be restricted to narrower opening. Additionally, a vertical divider descends from the ceiling in order to disrupt the counter-clockwise flow pattern that occurs later in the transient. Figure 2.20 shows that indeed this counter-clockwise mixing was curtailed. The flow was broken into two circulating flows. However, warmer water builds up underneath the flat plates, as shown in Figure 2.21, which seems to be slightly detrimental.

One final configuration was attempted and is displayed in Figure 2.22. One long vertical plate was placed above the coil with the idea that decay period mixing would be discouraged and that the formation of the boundary layer along this plate would slow the plume as it rose above the coil. Figure 2.22 shows that the flow was broken into two counter-rotating flow patterns: one on each side.

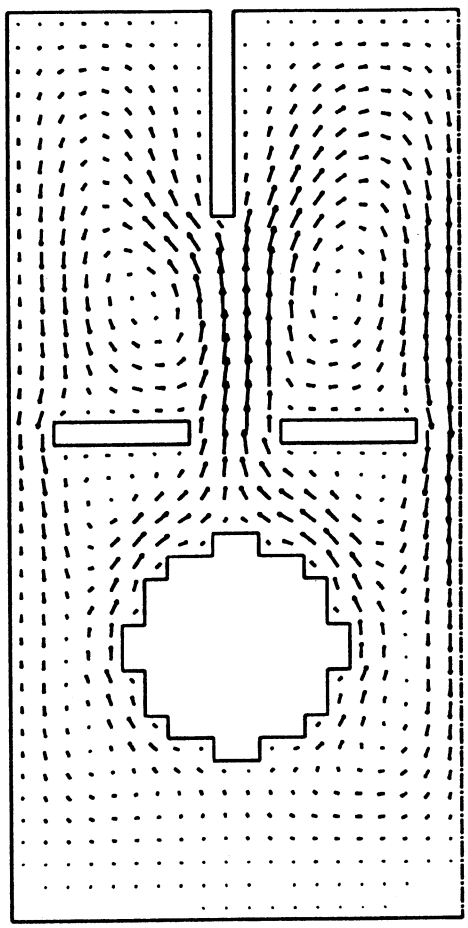

Figure 2.20 Velocity Vectors at Time of 50 Seconds for Two Plate and Divider Geometry

Max. Velocity = 1.61×10^{-3} m/s

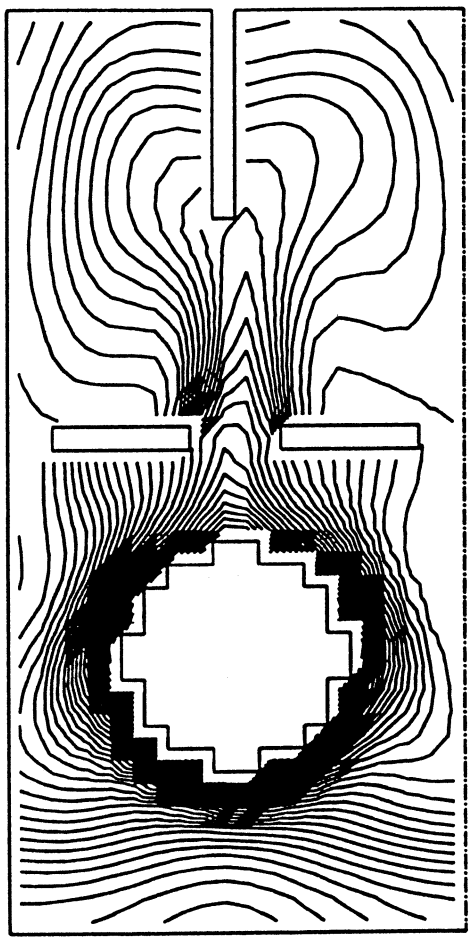

Figure 2.21 Temperature Contours at Time of 50 seconds for Two Plate and Divider Geometry, Max. Temp.= 305 K Min. Temp.= 301.3 K

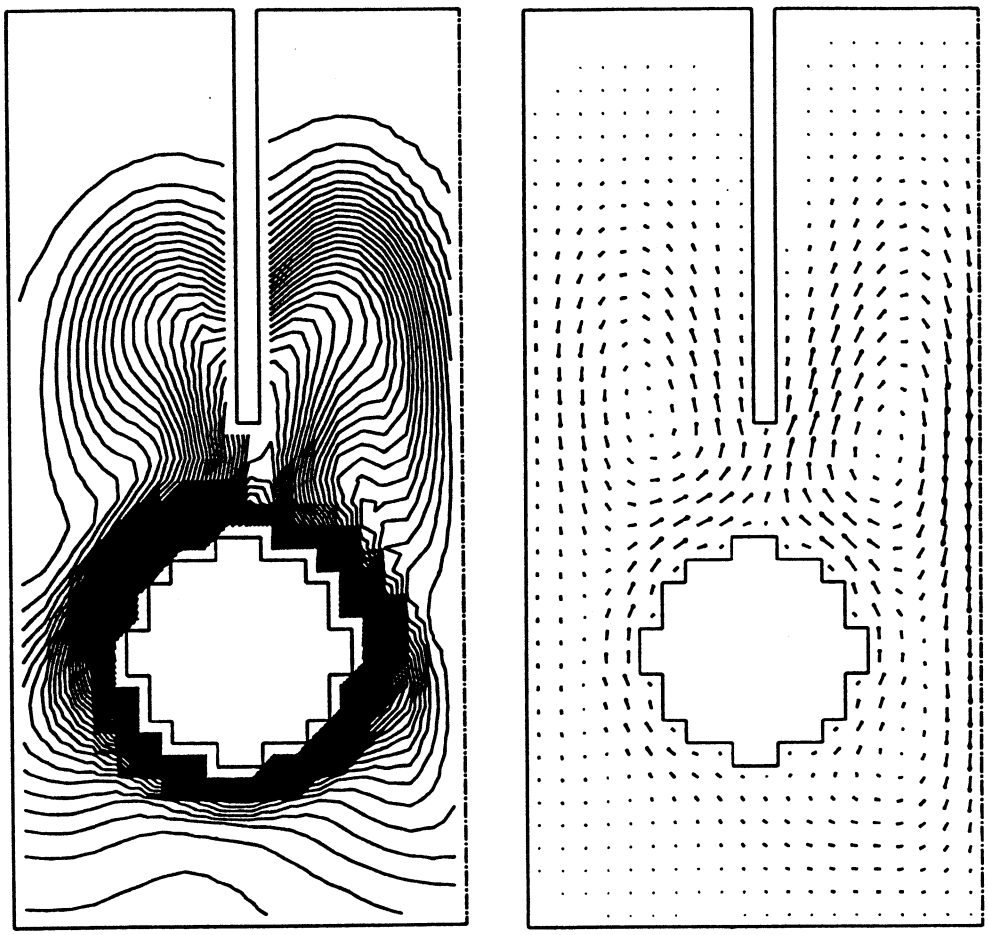

Figure 2.22 Temperature Contours and Velocity Vectors at Time of 10 seconds for Single Divider Geometry, Max. Temp.= 305 K, Min. Temp.= 300 K

Max. Velocity = 3.293×10^{-3} m/s

2.5.2 Nusselt Number and Temperature Results

The Nusselt number variation with time is plotted in Figure 2.23 while the bulk temperature response is plotted in Figure 2.24 for all of these variations and for the case with no flow impediments.

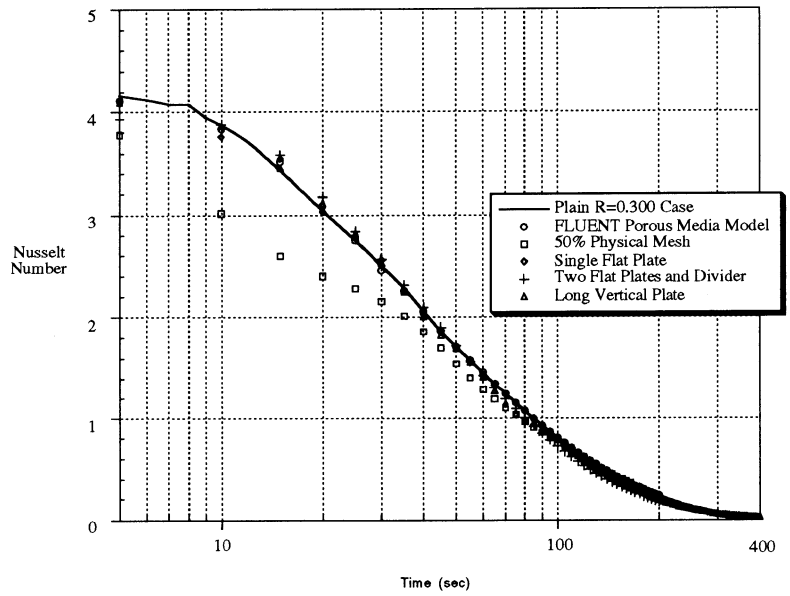

Figure 2.23 Transient Nusselt Number Response for Flow Impediment Geometries

As Figure 2.23 shows, several of these situations had no effect on the heat transfer including the FLUENT porous media model, the single flat plate geometry, and the long vertical plate. The 50% physical mesh geometry had a major detrimental effect on heat transfer. The two flat plates and divider geometry seems to be the most promising with a slightly higher initial Nusselt number.

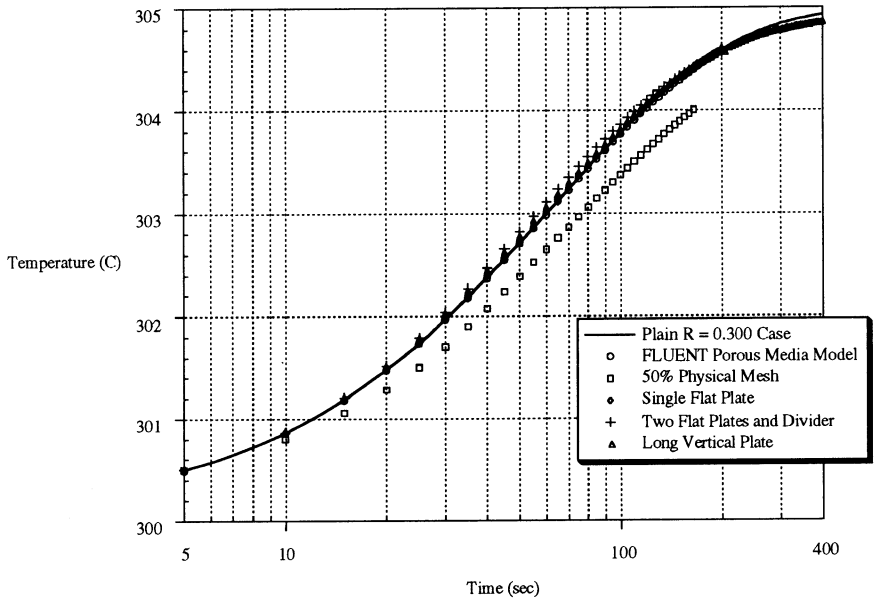

Figure 2.24 Transient Bulk Temperature Response for Flow Impediment Geometries

The situation with no flow impediment modifications, still charges the tank most effectively. The 50% physical mesh geometry heats the bulk temperature of the tank most slowly. Although the two flat plate and divider geometry shows some promise, the anticipated "inspired geometric modification" was never discovered.

2.6 Vertical Shroud Heat Transfer Enhancement

Sparrow and Pfeil (1984) showed that a vertical shroud around a horizontal pipe could greatly increase the heat transfer by creating a vertical channel for the convection plume and separating the warm, rising fluid from the cooler, descending fluid. Feiereisen (1984) attempted to do this experimentally. As discussed in Chapter 1, he placed a

vertical cylinder around a vertical bayonet style in-tank heat exchanger. However, he encountered problems with sizing the entrance and exit flow openings and, ironically, decreased the heat transfer.

FLUENT was used to study, with the same general geometry as Feiereisen, the effects of varying length chimneys above the coil. Because of grid sizing problems, the chimney was not extended alongside the coil. Three configurations were simulated as shown in Figure 2.25. In all three, two vertical plates are placed above the coil at the same width as the diameter of the coil (0.0045 m). In the first geometry, Figure 2.25a, the vertical chimney is 0.00855 m long and only one grid point (0.00045 m) separates it from the coil. This leaves 0.00225 m, or 1/8 th of the of the total tank height, above the chimney for the heated water to exit the chimney. The second geometry, Figure 2.25b, uses shorter vertical plates. They are only 0.0072 m high but still start the same distance from the tank ceiling. This means that the bottom of the shroud has been lifted 3 grid points over the first one. The third geometry, Figure 2.25c, has the shortest vertical plates at 0.00585 m long. This geometry has the greatest spacing between the coil top and the vertical plates.

It was expected that the middle length vertical shroud would have the best heat transfer of the three lengths. The assumption was that the longest plate length would choke the flow around the coil. It was also assumed that the shortest plate length would not channel the flow very well and have a minimal effect on heat transfer.

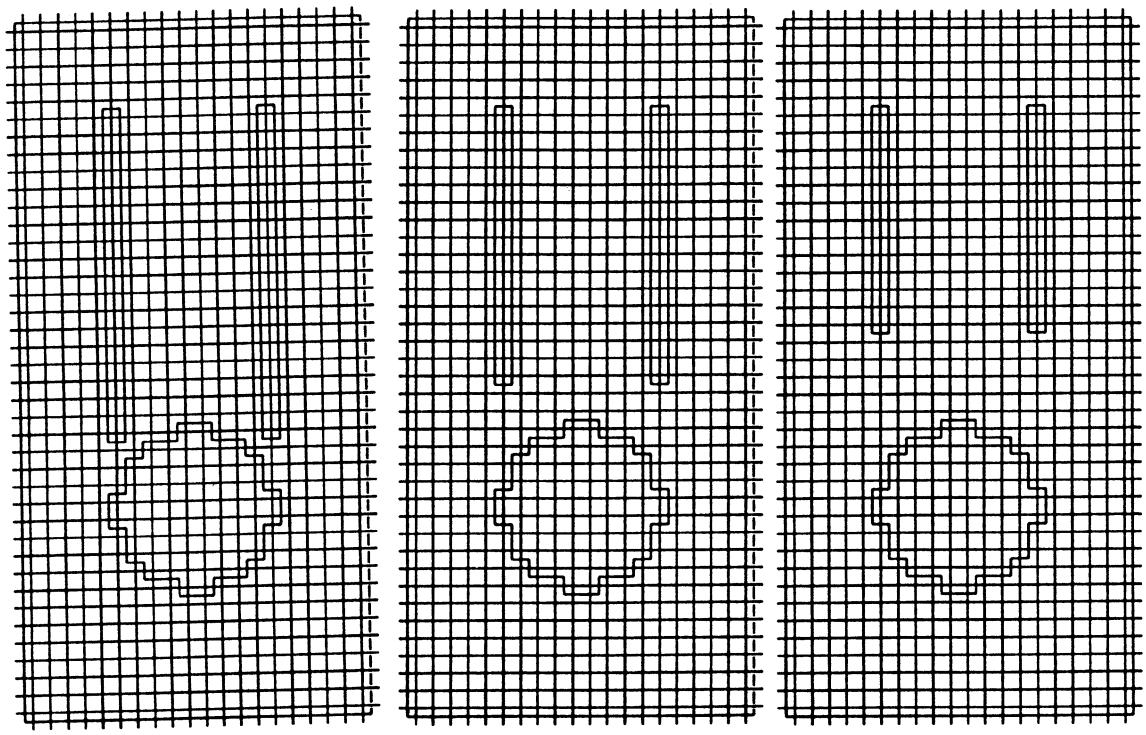

a) Long Shroud b) Medium Shroud c) Short Shroud

Figure 2.25 Three Different Vertical Shroud Length Grids

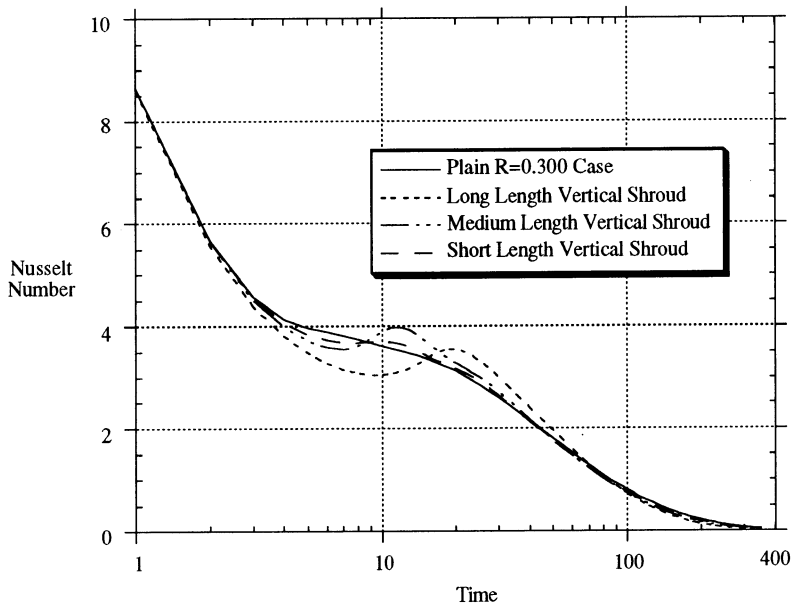

Figure 2.26 Transient Heat Transfer for Three Vertical Shroud Lengths

Figure 2.26 illustrates the transient heat transfer for all three vertical shrouds and the plain coil case and shows some unexpected results. All three geometries decreased the heat transfer from the coil prior to about 8 seconds but their heat transfer response crossed over the plain coil case at that point and dramatically extended the heat transfer at the end of the plain case quasi-steady period. It should be noted that even the shortest length shroud improves the heat transfer when, it was expected, that it would have no effect on the heat transfer.

The presence of the vertical plates close to the coil, in the case of the longest shroud, does initially adversely affect the heat transfer. It drops well below the plain, unshrouded case early in the transient. However, the heat transfer is dramatically increased again when a circulation flow around the vertical plates forms. The flow rises

on the inside of the enclosure and then descends on the outside of the enclosure. Only some flow passes through the vertical shroud. This is evident in the velocity maps for several time steps shown in Figure 2.27. Initially, in Figure 2.27a, the fluid cannot readily rise between the shrouds and recirculates back around the coil. This has the effect of significantly reducing the heat transfer. However, as can be seen in Figure 2.27b, once an upward flow is established around the shroud, the velocities around the coil and the shroud increase dramatically. This increased velocity has the effect of increasing the convection coefficient in this area and thereby the overall heat transfer coefficient. In contrast to the flow field of Figure 2.27, Figure 2.28 shows the flow field of the medium length vertical shroud. In this case, the fluid flows upward through the center of the shroud and back down on the outside of the coil. Figure 2.29 shows the temperature contours at a time of 30 seconds for both the long shroud case and the unshrouded case. Again, the warmer fluid is between the shroud walls. In addition, there is a significant degree of thermal stratification both within and outside the shroud.

Figure 2.30 shows the bulk temperature response for the vertical shroud geometries. Contrary to the expected outcome, the case of the longest vertical shroud increases the bulk temperature most quickly. The heat transfer is increased both by the pinched flow and increased stratification keeping a higher Nusselt number longer into the transient. In the long shroud case, the bulk temperature of the fluid within the tank reaches 304 C in 92 seconds. The unshrouded case has the worst temperature response. The bulk temperature reaches 304 C in 115 seconds. Of course, the unshrouded case, with R = 0.300, is the best of the cases studied with varying coil heights.

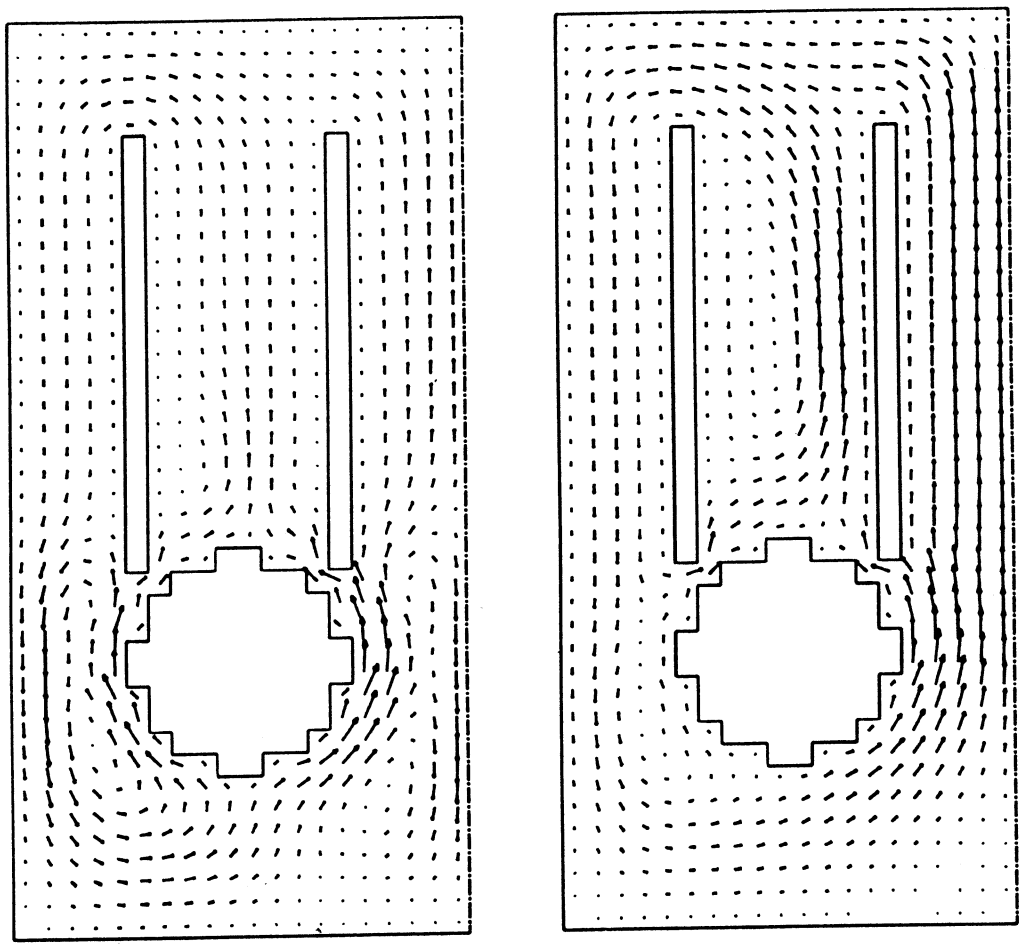

a) 5 seconds

Max. Velocity = 1.23 x 10^{-3} m/s

b) 20 seconds

Max. Velocity = 3.36 x 10^{-3} m/s

Figure 2.27 Velocity Vectors for Longest Vertical Schroud

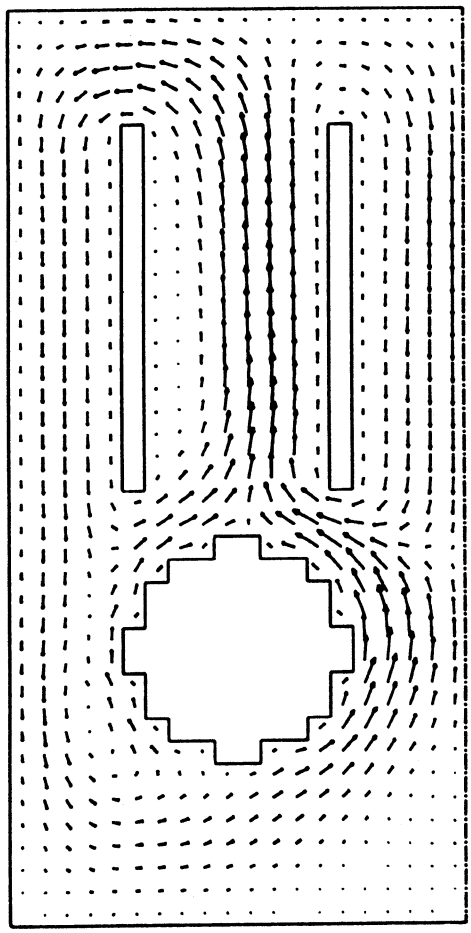

Figure 2.28 Velocity Vectors at Time of 20 seconds for Medium Length Vertical Schroud

Max. Velocity = 2.19×10^{-3} m/s

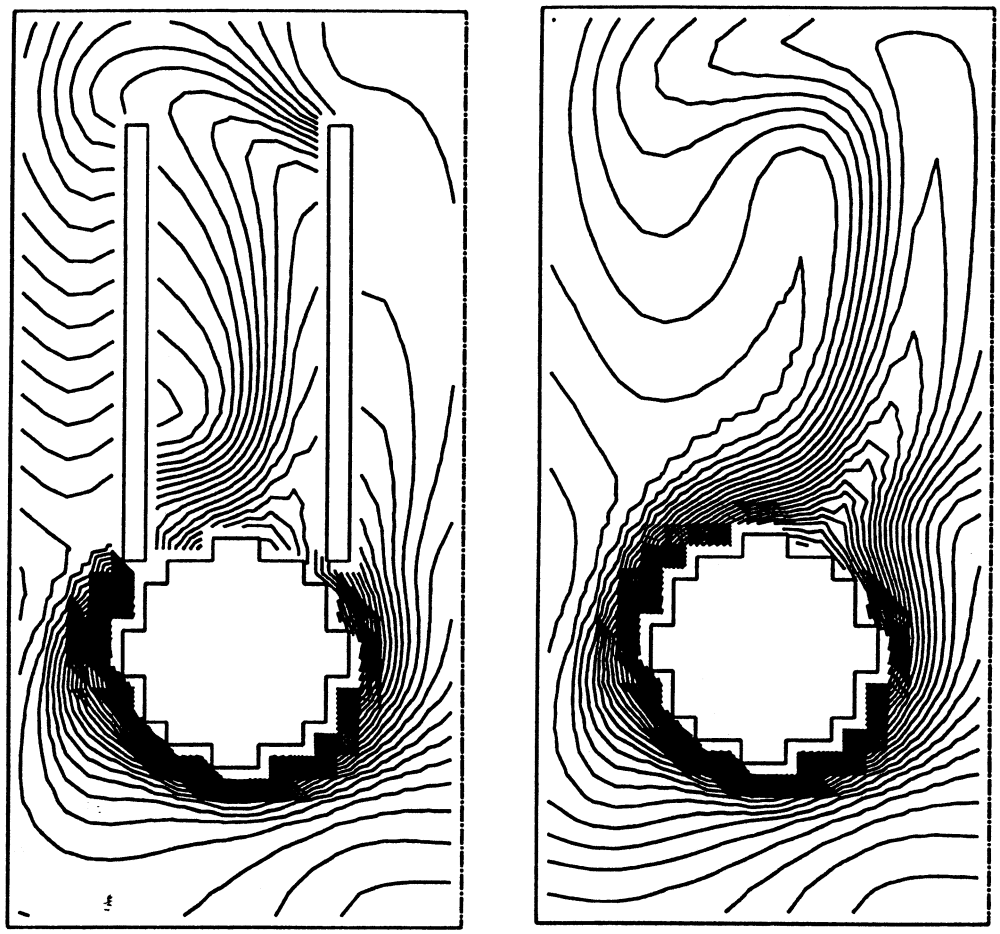

a) Long Vertical Shroud

Max. Temp.= 305.0 K

Min. Temp.= 300.4 K

b) Unshrouded Case

Max. Temp.= 305.0 K

Min. Temp.= 300.4 K

Figure 2.29 Temperature Contours at Time of 30 seconds

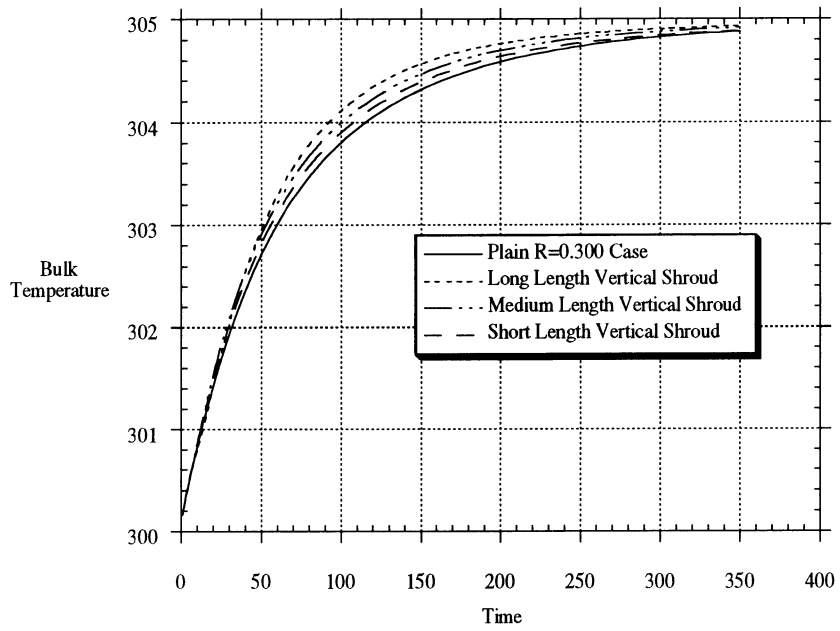

Figure 2.30 Transient Temperature Response of Fluid Within the Cylinder For All Three Vertical Shroud Lengths

2.7 Summary of Numerical Analysis

The first main area of study in this numerical study concerns the optimization of the height of the coil within the enclosure. The charging rate refers to the rate of increase of the bulk temperature of the fluid within the enclosure with respect to time. The charging rate is a direct result of the heat transfer throughout the transient. As can be seen in Figure 2.12, the middle coil height (R = 0.3) charges the tank most quickly. The reason for this can be seen by examining Figure 2.11. If the coil is placed too high within the enclosure, the quasi-steady period is shortened. Because the bulk temperature rises faster higher within the enclosure, the quasi-steady period drops off quickly. At the other

end, if the coil is placed too low within the enclosure, the presence of the enclosure floor and the outside wall interfere with the fluid flow and lowers the Nusselt number during the quasi-steady period. The conclusion from these numerical runs is that an optimum coil height exists and that it is located, for this geometry, in the vicinity of R = 0.3.

Another aspect that is examined by this numerical research deals with the performance of several geometries designed to improve thermal stratification within the enclosure. Five different geometries were studied ranging from a porous media to a single vertical plate above the coil. Although these geometries did modify the flow field within the enclosure, none improved the stratification in a way that improved the charging time. In fact, in several cases, the heat transfer rate was diminished. This was especially true of the imposed 50% physical mesh shown in Figure 2.23. The prevailing trend was that any interference with the ascending plume resulted in the plume flow recirculating down and back through the coil boundary layer, as illustrated in Figure 2.17. Immediate recirculation of the plume fluid is not desirable because this keeps warmer water flowing around the coil and thereby decreases the heat transfer driving force.

The final area of study was that of the effect of vertical shrouds on the heat transfer from a coil. Figure 2.24 illustrates the three shroud configurations used. It was found that all three configurations improved the charging rate of the enclosure fluid. As Figure 2.26 demonstrates, the Nusselt number for the shroud case is lower at the beginning of the quasi-steady period but then rises at the end of the quasi-steady period. Keeping in mind that a log scale is used for the time, this increase at the end of the quasi-steady period is of considerable importance to the charging time. Figure 2.30 shows that all three shroud geometries increase the charging rate. The longest vertical shroud is most effective at shortening the charging time.

CHAPTER
THREE

EXPERIMENTAL ANALYSIS OF A COILED TUBE WITHIN A CYLINDER

As discussed in Chapter 1, the primary focus of this research is experimental work to validate previous numerical results concerning the geometry of a coil within a cylinder and to examine the effects of the position of the coil within the tank. Experiments by Reindl (1992) were unsuccessful due to an oscillating coil wall temperature. Therefore, a new method was chosen for the present work. Instead of using electrical resistive heating within the coil, constant temperature water was pumped through the coil. This method solves the problem of an oscillating coil wall temperature but has some inherent problems of its own.

In this experiment, the transient Nusselt number is calculated based on the measured surface temperature of the coil and the bulk temperature of the fluid within the enclosure. The bulk temperature will be calculated based on the expansion of the fluid within the tank. The transient heat transfer response can be quantified with the examination of these values through time.

3.1 Experimental Setup

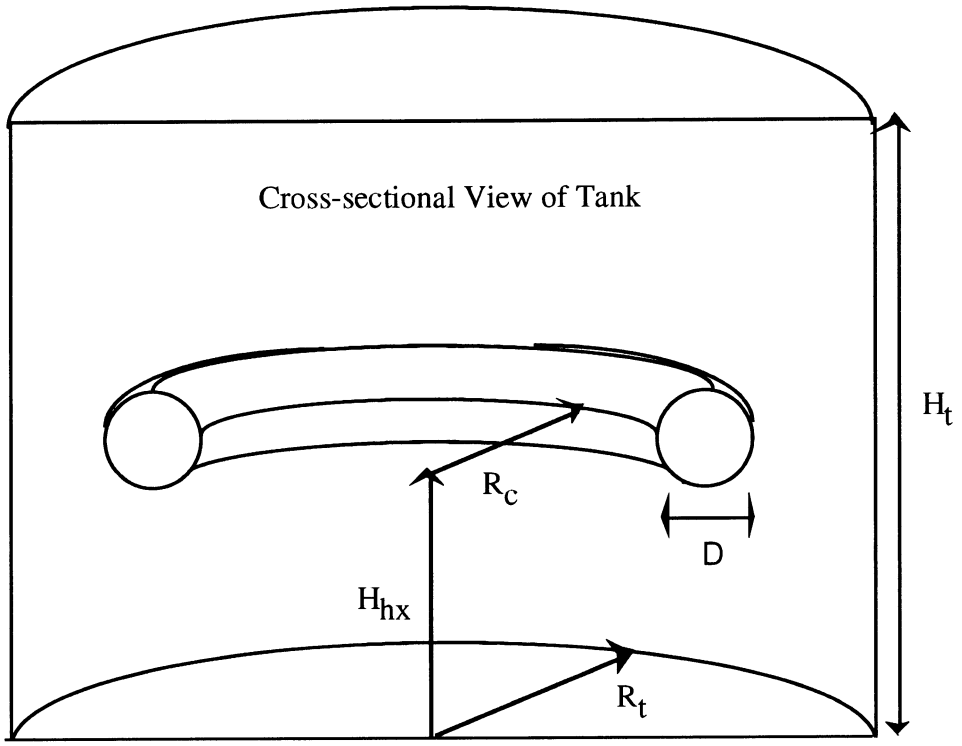

Figure 3.1 Theoretical Experimental Setup to Reflect Numerical Setup

Figure 3.1 illustrates the goal of the design of this experiment which is to make the experiment reflect, as closely as practical, the conditions represented in the numerical analysis of Reindl (1992).

3.1.1 Design Considerations

The bulk temperature is found by the thermal expansion of the fluid within the tank vertically into a tube extending above the tank. Therefore, it is important to reduce the thermal expansion of the cylinder and the top and bottom plates. An enclosure material with a low thermal expansion coefficient was sought to reduce heat losses. A

low thermal conductivity would help preserve any thermal stratification within the tank that could be destroyed by vertical conduction within the cylinder walls. A transparent material for the enclosure was desired to facilitate the use of flow visualization techniques. Finally, the material had to be smooth to be similar to the smooth walls of the numerical modeling.

The heat exchanger was designed to be, as close as possible, to the one used in Reindl's numerical simulations. Therefore, the pipes that supply water and support the coil must be as unintrusive as possible. There were to be no thermocouple wires close to the coil with the fear that they would interfere with the flow field. The surface of the coil should be smooth and the coil should be as round as possible, both cross-sectionally and radially. Additionally, the heat exchanger must have high thermal conductivity and low thermal capacitance so as not to hamper the heat flow from the supply fluid to the tank fluid.

The water supplied to the coil had to be of as constant a temperature as possible. It should also be of sufficient flow rate to produce a large interior heat transfer and a small inlet to outlet temperature drop. However, if the flow rate rose too high it could damage the coil.

3.1.2 Physical Apparatus

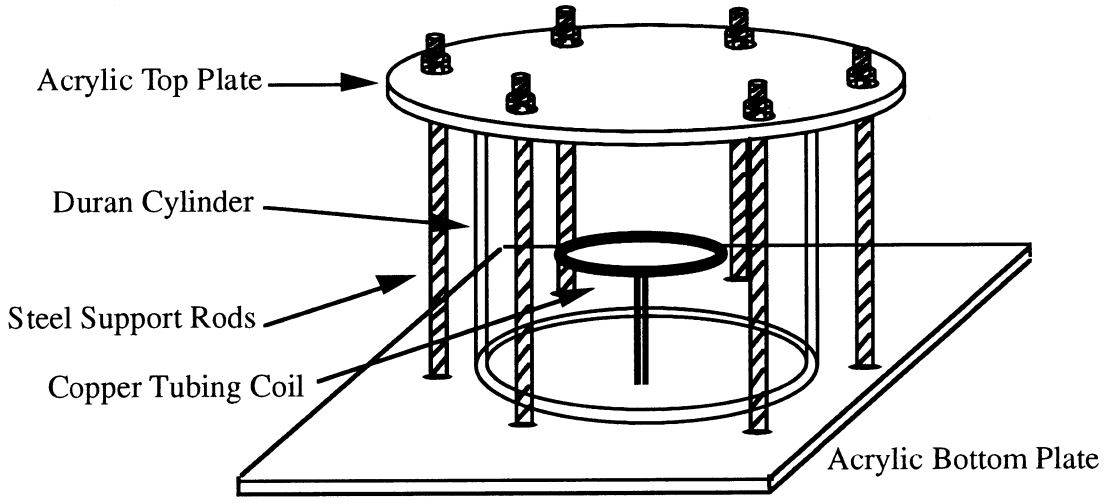

Figure 3.2 Experimental Enclosure Design

Keeping all these design considerations in mind, materials for the experiment were selected. The vertical cylinder, shown in Figure 3.2, was composed of a commercial borosilicate glass, Duran. The top and bottom plate will expand in all directions, as well. However, if the top and bottom plate are allowed to expand, the top and bottom plane of the enclosure should remain flat. With this in mind, acrylic plastic was used because it is considerably easier to work with than Duran and is less expensive. These materials meet the design requirements as they have a low conductivity, low thermal expansion (especially the Duran), transparent, and smooth. The relevant properties for Duran and acrylic are shown in Table 3.1. In the course of the present study, considerable research was done into finding larger Duran or fused quartz enclosures. A larger size would be prohibitively expensive to procure. An alternative, for future experiments, would be Invar which is a nickel-iron alloy with a very low thermal expansion coefficient. The thermal expansion of Invar is under 2×10^{-6} in./in.-C while the thermal expansion

coefficient for borosilicate glass is 3.85 x 10^{-6} in./in.-C.

Property	acrylic plastic	Duran® (borosilicate glass)
Thermal Conductivity	1.25 W/m-C	1.14 W/m-C
Specific Heat	1.19 kJ/kg-C	0.711 kJ/kg-C
Density	2676 kg/m^3	2230 kg/m^3
Max. Cont. Temp.	82 C	500 C
Linear Expansion Coeff.	7.46 e-6 1/K	3.25 e-6 1/K

Table 3.1 Material Properties of Enclosure Materials (at 33 C)

The Duran cylinder radius is 10.35 cm while the height is 20.7 cm. The bottom of the cylinder is bonded to the bottom Acrylic plate with silicone. To facilitate the removal of the top plate, there is a layer of neoprene rubber that is bonded, with silicone, between the top of the cylinder and the top acrylic layer. The vertical tie rods shown in Figure 3.2 were only tightened to allow the silicone to seal and when the apparatus needed to be moved. They were loosened during experimental runs so the top plate could thermally expand freely. It expands in all directions but the bottom surface should remain in place. The enclosure expansion is accounted for in the bulk temperature calculation as discussed in Section 3.3.

There are two holes within the enclosure. On the top of the tank, there is a hole through which the tank fluid can expand. The second is in the bottom of the tank through which pass the inlet and outlet flow pipes for the heat exchanger coil and the coil thermocouples. This hole is sealed with a fabricated compression fitting and O-ring.

The heat exchanger itself was difficult to design and machine. Figure 3.3 shows the design of the circular heat exchanger coil. The main body of the coil was constructed

of copper formed into a circular shape and 0.0127 m in diameter (0.5 inches). The copper has a high conductivity (401 W/m K) and can be sanded very smooth so both those design goals are met. The two ends of the coil were soldered together with a stainless steel dam in between so that water does not flow between. Then, a hole was cut into the coil on each side of the dam and a 0.00635 m (1/4 inch) stainless steel tube was soldered onto each hole. These pipes are 0.3084 m (12 inches) long. This longer length was used so that the pipes can reach easily out of the enclosure even if the coil is at the top of the enclosure. These pipes supply the heated water to the coil, support the coil within the enclosure, and house the thermocouples placed within the coil (described in the next section). These pipes were potted within a larger 0.016 m (5/8 in) piece of conduit. This larger pipe is necessary because of the available compression fittings to route the pipes through the bottom of the tank. This piece of steel conduit fits tightly within the modified electrical compression

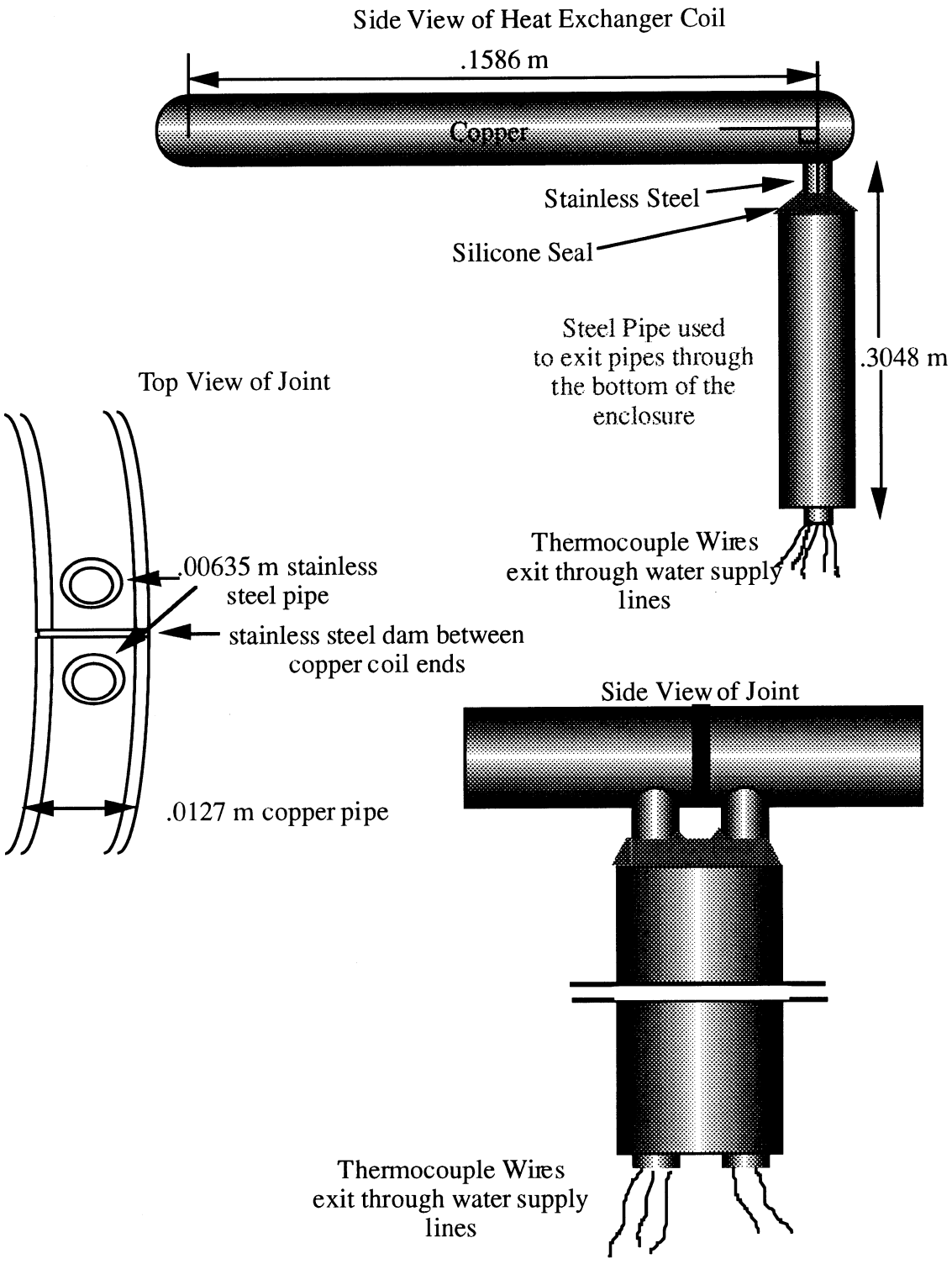

Figure 3.3 Circular Heat Exchanger Design

fitting in the bottom plate. The smaller pipes are sealed and supported within the larger pipe with silicone sealant. Except for this seal, there is open air between the smaller pipes and the larger pipe.

Questions have arisen concerning the effects of conduction within the heat exchanger apparatus especially between the inlet and outlet side of the coil, between the inlet and outlet pipes, and also along the support pipe. The problems of conduction between the inlet and outlet sides of the coil and conduction between the inlet pipe and outlet pipe are moot as a constant temperature around the perimeter of the coil is desired to correspond to the numerical results. Vertical conduction along the supporting pipe is still of some concern and in future experiments the supporting pipe should be replaced with a low thermal conductivity material.

Figure 3.4 shows the heated water supply system and its connection to the heating coil and enclosure. The main components of the heated water system include: a constant temperature water bath, a water pump, a rubber expansion bladder for controlling vibration, and connecting tubing. The constant temperature bath is a Magic Whirl Constant Temperature Bath. The bulk of the heating is done by the constant temperature bath. It can hold the temperature constant and keep the supply fluid well mixed. With proper insulation, the bath temperature is quite constant. Two water pumps were used in this experiment. The first was a 1/12 hp centrifugal pump that was partially submersible. This pump was replaced midway through the experiment with a 1/2 hp TEEL Swimming Pool pump in order to increase the fluid flowrate. The new pump required two additional valves and the appropriate fittings. Since the pump was probably too powerful, a shunt valve was installed to allow a portion of the water to bypass the coil. Because the thermal mass of the TEEL pump reduced the initial temperature of the supply water, the Coil Shutoff Valve was installed so that water could be pumped through the pump before it was passed through the heat exchange coil and the enclosure. The pump was preheated

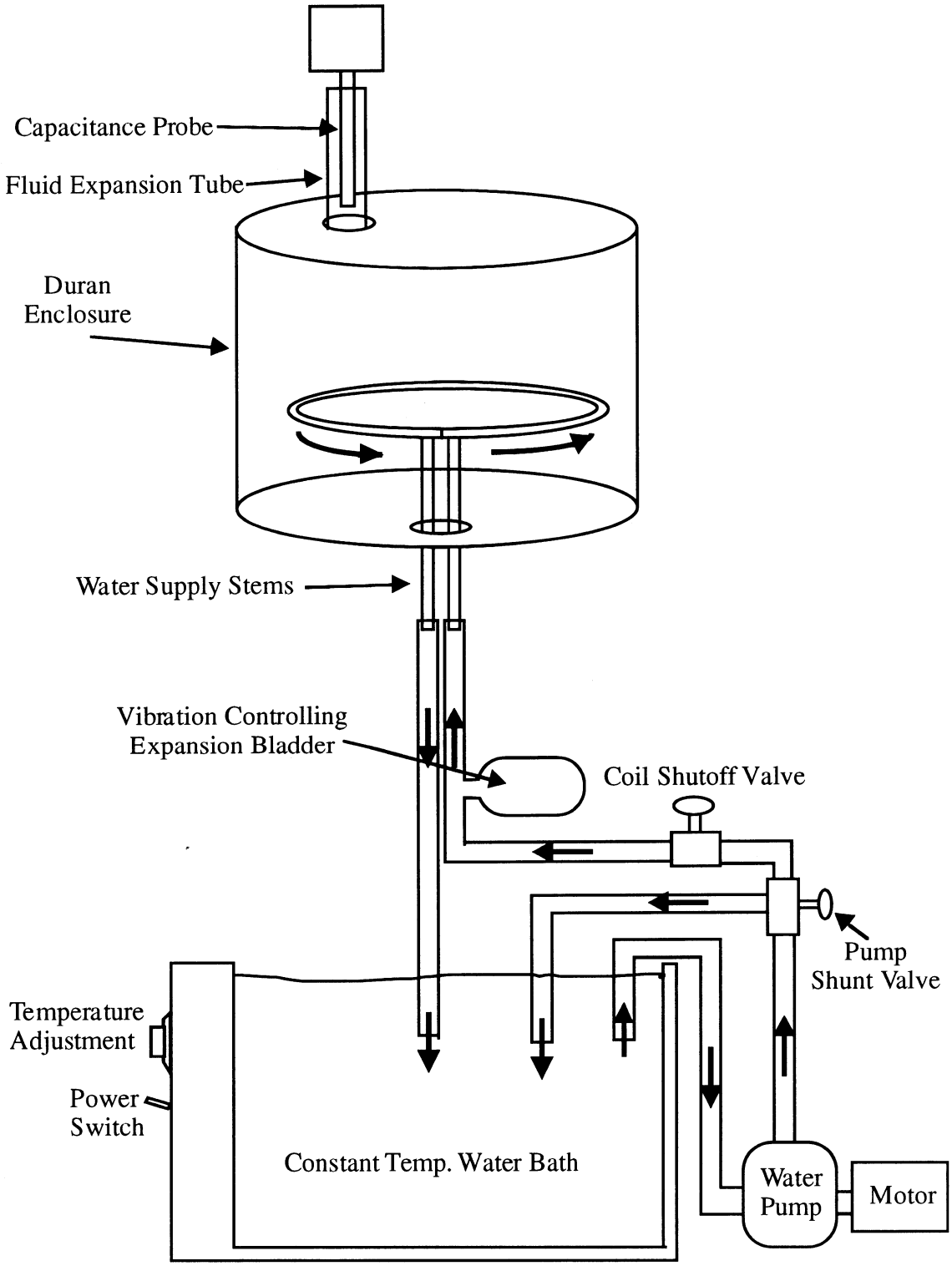

Figure 3.4 Heated Water Supply Setup

for several hours prior to passing water through the coil to stabilize the temperature. With the original pump, the constant temperature bath did most of the heating. However, the second pump generated so much heat that the water within the constant temperature bath actually rose above the setpoint temperature (by 3 to 6 C) after all insulation was removed from the fluid lines and top of the bath.

The fluid expansion tube and capacitance probe are also shown in Figure 3.4. They extend from the top of the enclosure through a small hole and also extend out of the insulation that covers the enclosure. There is a clear plastic tube into which the fluid expands which is 0.0305 m (1 3/16 in.) in diameter.

With the 1/12 hp pump, the tubes connecting the water supply to the coil were all flexible Tygon tubing and latex tubing. The latex tubing was used from the expansion bladder to the coil inlet to assist in noise reduction because it absorbs water pulsation better than the Tygon tubing. With the 1/2 hp pump, pipe fittings were included from the pump through the two valves. However, after the coil shutoff valve, flexible tubing is used.

3.1.3 Data Acquisition Apparatus

The important information in this experiment include the ambient temperature, the coil surface temperature, the height of fluid in the expansion tube, the temperature of the constant temperature bath, and, of course, time. All of the data is fed to an analog to digital converter board[1]. The data is then recorded by an IBM AT personal computer.

The temperature of the coil wall is monitored by 5 thermocouples placed evenly around the coil surface as shown in Figure 3.5. Two more thermocouples are placed in

---

[1] Model WB-AA1 High Resolution interface card from Omega Engineering, Inc. Stamford, CT

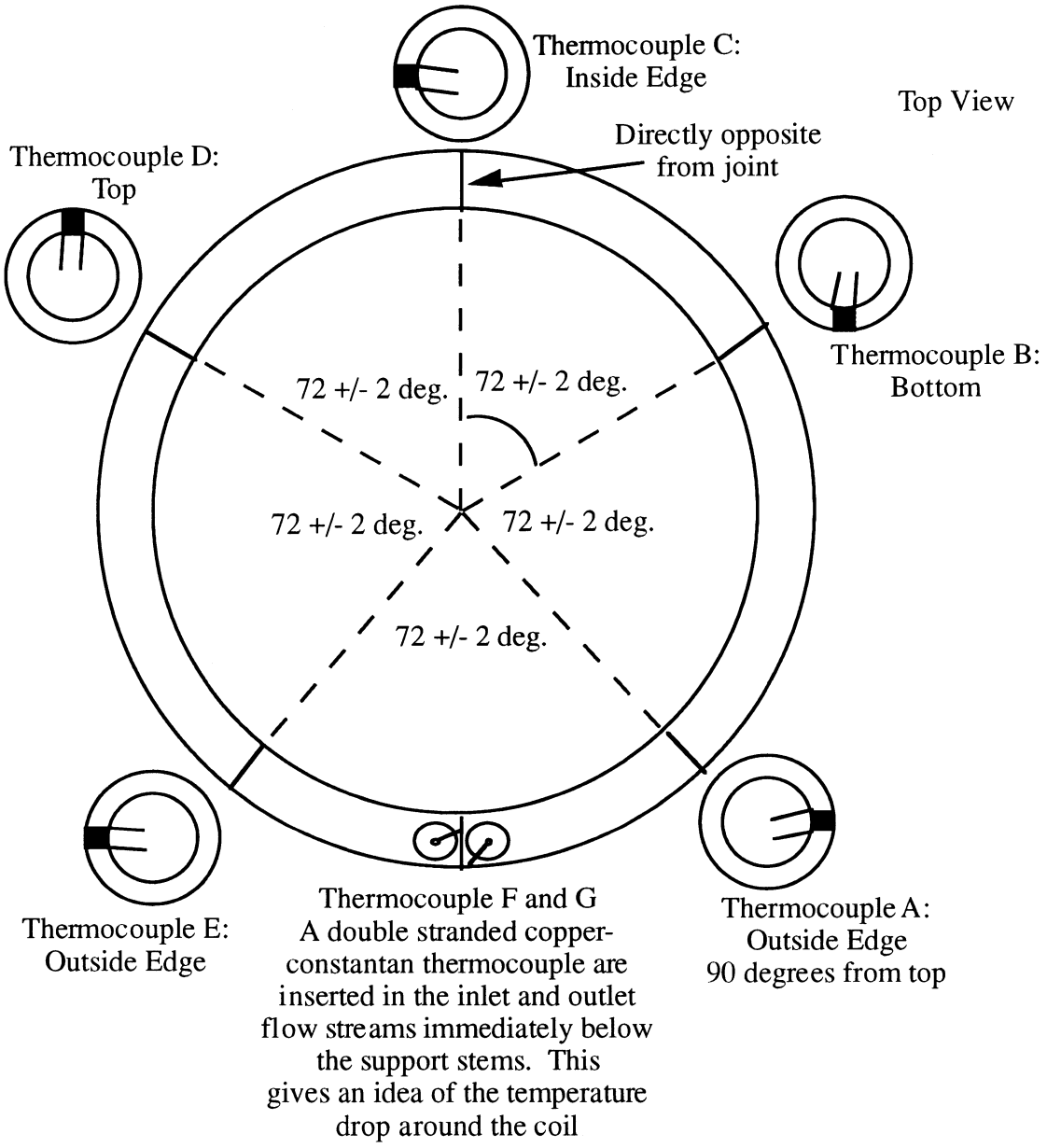

Figure 3.5 Coil Thermocouple Setup

the inlet and outlet flow streams directly below the support stems. The thermocouples are 36 AWG (0.127 mm, 0.005 in conductor diameter) copper/constantan (type T) with

Teflon insulation[2] The type T thermocouple was selected because it provides acceptable error characteristics (0.5 C, 0.9 F) for thermocouple measurements in the temperature range of interest. The five thermocouples are interesting because the constantan wire is directly soldered to the copper coil surface as depicted in Figure 3.5. Small holes were drilled in the surface of the coil and the constantan lead was passed through the hole and soldered in place. The lead is then fed through the inside of the coil and out through either the inlet or outlet stem. The thermocouple circuit is completed by a copper lead that is soldered to the surface of the coil at the joint. The figure also shows that the thermocouples are evenly distributed along the length of the coil and around the surface of the coil. This was done in an attempt to account for variations in the temperature with position along and around the coil. These thermocouples were calibrated several times with an ice bath and at an ambient temperature (22 C) with a precision mercury thermometer with an error of +/- 0.005 degrees.

The entire data acquisition setup is shown in Figure 3.6. Notice that the pump shown is different than the from the one shown in Figure 3.4. The pump shown here is representative of the first, smaller pump used for smaller flow rates. There are nine thermocouples used in the experiment. In addition to the five within the heat exchanger coil, there is a thermocouple at both the inlet and outlet. Also, there is a single thermocouple within the constant temperature bath and one that is used to measure the ambient temperature. The ambient thermocouple is located a few centimeters from the outside of the insulation that is placed around the enclosure.

Because the thermocouple values were measured using an A/D board, it would be convenient to measure the height of the fluid within the expansion tube with an instrument whose output can be fed to an A/D board. This is accomplished with a level transmitter[3]

---

[2] Model TT-T-36 T-type thermocouple from Omega Engineeering, Inc; Stamford, CT

[3] Model 700-1-22 Sensor from Drexelbrook Engineering; Horsham, PA

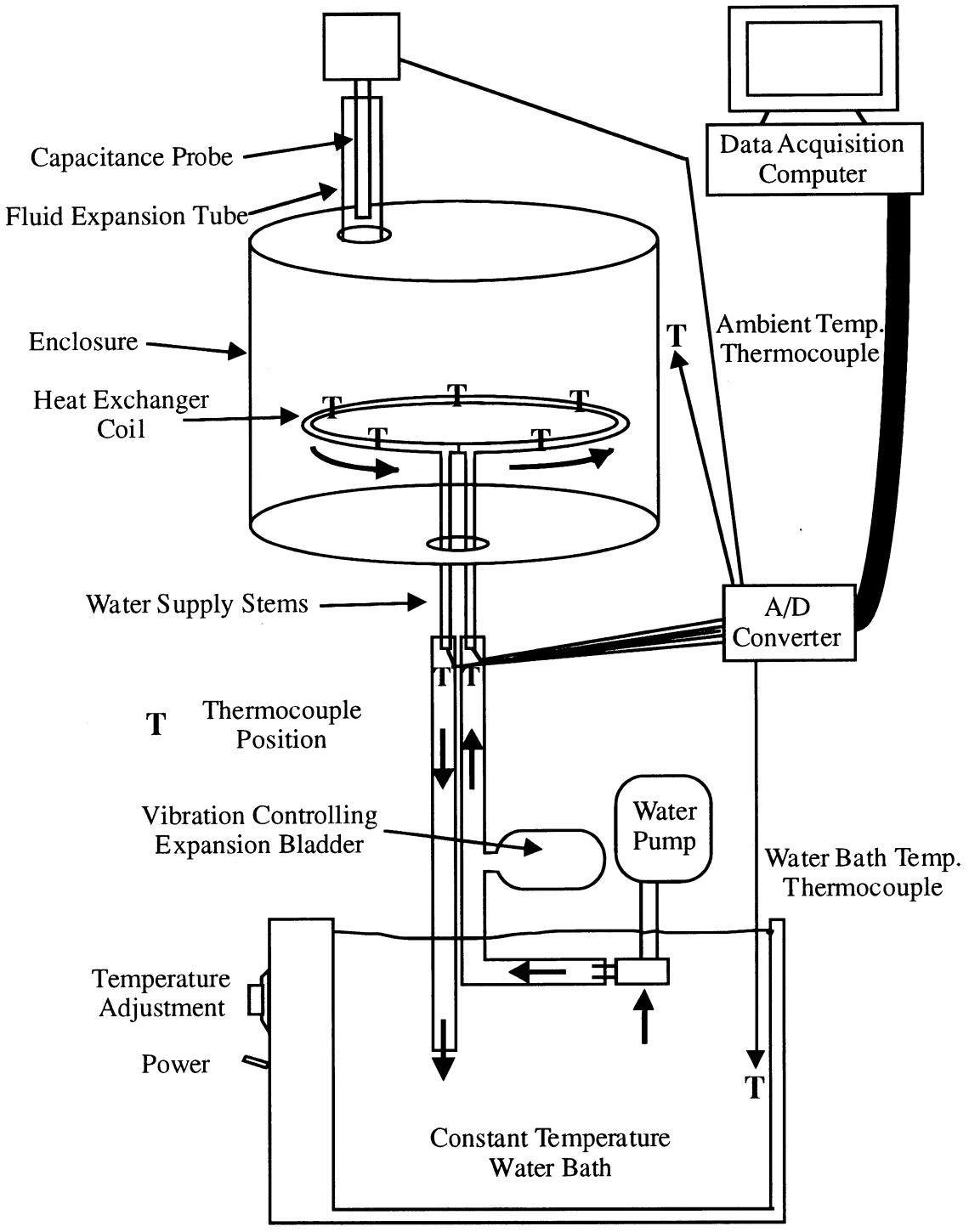

Figure 3.7 Experimental Data Acquisition Setup

(Capacitance probe) which runs vertically within the expansion tube and is connected to a

signal amplifier[4]. The output is fed into the A/D board. The capacitance probe is calibrated by adding fixed amounts (20 ml) of water to the fluid expansion tube and monitoring the response of the probe. Using this apparatus, Reindl (1992) found the response was non-linear unless a single copper ground was also inserted into the fluid expansion tube in parallel to the capacitance probe. In the course of the current experiment, it was found that the results were linear but not completely reproducible as shown in Figure 3.7.

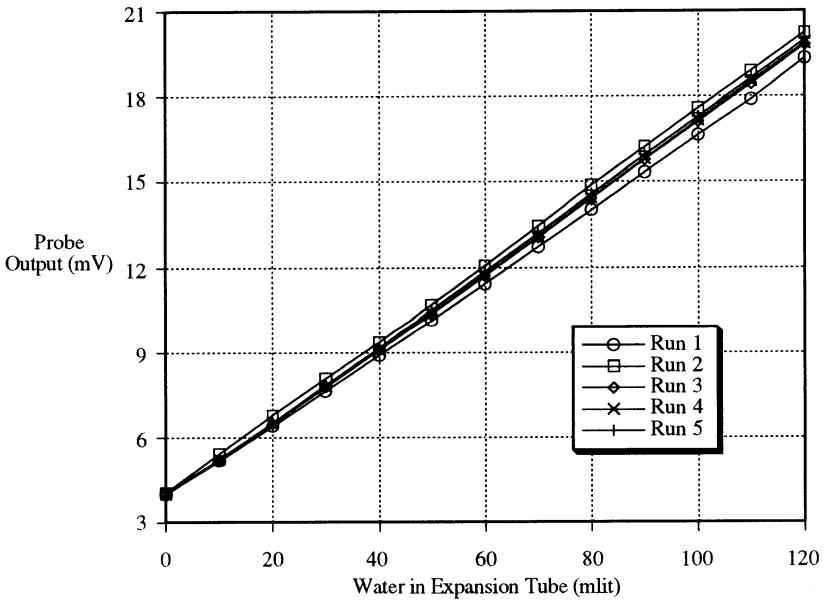

Figure 3.7 Early Capacitance Probe Calibration Results

The deviations between calibration runs were too great to allow for these experiments which depend on this calibration for the bulk temperature. Extensive research was conducted into the non-repeatable results. Because the equipment had been

---

4 Model 408-2200 two-wire transmitter from Drexelbrook Engineering; Horsham, PA

recently moved, it was assumed that the new environment was affecting the results through some sort of interference. After testing the equipment completely, the manufacturer was contacted. It was discovered that, because de-ionized water was being used for the experiment for purity reasons, the capacitance probe signal was not being saturated because of the lack of impurities in the water. The lack of saturation meant that the probe was susceptible to any slight variations in conductivity of the water within the tube. A susceptibility to property variations would have gone unnoticed if the water had been stored and reused as in Reindl's work rather than stored in separate containers as is the current practice. The manufacturer suggested an additional grounding wire. The addition of an additional ground was done with much improved results as shown in Figure 3.8.

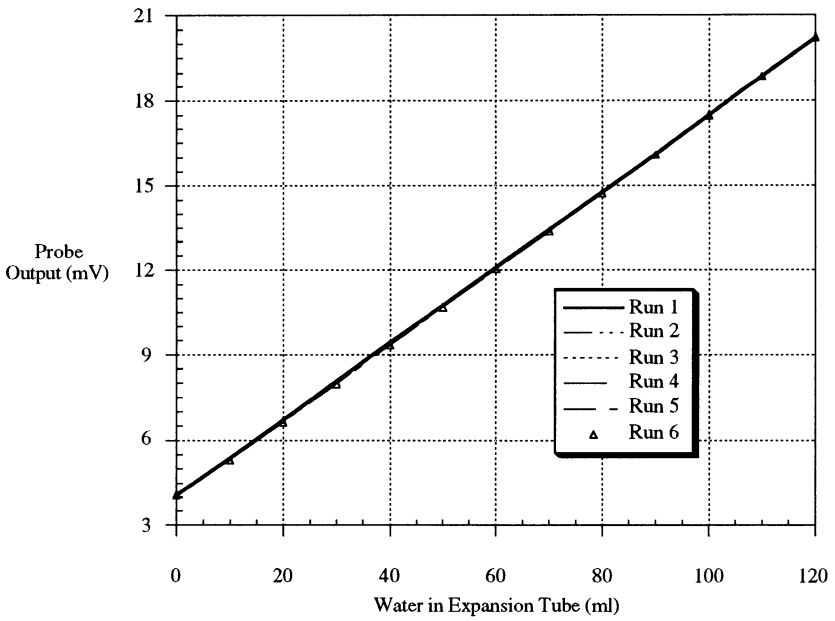

Figure 3.8 Improved Capacitance Calibration Results

In spite of an additional ground, as several changes of water within the enclosure

would be needed during the course of the experiment, the capacitance probe was calibrated before and after most runs. This constant calibration was especially important if some time had past, because of oxidation impurities introduced by the copper, or if new water had to be introduced into the enclosure.

Reindl (1992) also demonstrated that a linear relationship exists between the bulk fluid temperature and capacitance probe outlet. The straight line fitted data explains 99.2% of the actual bulk temperature results.

3.1.4 Assumptions

Several assumptions are made in the determination of these results. In the numerical study done by Reindl (1992), the Boussinesq approximation was used. The Boussinesq assumption assumes that all the fluid properties are constant during the experiment except for the density. As the experimental temperature difference is roughly 20 C, the Boussinesq approximation range (2 C) is exceeded so that the effect of varying fluid properties may be significant. The two properties that show the greatest temperature response are viscosity and the volume expansion coefficient. Reindl (1992) did several numerical runs with variable properties. He found that if the properties were evaluated as constants at a suitable temperature, the results approached the variable properties result. The properties are evaluated at a mean temperature which is the average of the initial fluid temperature and the coil wall temperature.

Radiation heat loss was neglected in the numerical study. Reindl (1992) proved that the experimental radiation heat transfer was negligible. The path lengths for the radiation in this range are so small (<< 1 mm) that the temperature differences are very small. Therefore, the net radiation heat transfer is negligible.

The enclosure in the numerical study was adiabatic while the experimental

enclosure is not adiabatic. It is assumed that conduction within the enclosure material (borosilicate glass and acrylic) is negligible and that it does not interfere with the thermal stratification in the fluid. As stated earlier, the enclosure is insulated with two layers of foil faced bubble type insulation which cuts down dramatically on the heat loss. Additionally, if the heat loss can be characterized, the Nusselt number values can be corrected for the transient heat loss from the tank.

Following the lead of Reindl, the heat loss is characterized by performing "cool down" experiments. The enclosure is heated as it would be during a normal experiment. However, after complete heating of the enclosure fluid, it is allowed to cool and the transient bulk temperature response and the ambient temperature are used to calculate an average heat loss coefficient. An energy balance on the enclosure during one of these cool down runs gives

$$\overline{h_L} A_o(\overline{T} - T_\infty) = (mc)_{tank}\frac{d\overline{T}}{dt} \qquad (3.1)$$

where

$\overline{h_L}$ is the surface average heat loss coefficient; dependent on bulk temperature

A_o is the external area of the insulated enclosure

$\overline{T}$ is the bulk temperature of the fluid within the enclosure

T_∞ is the ambient temperature of the air surrounding the insulation of the enclosure

$(mc)_{tank}$ is the mass capacitance of the enclosure and working fluid

t is the time.

The assumption is that the heat transfer coefficient, $\overline{h_L}$, is a function of the Rayleigh number and that the heat loss can be represented by the following correlation.

$$\overline{Nu_L} = C_o \overline{Ra}_H^n \qquad (3.2)$$

In this correlation, C_o is a correlating constant, and n is a correlating exponent. The

characteristic dimension for the Rayleigh number is H, the total insulated enclosure height. The characteristic temperature difference used in the Rayleigh number is $\overline{T} - T_\infty$. By solving Equations 3.1 and 3.2 simultaneously, the bulk temperature can be found to be

$$\overline{T} = T_\infty + \left[\frac{nC_0 k_{air} A_0}{H(mc)_{tank}}\left(\frac{g\beta H^3}{\nu\alpha}\right)^n_{air} t + \left(\overline{T}_0 - T_\infty\right)^{-n}\right]^{-1/n} \tag{3.3}$$

In this equation, $\overline{T}_0$ is the initial bulk fluid temperature. The properties are evaluated at the mean film temperature $((\overline{T}_0 + T_\infty)/2)$ and the subscript "air" denotes a property of the air surrounding the enclosure. The results of four cool down runs are averaged and coefficients of n=1/4 and $C_0 = 0.1210$ fit the data best and explain 94.1% of the variation in the experimental cool down results. Characterizing the heat loss as a function of the enclosure Rayleigh number, the enclosure heat loss can be estimated using Equation 3.4.

$$q_L = \frac{0.1210\overline{Ra}_H^{1/4} A_0 k_{air}}{H}\left(\overline{T} - T_\infty\right) \tag{3.4}$$

3.2 Experimental Procedure

Because of the complex timing required to run these experiments, an explanation of the standard experimental procedure must be included. Two slightly different procedures were used depending on the pump used.

The first step in conducting a run is to fully examine the apparatus for leaks. Between runs, small leaks may develop, especially around the compression fitting on the bottom of the enclosure. Secondly, the thermocouples should be checked for short circuits via the data acquisition computer. After checking the system, an initial capacitance

probe calibration is conducted by measuring the millivolt output of the data acquisition equipment for each incremental (20 ml) addition of water to the fluid expansion tube. The water used for the calibration should be the water that will expand into the tube during the experiment. This initial calibration and the final calibration after the run are necessary due to the probe sensitivity to water impurities, as discussed earlier. Following this calibration, the enclosure is sealed and the fluid tube is filled to a point well within the capacitance probes calibrated range.

With the 1/12 hp pump, at this point, the constant temperature water bath was turned on to preheat the water that would be pumped through the coil heat exchanger. This preheating would last approximately 3/4 hours. Also, at this time, the insulation was placed around the enclosure to reduce any thermal stratification within the enclosure due to ambient conditions. The insulation was left on at least one hour prior to initiating heating.

With the 1/2 hp pump, the preheating included both turning on the constant temperature bath and the pump. If it is not preheated, the thermal mass of the pump will initially absorb a great deal of energy from the water and the desired constant coil wall temperature will not be attained. Also, after warming up, the pump adds a great deal of energy to the water. If the water system is insulated, the pump can raise the water temperature at least 10 C above the setpoint. With the insulation removed, there is about a 3 C rise in temperature above the setpoint. It can take as long as three hours for the water supply temperature to stabilize.

With the physical apparatus prepared, the data acquisition equipment is prepared. The file name and the data taking time increment is determined. At this point, the run is started. After two preliminary readings to establish an average of the initial conditions, the heated water supply pump is turned on. With the 1/12 hp pump, this involved merely plugging in the pump. With the 1/2 hp pump, this involved opening the coil bypass valve. Both of these procedures, although not instantaneous, started the flow of water

through the coil within a second of the desired time.

At the desired ending point, the data acquisition was halted. The pump and constant temperature bath were shut off while the enclosure insulation was removed to allow the fluid to return to ambient conditions for the next run. Last, another capacitance probe calibration was done unless an identical run was to be conducted the next day. The enclosure was allowed to cool overnight which allowed more than enough time for it to return to ambient conditions.

3.3 Determining Bulk Temperature, Nusselt Number, and Effectiveness

Three main quantities have been selected to report these data. These quantities are the bulk temperature of the fluid, the Nusselt number, and the effectiveness as a function of the temperature difference between the bulk temperature and the ambient temperature.

The bulk temperature is found, as discussed above, based on the amount of water that expands into the fluid expansion tube above the coil. This method allows a better average bulk temperature than a single or even several thermocouples would allow. Additionally, there are no thermocouples within the enclosure which could possibly interfere with the fluid flow development. This method requires a linear relationship between the temperature and specific volume for the working fluid. To see why this is true, consider two fluid filled tanks. One is a fully mixed tank with a temperature increase of 20 degrees while the other is a stratified tank in which half the water has increased 10 degrees while the other half has risen 30 degrees. The average bulk temperature of both of these tanks is identical (the initial temperature plus 20 degrees). However, if the temperature to specific volume relationship is not linear the amount of fluid that had expanded into the fluid expansion tube would not be the same for both cases. To that

end, Figure 3.9 illustrates the temperature-specific volume relationship for water.

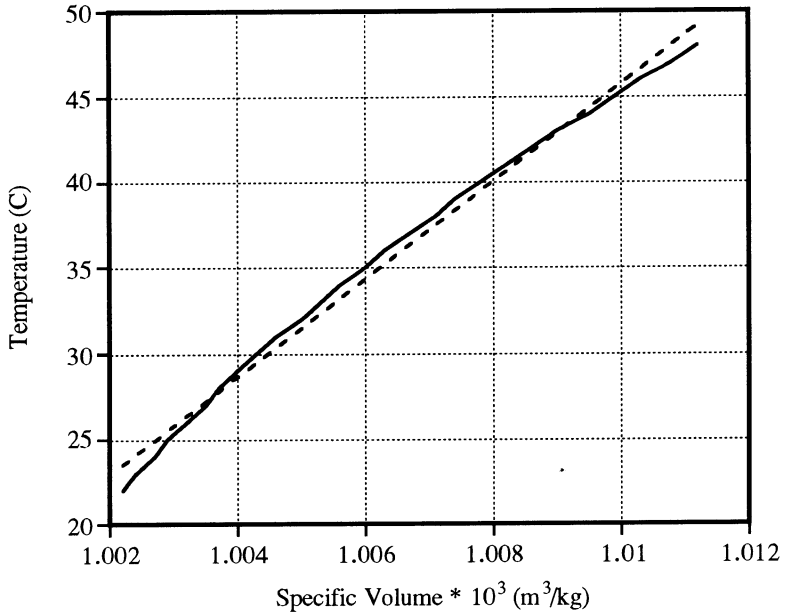

Figure 3.9 Temperature - Specific Volume Relationship for Water

From 20 C to 45 C, the temperature range covered by this study, the temperature-specific volume relationship is relatively linear with the above linear curve fit explaining 99.7% of the variation.

Additionally, the thermal and mass losses from the fluid within the expansion tube are considered to be negligible. This assumption is viable as only 1.5% of the total volume of the tank is held within the expansion tube. Additionally, the free surface within the expansion tube is small (~ 2 cm^2) which justifies a negligible evaporation rate.

Although it is diminished by the use of the Duran glass for the enclosure cylinder, the thermal expansion of the tank needs to be accounted for in the bulk temperature calculation. A first order estimate is added that assumes linear expansion in both the circumferential and vertical directions. The change in capacitance probe output due to the

expansion is given by Equation 3.5. This equation comes from Reindl (1992).

$$\Delta ma)_{corr} = \frac{\pi D_o H_o \alpha_{exp} \Delta\overline{T}}{31.435}\left[3\left(1+\alpha_{exp}\Delta\overline{T}\right) + \alpha_{exp}^2 \Delta\overline{T}^2\right] \qquad (3.5)$$

where

D_o is the enclosure diameter

H_o is the enclosure height

α_{exp} is the linear expansion coefficient for Duran

and $\Delta\overline{T} = (\overline{T}\,(t) - \overline{T}\,(o))$.

This correction factor is added to the output of the capacitance probe to give a true bulk temperature reading.

Once the bulk temperature is determined, the heat transfer, represented by the Nusselt number, can be characterized. A simplified energy balance upon the enclosure results in the following

$$Q_{in} - Q_{out} = \frac{dU}{dt} \qquad (3.6)$$

Q_{in} is the quantity of interest and can be represented by the following equation

$$Q_{in} = \frac{k_w \overline{Nu}}{D} A_{coil}(T_{wall} - \overline{T}) \qquad (3.7)$$

Q_{out} is the losses from the enclosure as characterized by the cool down runs. The overall heat loss coefficient calculated by the cool down runs, as a function of bulk temperature, can be used to express the overall heat loss as follows.

$$Q_{out} = \overline{h}_L A_o(\overline{T} - T_{ambient}) \qquad (3.8)$$

The term $\frac{dU}{dt}$ represents the increase in internal energy of the fluid within the enclosure and can be found by using the change in the bulk temperature of the fluid within the enclosure.

$$\frac{dU}{dt} = (mc)_{tank}\frac{d\overline{T}}{dt} \tag{3.9}$$

When equations 3.7 to 3.9 are combined in equation 3.6 and solved for the convective Nusselt number, the result is

$$\overline{Nu} = \frac{(mc)_{tank}\frac{d\overline{T}}{dt} + \overline{h}_L A_o(\overline{T} - T_{ambient})}{2\pi^2 R_c k_w(T_{wall} - \overline{T_o})} \tag{3.10}$$

Equation 3.10 is used to determine the transient heat transfer response for the experimental results.

$\frac{d\overline{T}}{dt}$ is found by examining the overall behavior in $\overline{T}$. The simplest method for calculating the value of $\frac{d\overline{T}}{dt}$ is to subtract the bulk temperature of the data point preceding the data point of interest from the bulk temperature of the data point following the data point of interest. However, this method is quite noisy. The experimental data for the bulk temperature is fit to a five factor polynomial. $\frac{d\overline{T}}{dt}$ is found by taking the derivative of this polynomial.

$$\overline{T} = m_o + m_1 t + m_2 t^2 + m_3 t^3 + m_4 t^4 + m_5 t^5 \tag{3.11}$$

is the polynomial that represents the bulk temperature. An example of this curve fit is shown in Figure 3.10.

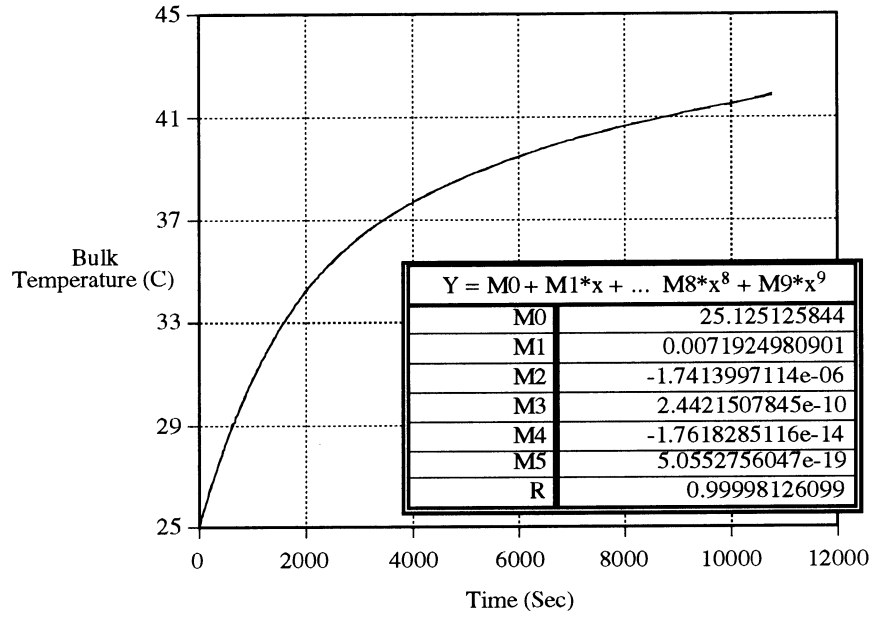

Figure 3.10 Typical Bulk Temperature Curve Fit

The resulting slope of this line, $\frac{d\overline{T}}{dt}$, is then

$$\frac{d\overline{T}}{dt} = m_1 + 2m_2t + 3m_3t^2 + 4m_4t^3 + 5m_5t^4 \qquad (3.12)$$

The curve fit of the bulk temperature, in all runs, accounts for at least 99% of the variation. Figure 3.11 illustrates the difference between calculating $\frac{d\overline{T}}{dt}$ using two data points and the new polynomial method. This illustrates that the fit is accurate and removes the noise from the data.

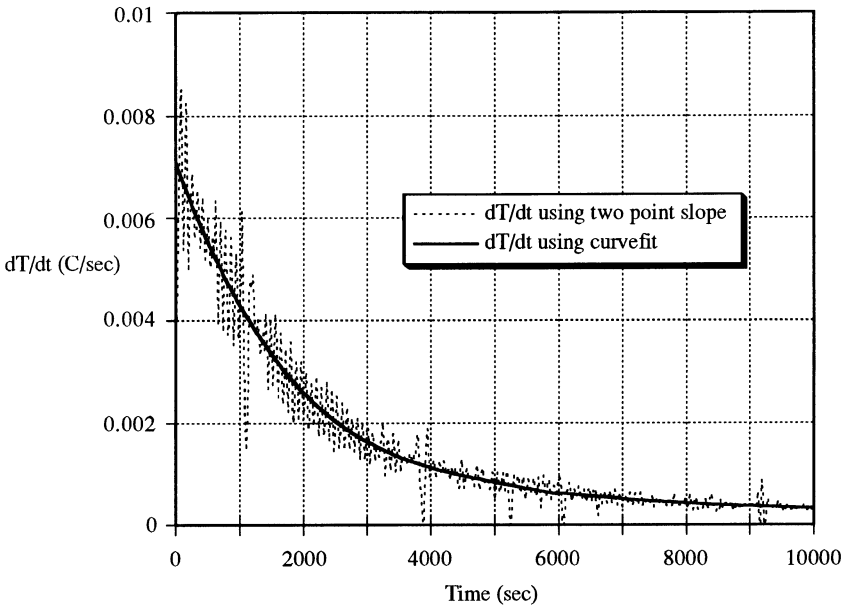

Figure 3.11 Calculation of dT/dt for use in the Nusselt Number Calculation

It is desirable to be able to characterize the performance of the coil heat exchanger. If the effectiveness of the coil can be determined as a function of the difference in temperature between the coil wall and the bulk fluid temperature and as a function of the fluid flow rate, then the heat transfer can be determined from the following equation.

$$q = \varepsilon q_{max} \tag{3.13}$$

where

$$q_{max} = \dot{m} C_p (T_{wall} - \overline{T}) \tag{3.14}$$

The effectiveness method of Farrington (1986) has been adapted in an attempt to characterize the heat exchanger performance.

$$\varepsilon = \frac{\text{actual heat transfer}}{\text{theoretical maximum heat transfer}} = \frac{\overline{h_o} A_{coil}(LMTD)}{(\dot{m}C_p)_{HX}(T_{wall} - \overline{T})} \tag{3.13}$$

where Farrington defines the log mean temperature difference to be

$$LMTD = \frac{T_{HX,in} - T_{HX,out}}{\ln\left[\frac{T_{HX,in} - \overline{T}}{T_{HX,out} - \overline{T}}\right]} \tag{3.14}$$

The log mean temperature difference has been altered to fit experimental constraints. The temperature difference across the heat exchanger, $\Delta T_{in\text{-}out}$, is determined from the two thermocouples placed in the flow stream directly below the supply stems as shown in Figure 3.7. These two thermocouples were calibrated by placing them next to the coil in the ice bath. The calibration was done (lying next to the coil in the ice bath) before being placed in the flow stream. In moving the thermocouples to the bottom of the supply stems, the calibration may be slightly less accurate. Therefore, the difference between these temperatures, $\Delta T_{in\text{-}out}$,is more accurate than the absolute value. In order to approximate the inlet temperature ($T_{HX,in}$), half the temperature difference across the stems is added to the average coil wall temperature. For the outlet temperature, half the temperature difference is subtracted from the average coil wall temperature. Placing these approximations into Equation 3.14, the log mean temperature difference used in Equation 3.13 is

$$LMTD = \frac{\Delta T_{in\text{-}out}}{\ln\left[\frac{\left(T_{wall} + \frac{\Delta T_{in\text{-}out}}{2}\right) - \overline{T}}{\left(T_{wall} - \frac{\Delta T_{in\text{-}out}}{2}\right) - \overline{T}}\right]} \tag{3.15}$$

Also, the use of the Farrington effectiveness equation requires the use of a Nusselt

number based on the instantaneous bulk temperature rather than the initial bulk temperature (as in equation 3.10). The expression for this Nusselt number formulation is given by Equation 3.16. The only change is replace the initial bulk temperature, T_o, by the instantaneous bulk temperature, $\overline{T}$, in the denominator. This minor change makes this Nusselt formulation consistent with the above effectiveness formulation.

$$\overline{Nu_\varepsilon} = \frac{(mc)_{tank}\frac{d\overline{T}}{dt} + \overline{h}_L A_o(\overline{T} - T_{ambient})}{2\pi^2 R_c k_w (T_{wall} - \overline{T})} \tag{3.16}$$

3.4 Typical Run Output

All the results of this experiment are derived from the experimental outputs of the coil wall thermocouples and the capacitance probe. Figure 3.12 shows the coil wall thermocouple outputs for a typical run using the 1/12 hp pump.

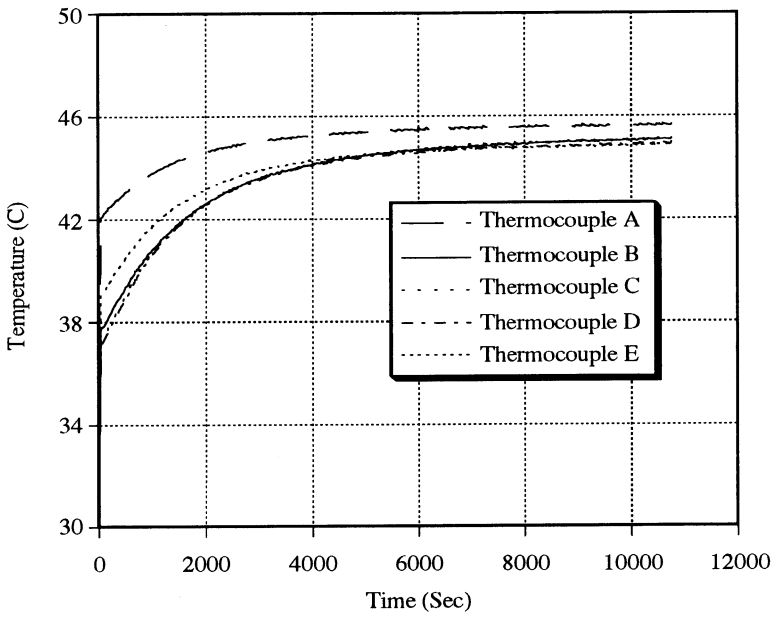

Figure 3.12 Typical Coil Wall Thermocouple Response

The average of these coil wall thermocouples is used as the Twall value. This value is combined with the bulk temperature and the bath temperature in Figure 3.13.

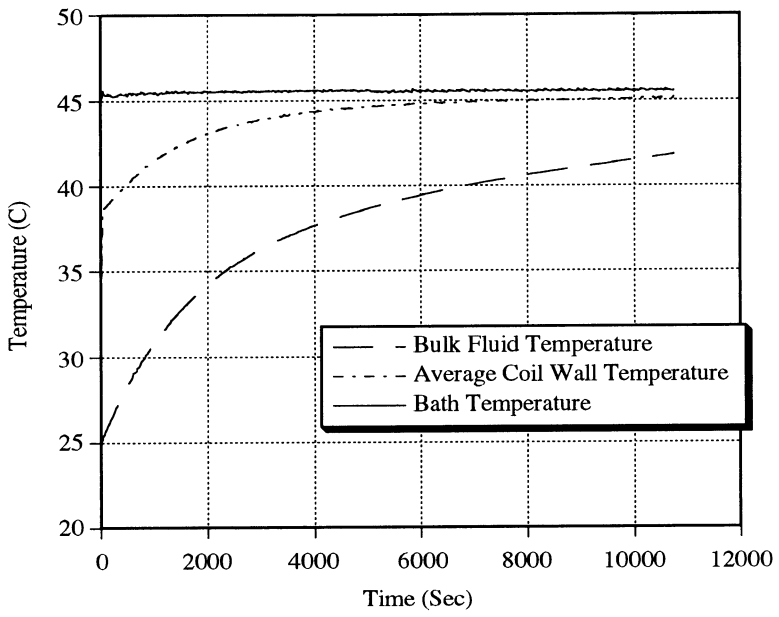

Figure 3.13 Typical Experimental Thermal Response

Using these temperatures, thermodynamic properties, and geometric properties, the transient Nusselt response can be calculated. Figure 3.14 shows the typical Nusselt response for both the standard Nusselt number formulation and for the effectiveness Nusselt number formulation. The particular run had a data taking interval of 20 seconds so that no early transient data is available.

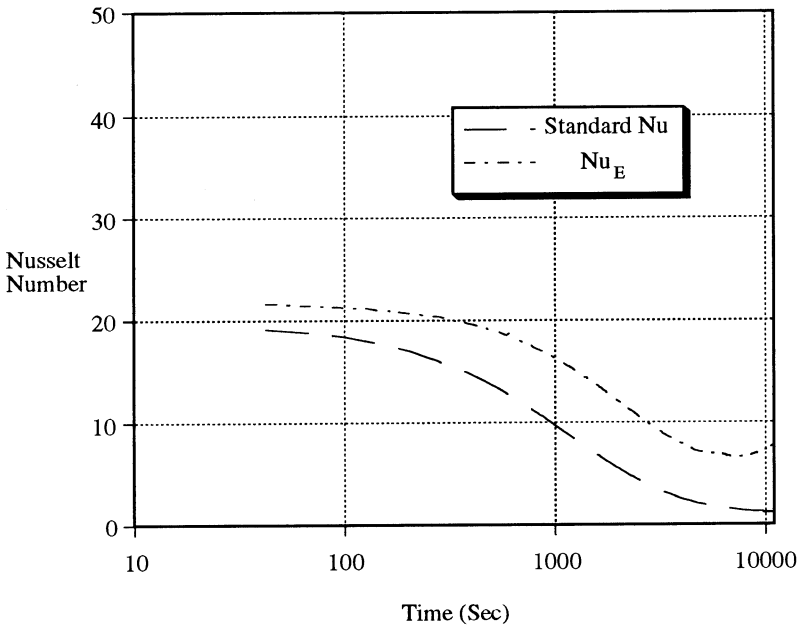

Figure 3.14 Typical Nusselt Response

Finally, the effectiveness can be calculated using Nu_ε and Equation 3.13. The effectiveness for this typical run is shown in Figure 3.15.

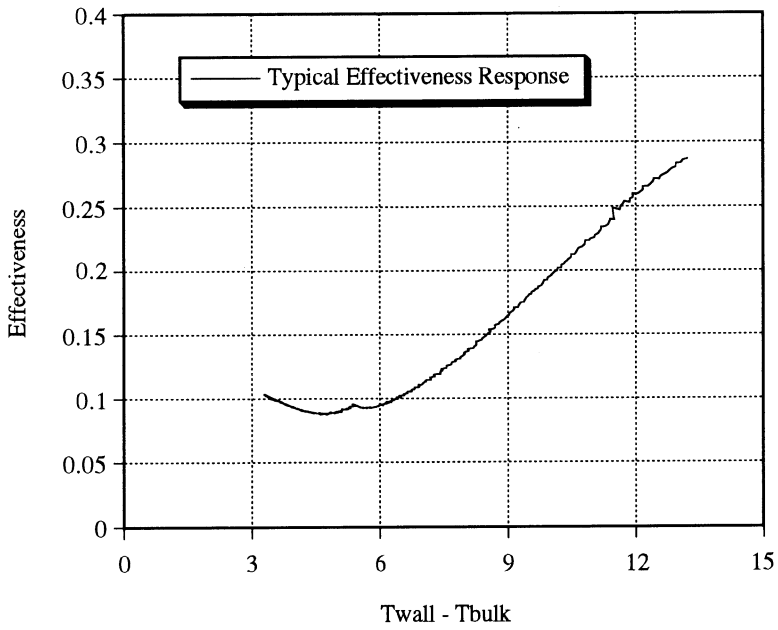

Figure 3.15 Typical Effectiveness Response

3.5 Uncertainty Analysis

The uncertainty related to an experimental result is crucial. It determines the merit of the results. The errors of constants and specific values were determined from manufacturer supplied data and from calibration results. The propagation of errors within this experiment was calculated using the root sum of squares method according to Kline and McClintock (1953). For an example of this method consider the following equation in which the the variables (X, Z) are independent of the coefficients (a, b) except that b and Z are determined using the same instrument so that they are correlated.

$$Y = aX + bZ \tag{3.17}$$

The error in Y can be written in terms of the errors in all the other variables and constants. The final term is necessary because b and Z are correlated by the fact that they are correlated.

$$(\delta Y)^2 = \left(\frac{\partial Y}{\partial a}\delta a\right)^2 + \left(\frac{\partial Y}{\partial X}\delta X\right)^2 + \left(\frac{\partial Y}{\partial b}\delta b\right)^2 + \left(\frac{\partial Y}{\partial Z}\delta Z\right)^2 + 2\left(\frac{\partial Y}{\partial Z}\right)\left(\frac{\partial Y}{\partial b}\right)\rho_{b,Z}\delta b\delta Z \qquad (3.18)$$

For this example, the final expression for the error in Y is given by the following equation.

$$(\delta Y)^2 = (X\delta a)^2 + (a\delta X)^2 + (Z\delta b)^2 + (b\delta Z)^2 + 2Zb\rho_{b,Z}\delta b\delta Z \qquad (3.19)$$

Values of constants and variables with constant error are listed in Table 3.1.

Property or Variable	Standard Value and Est. Error
A_o [m^2]	0.6911 +/- 0.007
T_o [C]	23.5 +/- 0.2
h_L	+/- 0.0082
time [sec]	+/- 0.5
D [m]	0.0127 +/- 0.00005
$(mc)_{tank}$ [J/C]	37987 +/- 1900
C_p [J/kg K]	4178 +/- 0.5
R_c [m]	0.0794 +/- 0.0005
$\dot{m}$ [GPM]	0.48 +/- 0.01
g	9.81 +/- 0.005
β[1/K]	361.9E-6 +/- 0.05E-6
k_w [W/m K]	0.628 +/- 0.0005
α [m^2/s]	1.514e-7 +/- 0.0005e-7
ν [m^2/s]	6.998e-7 +/- 0.0005e-7
Twall [C]	+/- 0.2
ΔT_{in-out} [C]	+/- 0.71

Table 3.1 Estimated Errors Table

The thermocouples are given an error by the manufacturer of +/- 0.5 C. The errors associated with the coil wall temperature (Twall) and the initial temperature (To) are both given as +/- 0.2 C. This is because the average of five thermocouples is used for these values. This results in the associated, smaller error.

The error analysis for the Nusselt number value begins by creating the expression

for the root sum of squares error. This is given by

$$\delta\overline{Nu}^2 = \left(\frac{\partial\overline{Nu}}{\partial\overline{h_L}}\delta h_L\right)^2 + \left(\frac{\partial\overline{Nu}}{\partial A_o}\delta A_o\right)^2 + \left(\frac{\partial\overline{Nu}}{\partial\overline{T}}\delta\overline{T}\right)^2$$
$$+\left(\frac{\partial\overline{Nu}}{\partial T_o}\delta T_o\right)^2 + \left(\frac{\partial\overline{Nu}}{\partial(mc)_{tank}}\delta(mc)_{tank}\right)^2 + \left(\frac{\partial\overline{Nu}}{\partial\frac{\partial\overline{T}}{\partial t}}\delta\frac{\partial\overline{T}}{\partial t}\right)^2 + \left(\frac{\partial\overline{Nu}}{\partial R_c}\delta R_c\right)^2$$
$$+\left(\frac{\partial\overline{Nu}}{\delta k_w}\delta k_w\right)^2 + \left(\frac{\partial\overline{Nu}}{\partial T_{wall}}\delta T_{wall}\right)^2 + 2\left(\frac{\partial\overline{Nu}}{\partial T_o}\right)\left(\frac{\partial\overline{Nu}}{\partial T_{wall}}\right)\rho_{T_o,T_{wall}}\delta T_o\delta T_{wall} \qquad (3.23)$$

After developing the partial derivatives and simplifying, the final root sum of squares expression for the error of the Nusselt number is

$$\delta\overline{Nu}^2 = \frac{1}{C_1^2}\left\{\begin{array}{c}\left(A_o(\overline{T}-T_o)\,\delta\overline{h_L}\right)^2 + \left(\overline{h_L}(\overline{T}-T_o)\delta A_o\right)^2 + \left(h_L A_o\delta\overline{T}\right)^2 \\ +\left(\left(h_L A_o(\overline{T}+T_{wall}-2T_o) - (mc)_{tank}\frac{d\overline{T}}{dt}\right)\frac{\delta T_o}{(T_{wall}-T_o)}\right)^2 + \left(\frac{d\overline{T}}{dt}\delta(mc)_{tank}\right)^2 \\ +\left((mc)_{tank}\delta\frac{d\overline{T}}{dt}\right)^2 + \left(C_2\frac{\delta R_c}{R_c}\right)^2 + \left(-C_2\frac{\delta k_w}{k_w}\right)^2 + \left(-C_2\frac{\delta T_{wall}}{(T_{wall}-T_o)}\right)^2 \\ +2C_2\left(h_L A_o(\overline{T}+T_{wall}-2T_o) - (mc)_{tank}\frac{d\overline{T}}{dt}\right)\frac{\delta T_o\delta T_{wall}}{(T_{wall}-T_o)^2}\end{array}\right\} \qquad (3.24)$$

where $C_1 = 2\pi^2 R_c k_w (T_{wall}-T_o)$ which is the denominator of the Nusselt expression (Equation 3.10) and $C_2 = \overline{h_L}A_o(\overline{T}-T_o) + (mc)_{tank}\frac{d\overline{T}}{dt}$ which is the numerator for the Nusselt expression. The typical results for the uncertainty analysis are illustrated in Figure 3.16. The Nusselt number has a typical error of +/- 1.0 during the quasi-steady period. This is an error of +/- 5 % during the quasi-steady period. The error during the conduction regime is significantly greater than 5 % while the error during the decay regime is considerably less than 5 %.

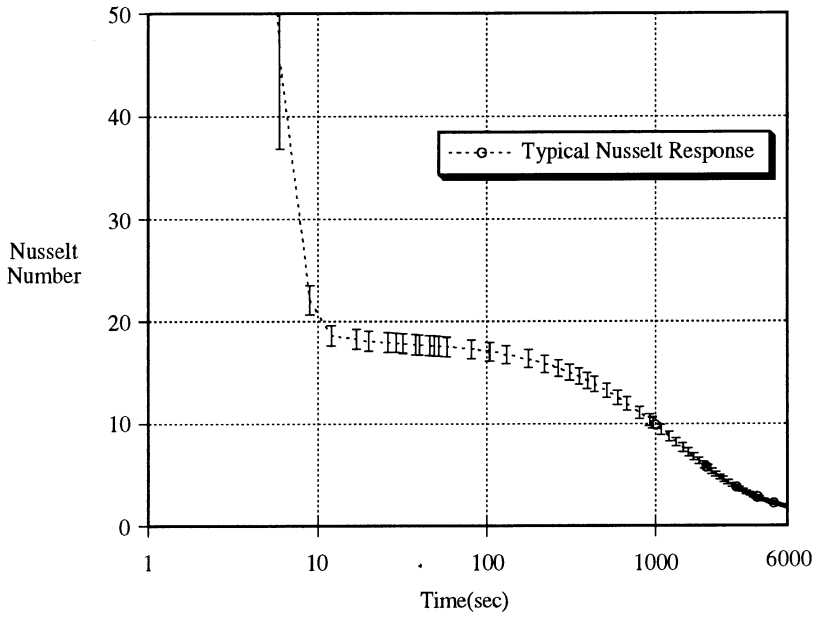

Figure 3.16 Typical Transient Nusselt Number Error

Additionally, the effectiveness error equation requires the error from $\overline{Nu}_\varepsilon$ as given in Equation 3.14. Following the same method used for the standard Nusselt formulation, the resulting root sum of squares equation is as follows.

$$\delta\overline{Nu}_\varepsilon{}^2 = \frac{1}{C_3^2}\left\{\begin{array}{c}\left(A_o(\overline{T}-T_o)\,\delta\overline{h_L}\right)^2 + \left(\overline{h_L}(\overline{T}-T_o)\delta A_o\right)^2 + \left(\left(h_L A_o + \left(\frac{C_2}{(T_{wall}-\overline{T})}\right)\right)\delta\overline{T}\right)^2 \\ + \left(-\overline{h_L}A_o\delta T_{amb}\right)^2 + \left(\frac{d\overline{T}}{dt}\delta(mc)_{tank}\right)^2 \\ + \left((mc)_{tank}\delta\frac{d\overline{T}}{dt}\right)^2 + \left(C_2\frac{\delta R_c}{R_c}\right)^2 + \left(-C_2\frac{\delta k_w}{k_w}\right)^2 + \left(-C_2\frac{\delta T_{wall}}{(T_{wall}-\overline{T})}\right)^2 \\ + 2\left(\overline{h_L}A_o\right)C_2\frac{\delta T_{amb}\delta T_{wall}}{(T_{wall}-\overline{T})^2}\end{array}\right\} \qquad (3.25)$$

The error for $\overline{Nu}_\varepsilon$ is represented in Figure 3.17. The error response is similar to the

standard Nusselt number formulation except during the decay region. During this region, the error is considerably larger because the $\overline{Nu}_\varepsilon$ value is larger than the standard Nu value.

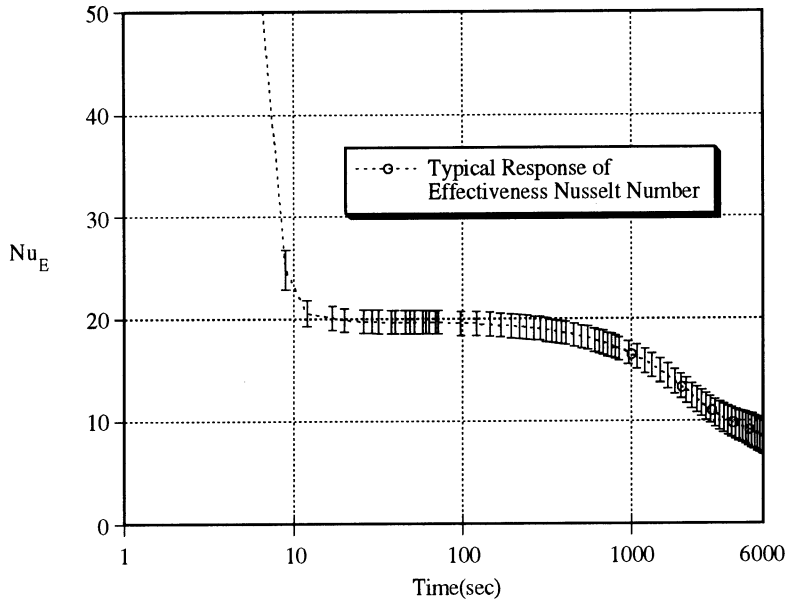

Figure 3.17 Typical Transient $\overline{Nu}_\varepsilon$ Error

The error for the effectiveness is found in a similar manner. The root sum of squares error expression is

$$\delta\varepsilon^2 = \left(\frac{\partial\varepsilon}{\partial k_w}\delta k_w\right)^2 + \left(\frac{\partial\varepsilon}{\partial\overline{Nu}}\delta\overline{Nu}\right)^2 + \left(\frac{\partial\varepsilon}{\partial D}\delta D\right)^2 + \left(\frac{\partial\varepsilon}{\partial LMTD}\delta LMTD\right)^2 + \left(\frac{\partial\varepsilon}{\partial\dot{m}}\delta\dot{m}\right)^2 + \left(\frac{\partial\varepsilon}{\partial A_c}\delta A_c\right)^2 + \left(\frac{\partial\varepsilon}{\partial T_{wall}}\delta T_{wall}\right)^2 + \left(\frac{\partial\varepsilon}{\partial\overline{T}}\delta\overline{T}\right)^2 \quad (3.26)$$

As before, the proper derivatives are taken and the expression is simplified to the following form.

$$\left(\frac{\delta\varepsilon}{\varepsilon}\right)^2 = \left(\frac{\delta h_o}{h_o}\right)^2 + \left(\frac{\delta A_c}{A_c}\right)^2 + \left(\frac{\delta LMTD}{LMTD}\right)^2 + \left(\frac{\delta \dot{m}}{\dot{m}}\right)^2 + \left(\frac{\delta T_{wall}}{(T_{wall}-\overline{T})}\right)^2 + \left(\frac{\delta \overline{T}}{(T_{wall}-\overline{T})}\right)^2 + \left(\frac{\delta \overline{Nu_\varepsilon}}{\overline{Nu_\varepsilon}}\right)^2 + \left(\frac{\delta D}{D}\right)^2 \quad (3.27)$$

Typical results for the error of the effectiveness are displayed in Figure 3.18. Obviously, the error at low (T_{wall} - T_{bulk}) values is very large. The percentage error at large (T_{wall} - T_{bulk}) values is still large at about 8%. This large error is caused by how far removed this result is from the data and also its sensitivity to temperature measurement error.

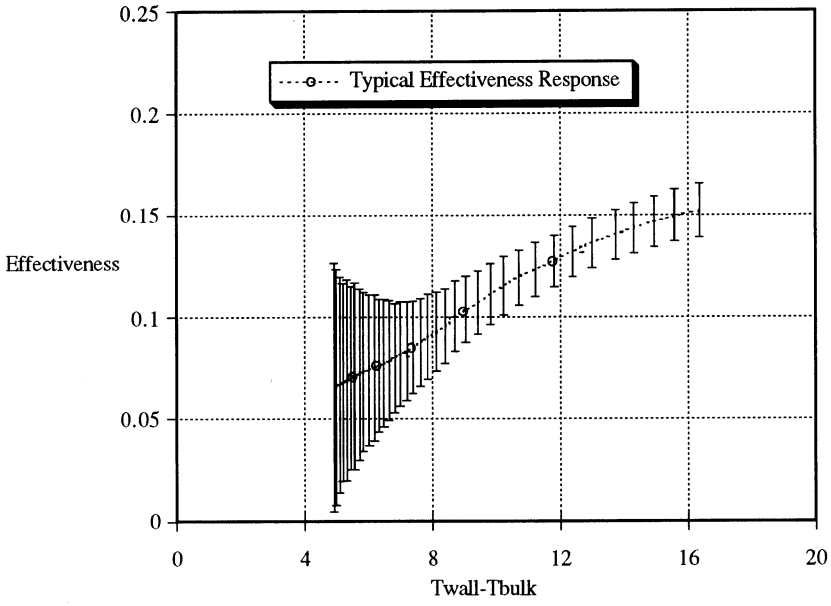

Figure 3.18 Typical Transient Effectiveness Error

The error equations for the Nusselt number and effectiveness require the derivation of several additional error equations including $\overline{h_L}$, $\overline{T}$, and $\frac{d\overline{T}}{dt}$. The uncertainty in the bulk temperature is found by analyzing the bulk temperature response as a function

of the change in capacitance probe output.

$$\overline{T} = a + b(\Delta ma) \tag{3.17}$$

The resulting error expression is

$$\delta\overline{T}^2 = (\delta a)^2 + \{(\Delta ma)\delta b\}^2 + \{b\delta(\Delta ma)\}^2 \tag{3.18}$$

where δa and δb are the errors associated with the coefficients from the linear regression formula. Because the regression accounts for over 99% of the variance in the data, an error of 1% is assigned to a and b. Typical results for the bulk temperature error are shown in Figure 3.19.

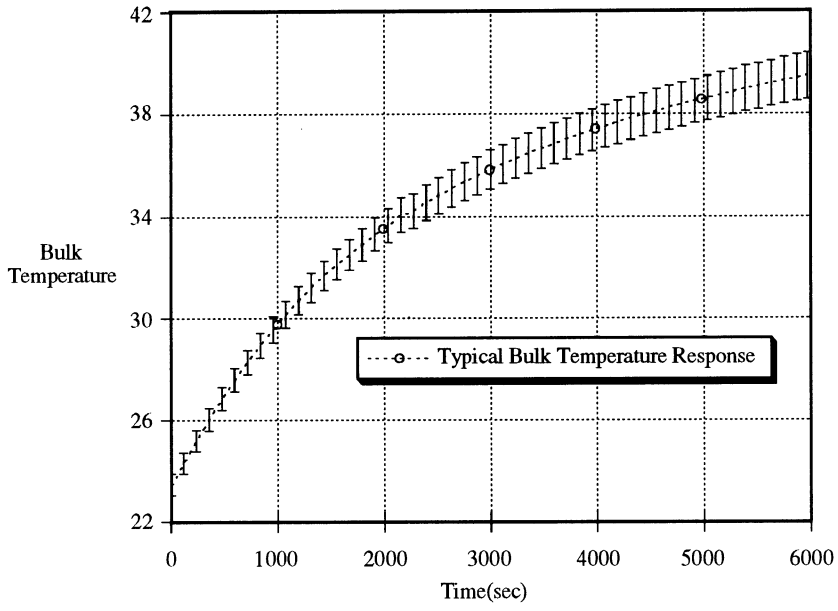

Figure 3.11 Typical Transient Bulk Temperature Error

The heat loss has been characterized by the cooldown runs as previously discussed. Again, the heat loss equation is

$$\overline{Nu_L} = C_o \overline{Ra_H}^n \tag{3.19}$$

where n = 1/4 and $C_O = 0.1210$. Rearranging this equation to single out the heat loss

coefficient gives

$$\bar{h}_L=\frac{C_o\, g^n\, \beta_{air}^n\, H^{3n-1}\,(\bar{T}-T_{amb})^n\, k_{air}}{H\, \nu_{air}^n\, \alpha_{air}^n} \tag{3.20}$$

The subscript air means that the properties are evaluated at a mean temperature of $T_{mean}=(T_{wall}-T_o)/2$, H is the insulated enclosure height, and T_{amb} is the ambient temperature.

The resulting error equation for $\bar{h}_L$ is

$$(\delta\bar{h}_L)^2 = n^2\left\{\left(\frac{\delta g}{g}\right)^2+\left(\frac{\delta\beta}{\beta}\right)^2+\left(\left(3-\frac{1}{n}\right)\frac{\delta H}{H}\right)^2+\left(\frac{\delta T_{amb}}{\Delta\bar{T}}\right)^2+\left(\frac{\delta\alpha}{\alpha}\right)^2+\left(\frac{\delta\nu}{\nu}\right)^2\right\} \tag{3.21}$$

From this equation, it is obvious that $\bar{h}_L$ is dependent on the bulk temperature. Therefore, the error in $\bar{h}_L$ was found for a large $\Delta\bar{T}$ and a small $\Delta\bar{T}$. The smaller error was approximately half the larger value. The larger value was used as a constant.

The uncertainty in $\frac{d\bar{T}}{dt}$ depends on two quantities. First, it depends on the error in the $\bar{T}$ values that were used for the curve fit. On top of this error is the error in the curve fit of $\bar{T}$. The percentage error in $\bar{T}$ has already been calculated. The polynomial curve fit in all runs accounts for at least 99% of the variation in the bulk temperature. The root sum of squares equation for the error in $\frac{d\bar{T}}{dt}$ is as follows:

$$\left(\delta\frac{\partial\bar{T}}{\partial t}\Big/\frac{\partial\bar{T}}{\partial t}\right)^2=\left(\frac{\delta\bar{T}}{\bar{T}}\right)^2+\left(\frac{\delta\text{curvefit}}{\text{curvefit}}\right)^2 \tag{3.22}$$

Figure 3.20 illustrates a typical result for the error in $\frac{d\bar{T}}{dt}$.

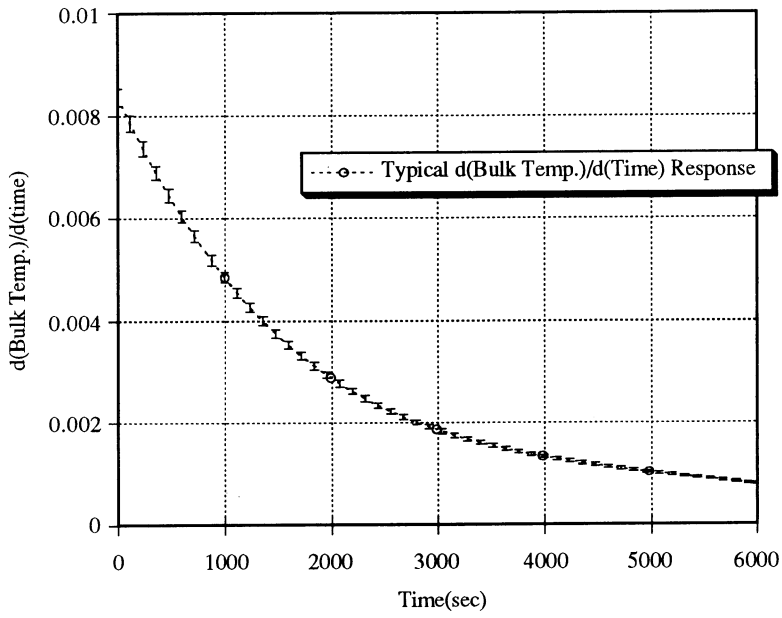

Figure 3.20 Typical Transient $\frac{d\overline{T}}{dt}$ Error

Table 3.2 summarizes typical results of the errors calculated by equations in this section.

$\frac{d\overline{T}}{dt}$	2 %
$\overline{h}_L$	1.5 %
$\overline{T}$	2 %
$\overline{Nu}$	5 %
$\overline{Nu_\varepsilon}$	6 %
ε	10 % to 110 %

Table 3.2 Table of Typical Error Results

CHAPTER
FOUR

EXPERIMENTAL RESULTS OF A COILED TUBE WITHIN A CYLINDER

Approximately 50 runs were conducted with the current experimental apparatus as discussed in Chapter 3. Many of these runs were useless because of problems with leaking, calibration, or procedural errors. The remaining data can be divided into two main groups based on the pump used. The data from the original 1/12 hp pump are useful for validating the previous numerical results of Reindl. This is due to a large number of replications that minimize the accompanying error. The new pump has been used to take data which examine the effect of coil height within the tank.

4.1 Results of a Typical Run

First, the output of a single run will be examined. Two basic pieces of actual data come from the apparatus. One of these is the output of the capacitance probe. The second is the output of the thermocouples within the tank. Figure 4.1 illustrates the response of the coil thermocouples. From Figure 3.6, Thermocouple A is closest to the inlet and

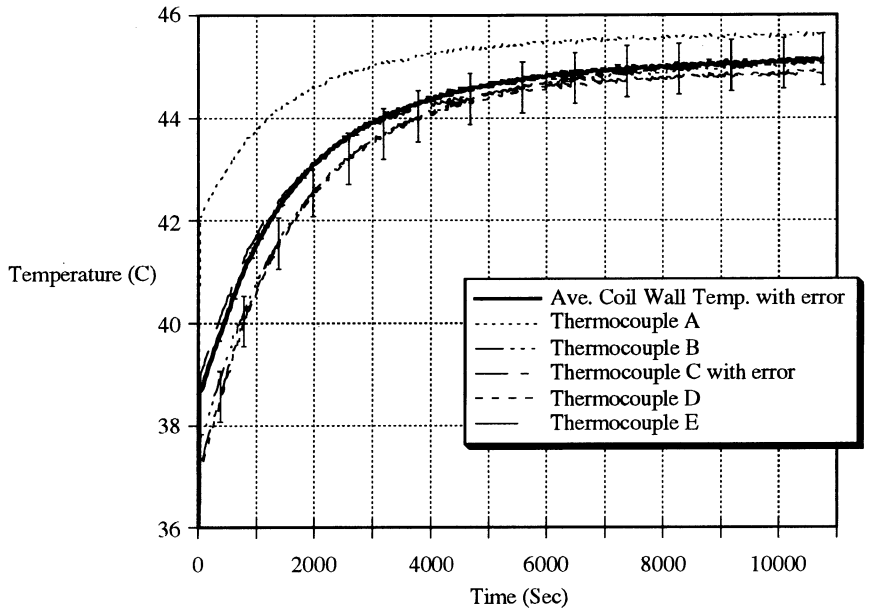

Figure 4.1 Typical Coil Wall Thermocouple Output

appropriately has the highest temperature response. After approximately 2500 seconds, all of the coil temperature readings fall within the error bars of a single thermocouple output. Thermocouple A is located closest to the entrance of the coil and has the highest temperature throughout the transient.

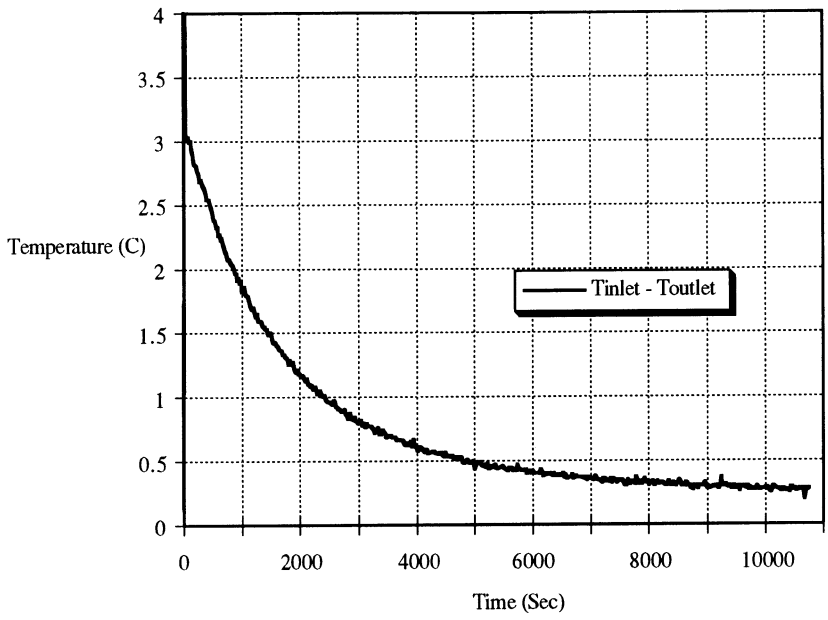

Figure 4.2 Typical Inlet to Outlet Temperature Drop

Figure 4.2 shows the difference in temperature between the two thermocouples at the base of the water supply stems. They are labeled Thermocouples F and G in Figure 3.6. The temperature drop starts at about 3 C and decays to less than 1 C in roughly 2000 seconds. The error for this measurement is +/- 0.71 C.

After calculating the bulk fluid temperature and the average coil wall temperature, Figure 4.3 can be plotted. The bulk temperature remains constant at approximately 45.5 C. The coil wall temperature jumps almost immediately to 39 C and then slowly, over the course of the transient, climbs the remaining 6 degrees. The bulk temperature gradually rises in response to the coil wall temperature. The error in the bath temperature is greater than the 0.5 C specified for the thermocouples since it is a single thermocouple swirling within a large bath.

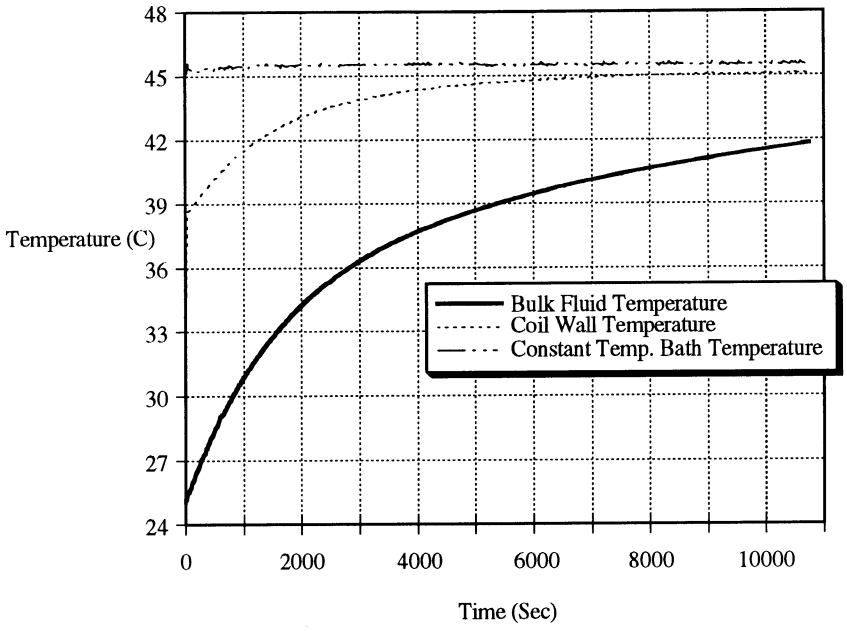

Figure 4.3 Typical Transient Thermal Response

Reindl formulated several scale analysis equations that calculated the expected duration of both the conduction regime and the quasi-steady regime. Because of an error in these equations when compared to the present results, the results using the small 1/12 hp pump were initially not considered to be very good. [It was later shown that they were quite good.] The assumed problem was a low flow rate. It was presumed that a higher flow rate would increase the initial temperature change in wall temperature and thereby approximate a step change in wall temperature more closely. A greater initial temperature change would approximate more closely the numerical geometry and produce better results. At this point, the 1/2 hp pump was ordered and installed, as discussed in Section 3.1.1.

The first data run using the new pump have the transient thermal response shown

in Figure 4.4. The new pump was adding heat to the system. Also, it was initially decreasing the bath temperature because of heating its thermal mass. The bath temperature is initially at 46 C but drops immediately to 42 C. These problems were corrected by removing all the insulation from the pump and constant temperature bath. Also, a valve was installed to preheat the pump.

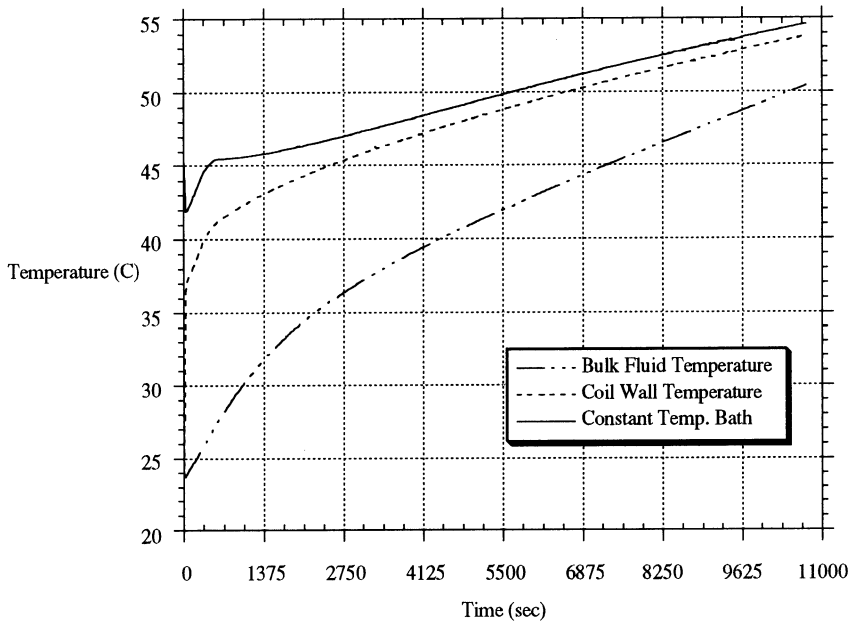

Figure 4.4 Unexpected Transient Thermal Response

Figure 4.5 illustrates the thermal response difference between the small pump and the large pump. The large pump does increase the initial coil wall temperature more quickly. This increase is an additional 2 C for this comparison. The trade off is that the bath temperature using the new pump, although much improved, still exhibits a gradual increase at the end of the transient. The different responses of the bath temperature is due primarily to the difference in initial fluid temperature.

The dependence of heat transfer on flow rate was further examined by choking the

flow of the small pump even further. It was found, and is illustrated in Figure 4.6, that there is a difference between the heat transfer response for these flowrates, however, it is not a significant difference considering the associated error.

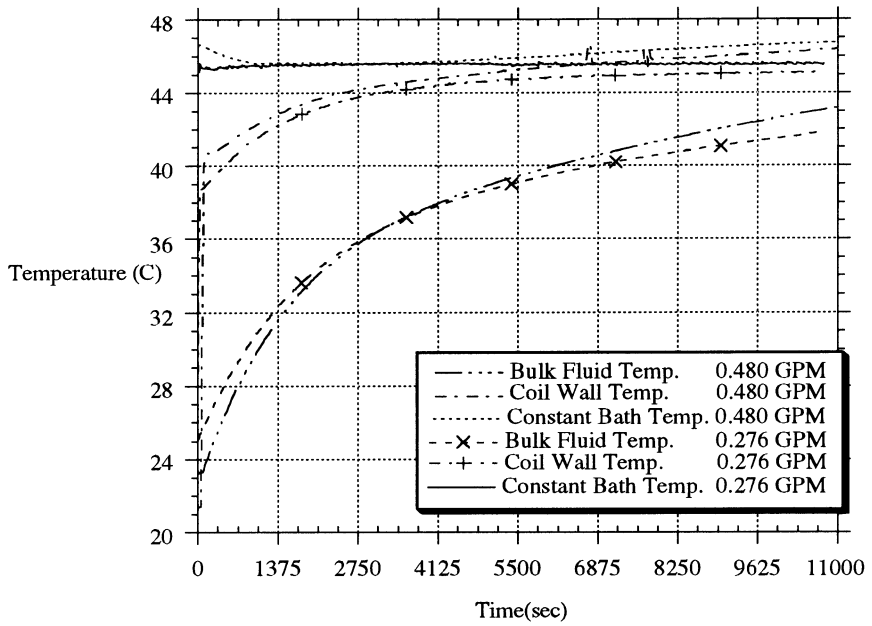

Figure 4.5 Comparison of Typical Small Pump (0.276 GPM) and Large Pump (0.48 GPM) Thermal Response

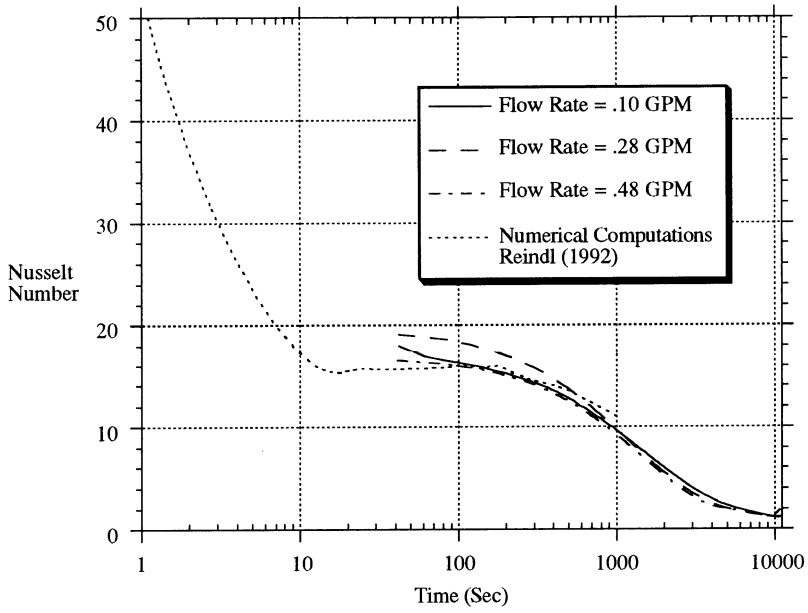

Figure 4.6 Comparison of Transient Nusselt Number for Three Flow Rates

4.2 Validation of Previous Numerical Results

Using Figure 4.6 as justification for using the medium flow rate, the small pump results will be used to validate the numerical results of Reindl discussed in Chapter 1. Five replicate runs were conducted with taking data every 20 seconds throughout the transient. Additionally, two short duration runs were done to examine the early transient. The data aquisition interval for these runs was 4 seconds. The results are plotted along with Reindl's numerical results for a Rayleigh number of 1×10^6 in Figure 4.7. A high degree of agreement exists between Reindl's results and these experimental results. This is especially true in terms of the duration of both the conduction regime and the quasi-steady regime. The Nusselt value within the quasi-steady regime is higher for the

experiments, but not dramatically so. Additionally, except for Run 4, the Nusselt numbers of the data runs are within the calculated error bounds. It should be noted that the time axis is represented in a log scale. This means most of the data is contained further along in the transient and that differences occuring early in the transient are magnified. Figure 4.8 illustrates the same results using the average of the five data runs. Note that the short duration run and the average of the longer runs also matched.

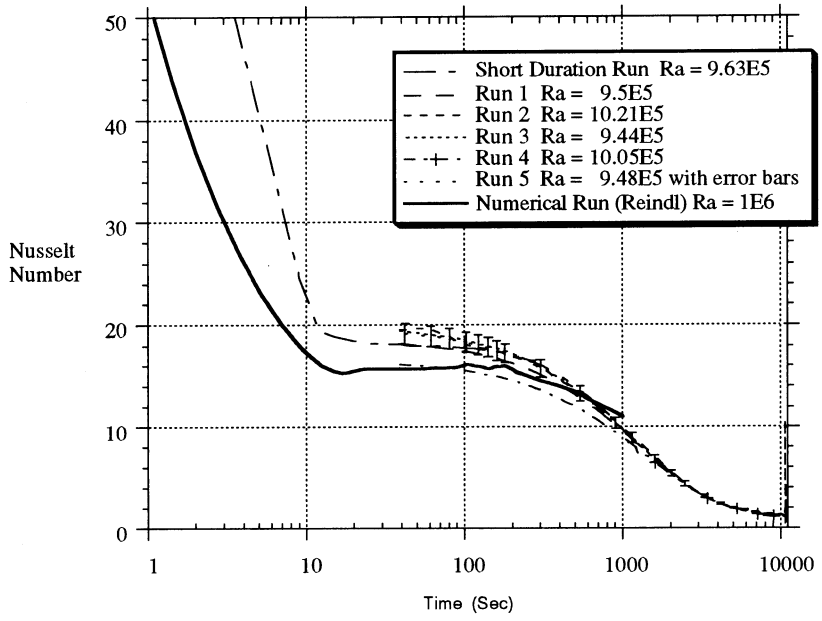

Figure 4.7 Transient Heat Transfer Response for Five Replications, Short Duration Run and Numerical Results

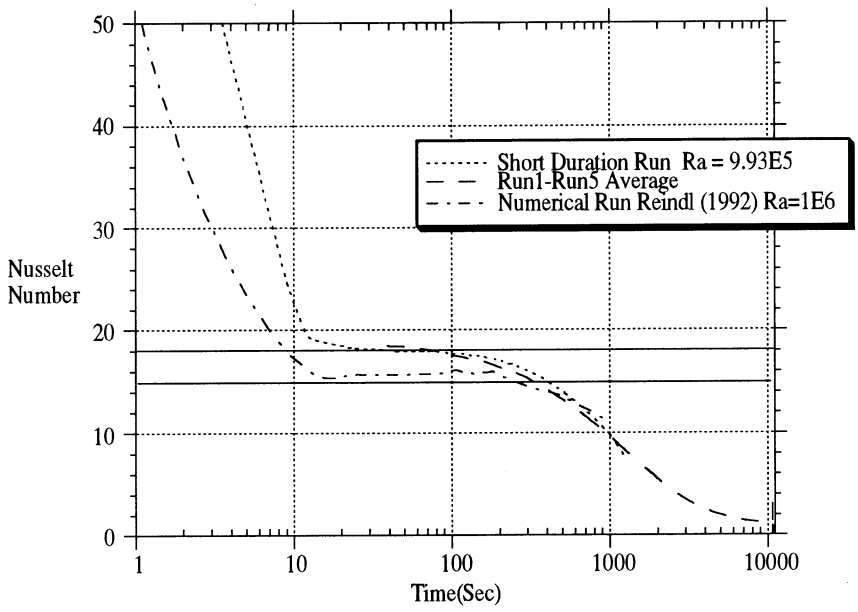

Figure 4.8 Transient Heat Transfer Response for Five Run Average, Short Duration Run, Numerical Results and Correlation Results

The range of values calculated by the correlations from Chapter 1 are also represented in Figure 4.8. Several results are observed when the experimental results are compared to the numerical results and the correlations. First, both the duration of the conduction regime and the quasi-steady regime for the experimental results agree well with the numerical results of Reindl. The main difference between the experimental results and the numerical results is in the Nusselt number during the quasi-steady period. The range of correlation values reported for this Rayleigh number includes both the numerical Nusselt value and the experimental Nusselt value. Another reason for the difference in quasi-steady Nusselt number values is the observed three dimensionality of the convective plume as it rises up from the coil. Figure 4.9 illustrates the shape of the

convective plume when viewed across the coil using a simple shadow graph technique. The top illustration shows the convective plume at the beginning of the quasi-steady period. These illustrations show that there is a three dimensional dependence of the heat transfer in the form of these Bernard-type cells. In the two dimensional model, complete axial symmetry was assumed in order to reduce the geometry to a two dimensional grid. Therefore, the three dimensional dependence is not represented in the two dimensional simplification. In fact, the numerical runs represent a vertical slice through the center of one of the rising convective cells.

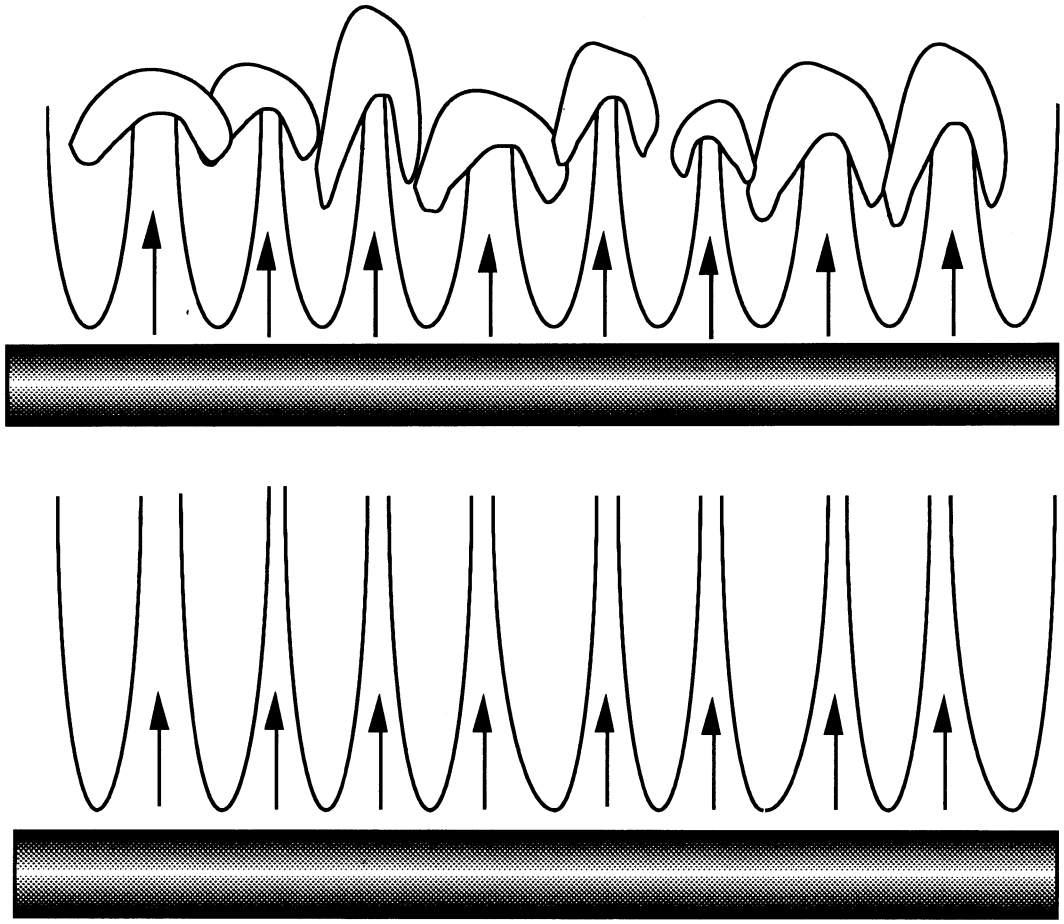

Figure 4.9 Flow Visualization Illustration

As previously discussed, a special formulation of the Nusselt number is needed to

calculate the effectiveness. This formulation is presented in Figure 4.10. The quasi-steady value and decay regime Nusselt number are both higher than that of the standard Nusselt formulation because the temperature difference in the numerator is also decreasing with time.

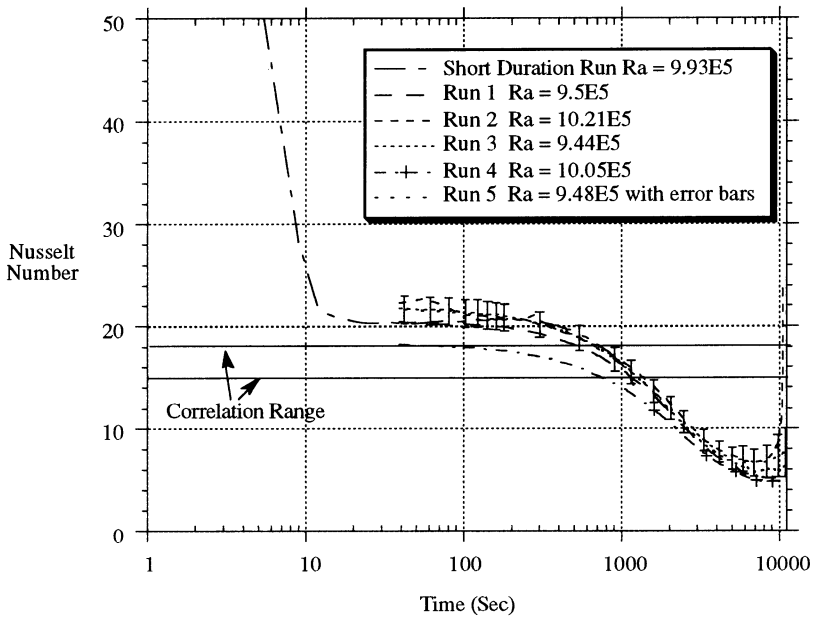

Figure 4.10 Transient Nu_ε Response for Five Replications and the Short Duration Run

The normalized bulk temperature response for the five replicate runs is given in Figure 4.11. Although there is considerable spread across the runs that grows through the transient, the error bars show that this degree of variance is not unexpected.

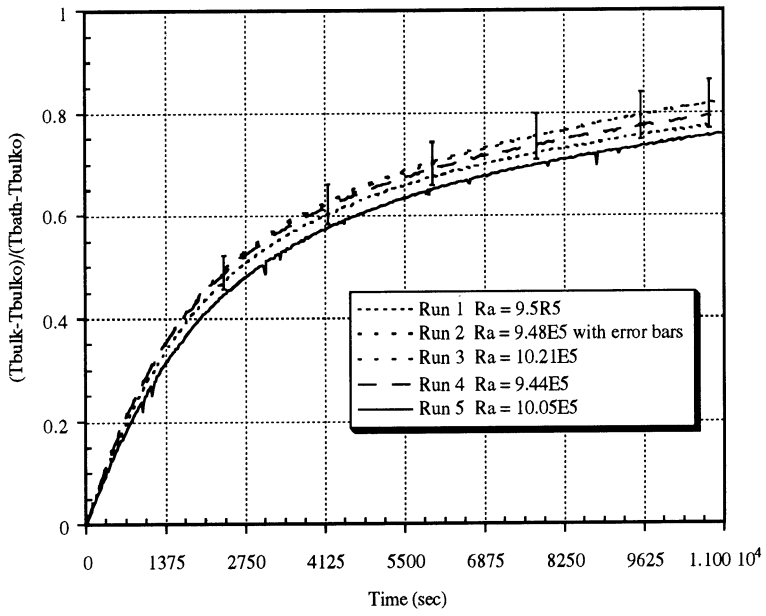

Figure 4.11 Normalized Bulk Temperature Response for Five Replicate Runs

The scale analysis equations developed by Reindl for his numerical results have not represented these experimental results as closely as his numerical results. Figure 4.12 illustrates several scale analysis results. The scale analysis estimate for the duration of the conduction regime (Equation 1.8), for these experimental parameters, is represented by dT_C1. This value is 0.95 seconds which is much less than the experimental value of 10 seconds. In Reindl's numerical runs, the non-dimensional form of the Navier-Stokes equations was used. In this formulation, the Rayleigh number was fixed and a nondimensional temperature difference of 1 degree was used. The size of the coil diameter was then calculated from the nondimensional Rayleigh number using the nondimensional temperature difference.

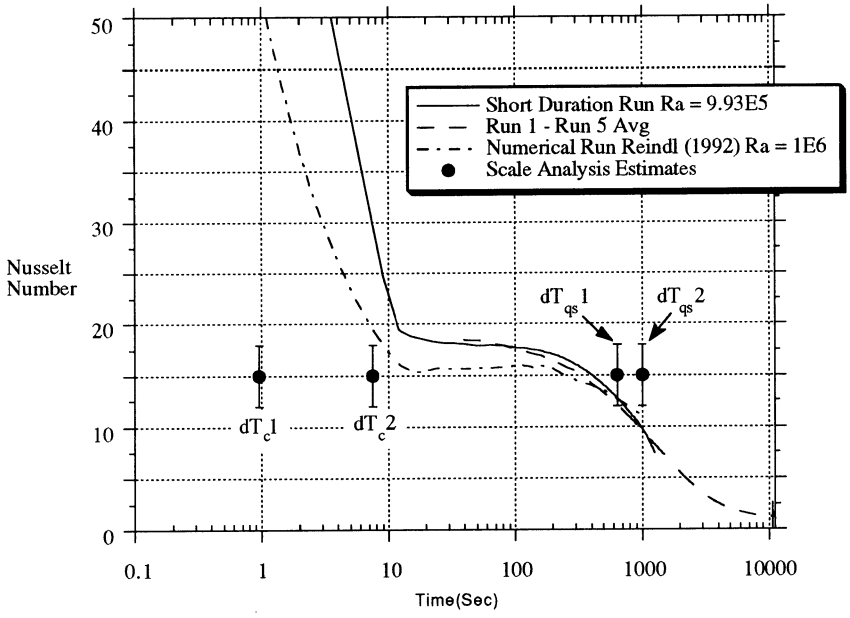

Figure 4.12 Scale Analysis Estimates

Therefore, the diameter used in Equation 1.8 is really a nondimensional diameter. In an attempt to reformulate Equation 1.8 entirely in terms of the Rayleigh number and removing the dependence on the nondimensional diameter, the coil diameter was expressed in terms of the Rayleigh number assuming a temperature difference of 1 degree. Rewriting Equation 1.8 using this expression gives

$$\Delta t_c = \left(\frac{\nu}{g\beta}\right)^{2/3} \frac{Ra_D^{1/6}}{\alpha^{1/3}} \tag{4.1}$$

This formulation gives the duration estimate represented by dT_c2 in Figure 4.12. This estimate is quite good for a scale analysis estimate.

The duration of the quasi-steady regime is also difficult to characterize. Reindl's

scale analysis estimate (Equation 1.9) radically overestimates the duration of the quasi-steady period. This result is represented in Figure 4.12 by $dT_{qs}2$. The duration estimate stems from the time it takes for the water above the coil to pass through the boundary layer. After consulting with Reindl, a new formulation was developed that uses the surface area of a toroid exactly instead of using a two dimensional approximation of a circle. This result is given by Equation 4.2.

$$\Delta t_{qsnew} = \frac{r_x^2\gamma(1-\eta+\phi)}{4\pi^2 R_x \alpha \phi^2 Ra_D^{1/4}} \tag{4.2}$$

This gives the result represented in Figure 4.12 by $dT_{qs}1$. The duration of the quasi-steady period can be estimated from the data as the point at which a noticable decrease in the Nusselt number begins to occur. The estimate from Figure 4.12 is 400 seconds. $dT_{qs}1$ gives a better result than $dT_{qs}2$, with a value of 635 seconds. The error in the time measurement is 0.5 seconds from the data aquisition apparatus. These scale analysis estimates are not within 0.5 seconds of the experimental duration values. However, these scale analysis estimates give an acceptable order of magnitude result.

The effectiveness of the five replicate runs is represented in Figure 4.13. Except for Run 5, all the runs fall within the error bars. As previously mentioned, effectiveness values at low temperature differences should be disregarded because the error is too large. Figure 4.14 illustrates the comparison between the effectiveness found by Farrington for different flow rates and these experiments. Because the geometries are different , a direct comparison is not possible. However, both data sets show that as the flow rate increases the effectiveness decreases.

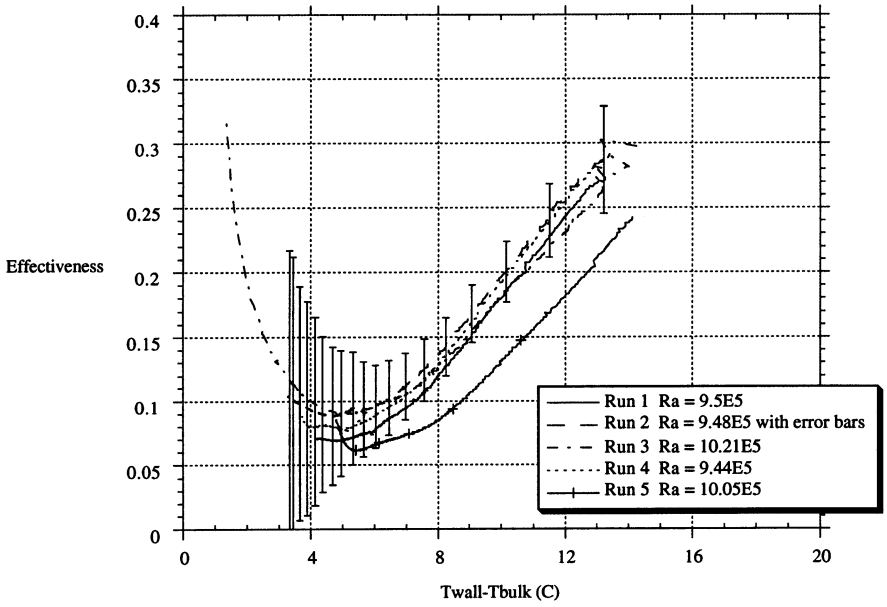

Figure 4.13 Effectiveness Response for Five Replicate Runs

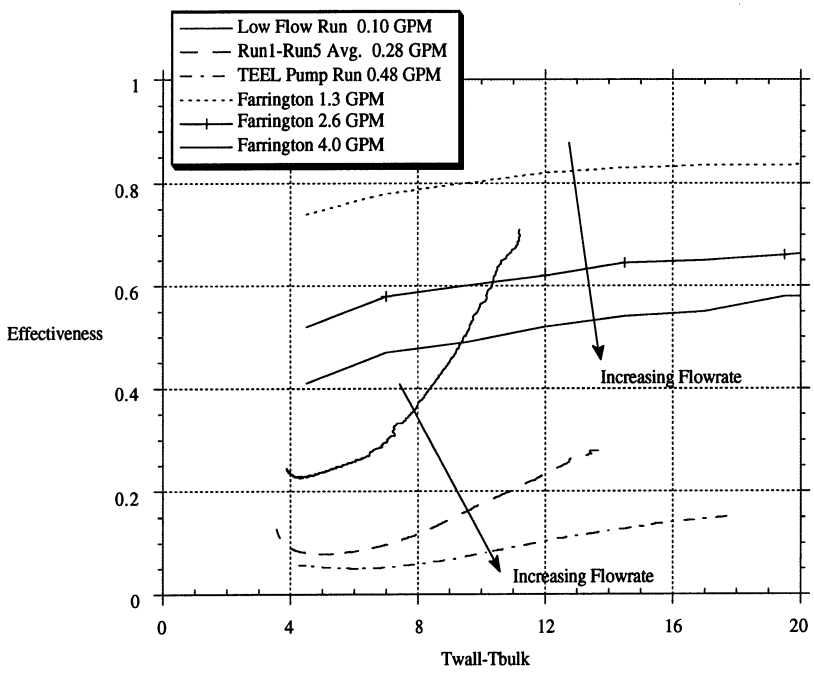

Figure 4.14 Effectiveness Results for Several Flow Rates and Results of Farrington

4.3 Coil Height Optimization Results

Using the 1/2 hp pump, data was taken at relative coil heights of R = 0.7, 0.4, 0.3, 0.2, 0.1, 0.029 (bottom of enclosure). For each of these relative heights, two data runs were conducted. The reproducibility between runs was quite high. Figure 4.15 illustrates this with the thermal response for the two runs at R = 0.4. Figure 4.14 shows the normalized bulk temperature response for these runs. They lie on top of each other and are obviously within the error bars.

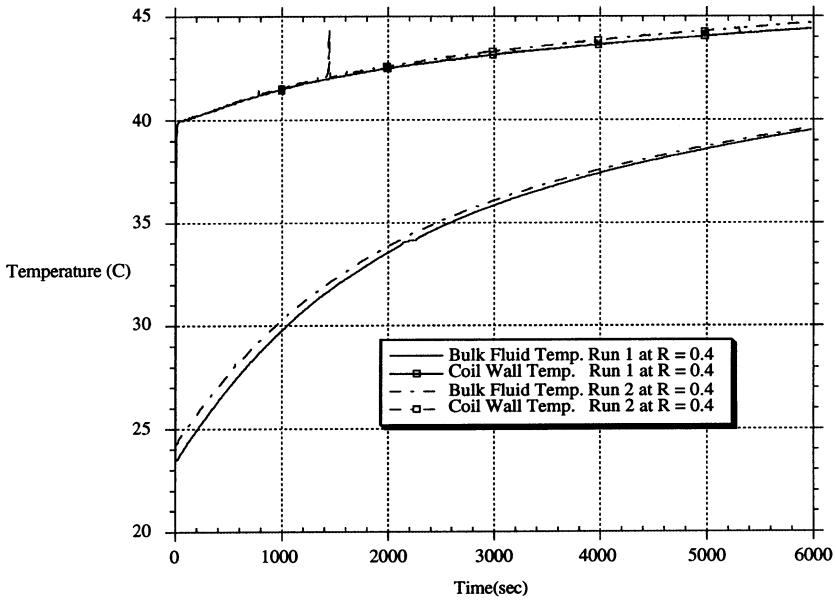

Figure 4.15 Thermal Response for Two Runs at R = 0.4

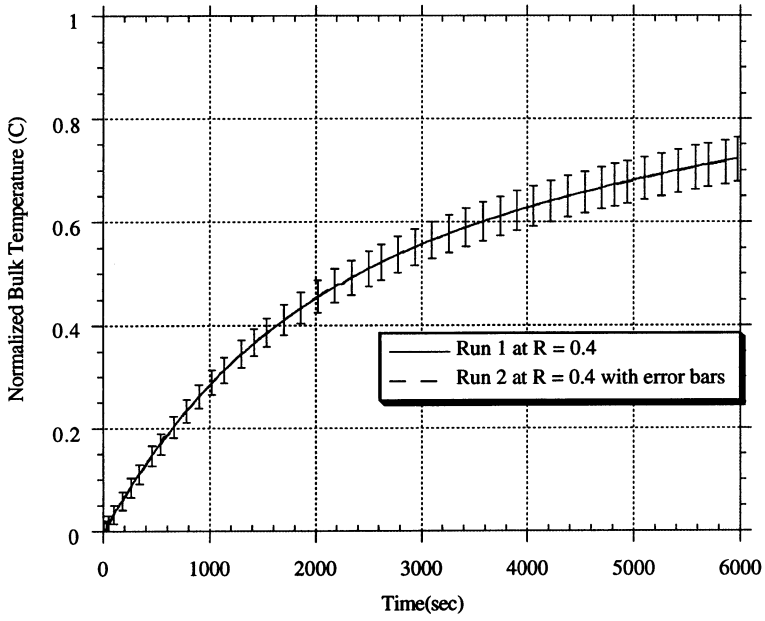

Figure 4.16 Normalized Bulk Temperature for Two Runs at R = 0.4

The transient heat transfer response for the two runs at R = 0.4 is given in Figure 4.17. Again, the reproducibility is excellent and there is good agreement to Reindl's results. Finally, Figure 4.18 shows good reproducibility in the effectiveness values as well.

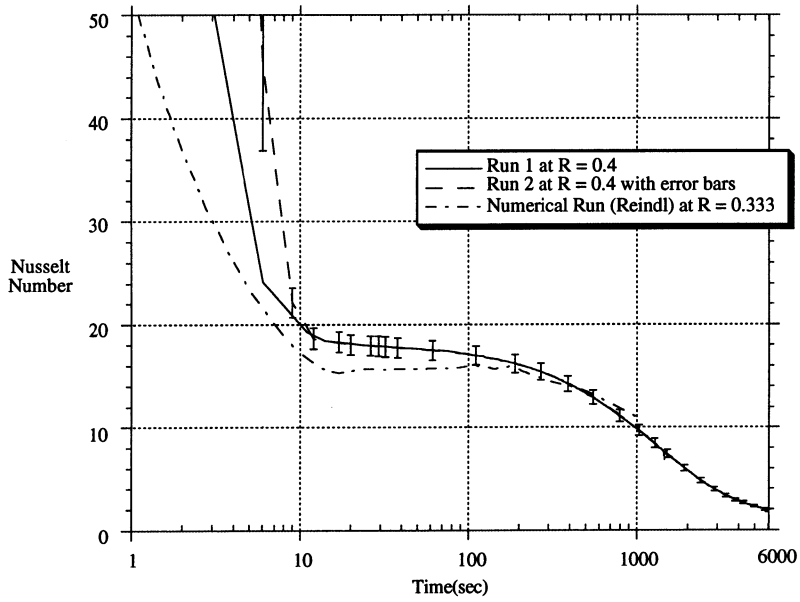

Figure 4.17 Transient Nusselt Response for Two Runs at R = 0.4

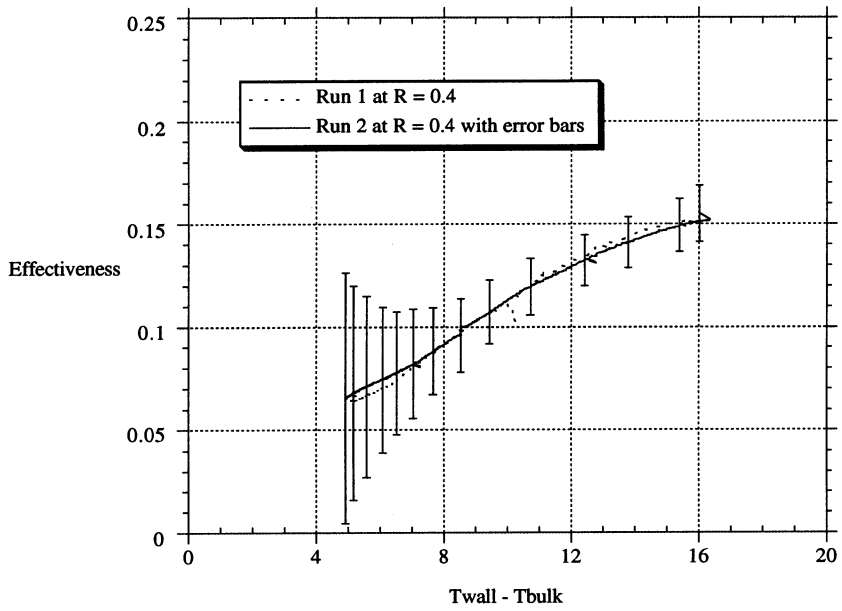

Figure 4.18 Effectiveness for Two Runs at R = 0.4

The transient heat transfer at various coil heights are compared to each other. Figure 4.19 shows that the conduction regime duration for all heights is basically identical. R = 0.1 has the lowest value of the quasi-steady Nusselt number, although the error bars overlap during the quasi-steady regime. Figure 4.20 examines the end of the quasi-steady regime. It shows that, surprisingly, R = 0.029 (bottom) has a long quasi-steady period with a relatively high Nusselt number. R = 0.1 has a longer quasi-steady period than R = 0.029 (bottom) but has a lower Nusselt value. R = 0.7 has the shortest quasi-steady regime which follows the theory.

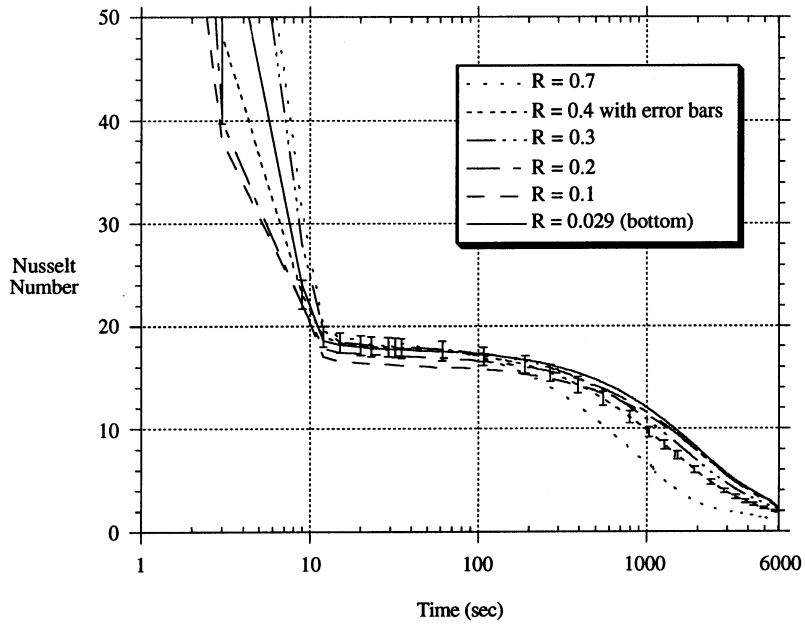

Figure 4.19 Transient Heat Transfer at Various Coil Heights

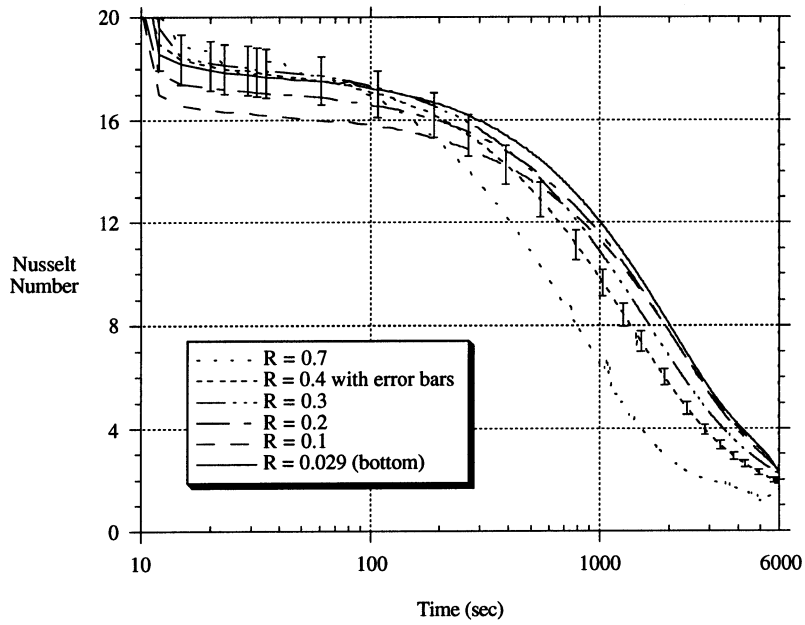

Figure 4.20 End of Quasi-Steady Regime for Various Coil Heights

Again, the performance at R = 0.029 (bottom) is the best during the decay regime as illustrated in Figure 4.21. This heat transfer performance transfers to the bulk temperature response as illustrated in Figure 4.22. According to this figure, the lower the coil, the quicker the tank heats up. The expected reduction of heat transfer by the floor of the enclosure did not occur.

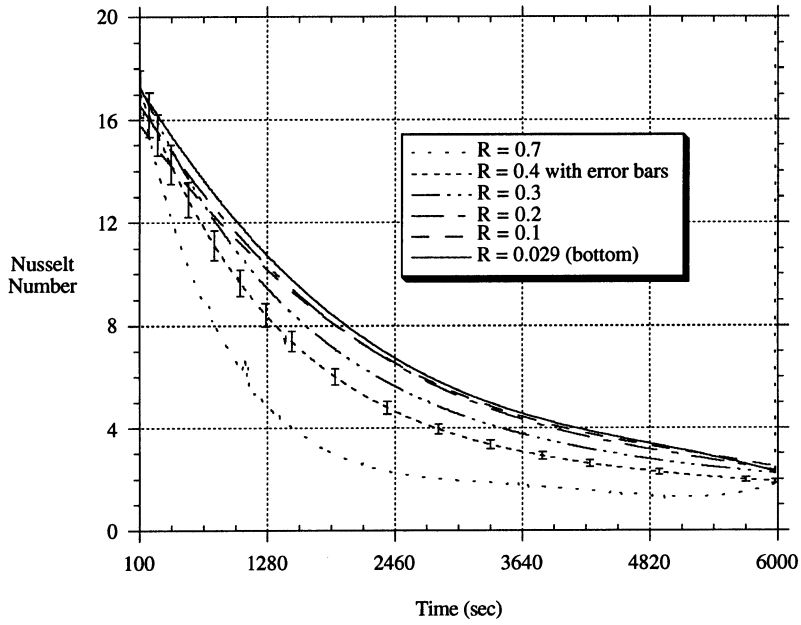

Figure 4.21 Decay Regime for Various Coil Heights

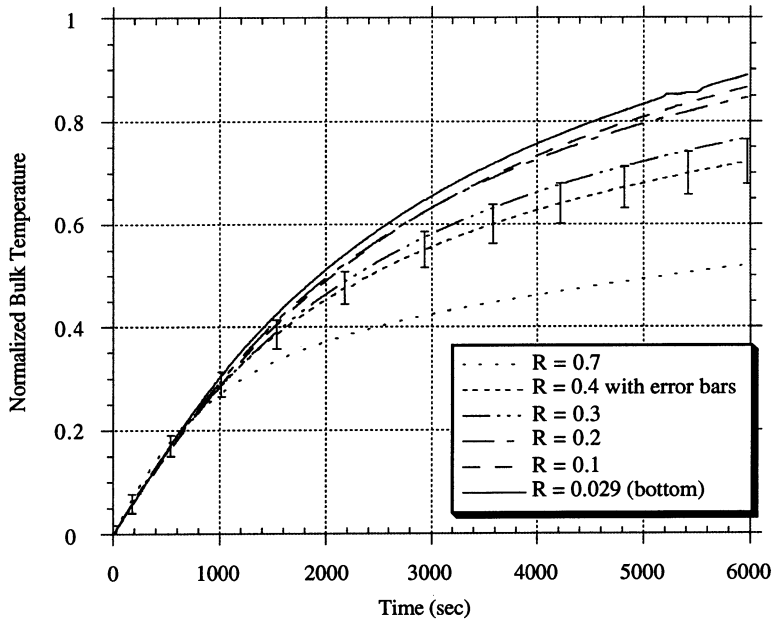

Figure 4.22 Normalized Bulk Temperature for Various Coil Heights

Figure 4.23 contains the scale analysis duration estimate for the quasi-steady regime. These estimates are made using Equation 4.2. Although it is difficult to determine the precise end of the quasi-steady regime, the correct trend is apparent and the scale analysis estimate for R = 0.7, especially, seems accurate.

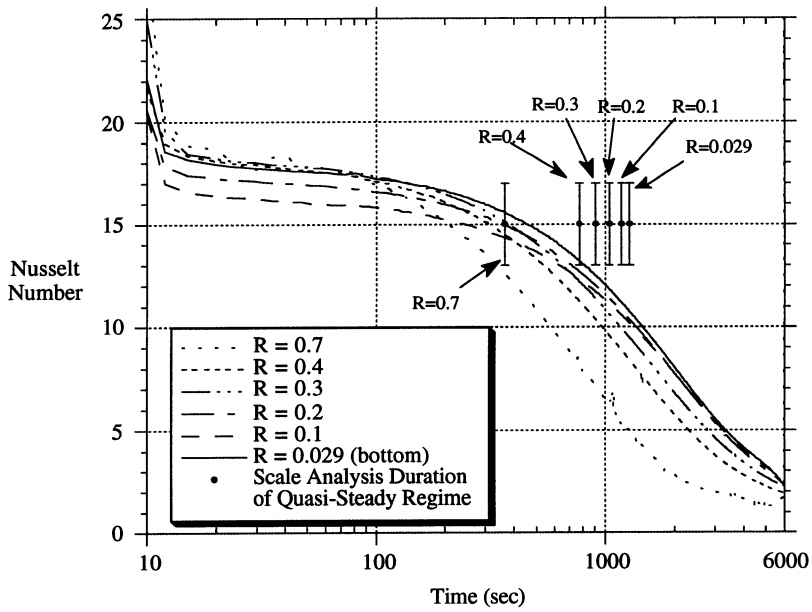

Figure 4.23 Scale Analysis Estimates for Various Coil Heights

Finally, Figure 4.24 contains the effectiveness as a function of Twall - Tbulk for the various coil heights. The trend seems to be the effectiveness curve flattens out as the coil height decreases. Again, any values with low temperature differences must be neglected because of the large error bars.

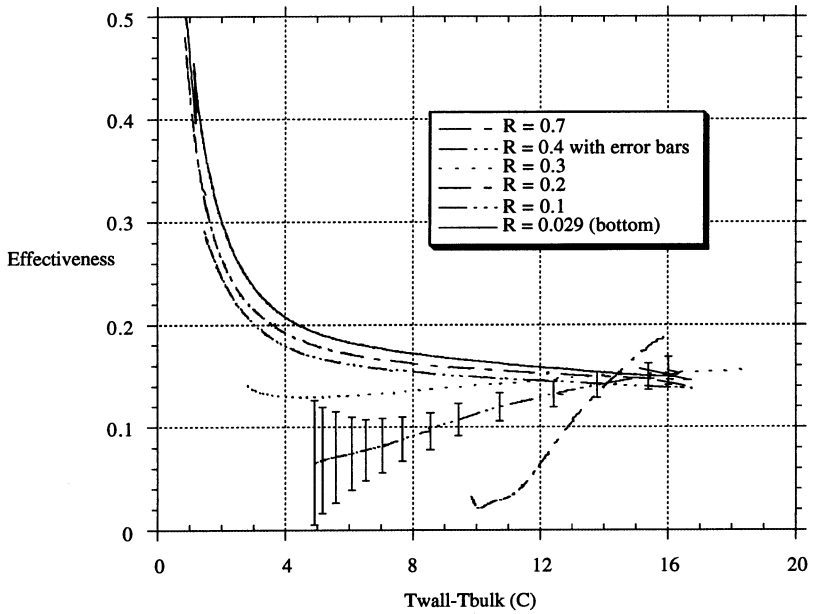

Figure 4.24 Effectiveness at Various Coil Heights

4.4 Summary of Experimental Analysis

An experimental technique has been developed to examine the transient heat transfer from a coil within a cylinder. The problems associated with the previously used resistively heated coil method have been eliminated. Flow visualization with the present method, using a shadow-graph technique, shows no indications of "pulsations" in the convective flow that leads to destruction of the quasi-steady period. Additionally, the experimental results from this apparatus are reproducible as illustrated by Figures 4.11 and 4.16.

The first main focus of the experimental side of this study deals with the validation of the prior numerical results of Reindl (1992). The current experimental geometry

"strains" the parameter range of the numerical solutions in that; the coil diameter relative to the enclosure size is considerably smaller for the experiment than for the numerical study, the relative radius of the toroid is larger in the experiment, and the relative height of the coil within the enclosure is not held constant in the experiment. This idea was purposely designed into the experiment. Because the parameter range used in the numerical analysis is strained by the experimental geometry, agreement between the experimental results and the numerical results would lend a great deal of validity to both the present study and the previous numerical result. Current experiments have shown good agreement to Reindl's numerical results. As shown in Figure 4.8, the average of five experimental runs and a short duration run agree well with the results of Reindl. The time duration of both the conduction regime and the quasi-steady regime are in excellent agreement. The main difference between the experimental results and the numerical results is the value of the Nusselt number during the quasi-steady period. The experimental results have a quasi-steady Nusselt number of 18.0 while the numerical results have a value of 15.5. There is some spread within the literature for the quasi-steady Nusselt number when it is assumed to be equivalent to a coil in an infinite medium. Morgan (1975), in his literature review, gives a range of average Nusselt numbers for $Ra = 1x\ 10^6$ of 14.45 to 18.17 which contains the current experimental results, although they are on the upper edge of the range. A possible cause of the difference between Nusselt numbers is the three dimensionality observed of the plume as it rises from the coil as shown in Figure 4.9. A three dimensional dependence is not taken into account by the numerical study because it assumes axial symmetry in order to reduce the geometry to a two dimensional grid.

The effect of the coil height within the enclosure was studied experimentally. The ratio of coil height within the enclosure to the total enclosure height (R) values that were tested including 0.7, 0.4, 0.3, 0.2, 0.1, and 0.029 (bottom). Figures 4.15 through 4.18 show that the results for the individual R value results are reproducible. An optimum R

value would charge the fluid in the enclosure most quickly, and it was expected, based on the numerical study reported in Chapter 2, that there would be an optimum R value in the middle of the R value range. It was theorized that a high R value would result in a short quasi-steady period because the fluid in the top of the enclosure would be charged before the bottom fluid. A low R value would result in a low quasi-steady Nusselt number because the presence of the floor of the enclosure would pinch the fluid entrainment into the coil boundary layer. Surprisingly, the optimum R value was found experimentally to be 0.029 (bottom). As Figure 4.20 indicates, the "knee" of the Nusselt number curve for R = 0.029 sticks out the furthest. Figure 4.20 also shows that R = 0.7 has the shortest quasi-steady period as the numerical results of Chapter 2 would indicate. Figure 4.21 shows that R = 0.029 has the maximum value during the decay regime while R = 0.7 has the minimum Nusselt number during the decay region. Finally, Figure 4.22 indicates that indeed R = 0.029 charges the tank quickest. R = 0.7 charges the tank most slowly.

These results indicate that the presence of the floor of the enclosure is not as major a factor in the transient natural convection from the coil as indicated by the numerical analysis. It can be assumed that the convective plume can entrain all the cool fluid it needs from the fluid beside the coil. This result is completely different than the results of the numerical study reported in Chapter 2. The probable explanation for the difference is that if the walls were also closer to the coil, as in Chapter 2, then the convective flow would not be able to entrain the necessary fluid from the volume on the sides of the coil. The presence of the floor will have a greater affect on the heat transfer if the walls are at a similarly short distance from the coil.

The effectiveness of the coil heat exchanger was also determined. In the effort to characterize the in-tank heat exchanger, it would be good to be able to quantify the effectiveness of the coil heat exchanger in terms of the temperature difference (Twall - $\overline{T}$) and the mass flow rate. Figure 4.13 shows the effectiveness for the five runs using the

1/12 hp pump. The effectiveness increases linearly with an increasing temperature difference from a 4 degree difference to the maximum difference of 14 degrees. Below a 4 degree temperature difference, the effectiveness appears to increase dramatically, but the large error bars in this range preclude definite conclusions. Figure 4.14 illustrates the flow rate dependence of the effectiveness and the comparison of the effectiveness results of the present study to the previous study done by Farrington (1986). As the figure shows, an increasing flow rate decreases the effectiveness of the coil. The lack of agreement between the results of the present experiment and the results of Farrington may be due to geometrical differences. Farrington's geometry consisted of a multiple turn coil while the present experiment incorporates a single coil turn.

Figure 4.24 shows the effectiveness results for the range of coil height ratios (R). As the coil is moved lower within the tank, the effectiveness becomes constant with respect to the temperature difference. Again, the effectiveness appears to increase dramatically below a 4 degree temperature difference, although the results in this range are uncertain.

CHAPTER
FIVE

Conclusions and Recommendations

This chapter discusses the results of the numerical study reported in Chapter 2 and the results of experimental study reported in Chapter 4. This chapter also makes recommendations for the expansion and continuation of this study.

5.1 Conclusions of the Numerical Analysis

Possible geometric modifications were examined using a fluid dynamics package (FLUENT). The first conclusion deals with the optimization of the coil height of the coil within the enclosure. An optimum coil height would charge the fluid within the tank most quickly. Three relative coil heights were studied; 0.5, 0.3, and 0.175, and the middle coil height (R = 0.3) was found to charge the tank most quickly. If the coil is placed too high within the enclosure, the quasi-steady period is shortened. The conclusion from these numerical runs is that an optimum coil height exists and that it is located, for this geometry, in the vicinity of R = 0.3.

Several geometries designed to improve thermal stratification within the enclosure were studied. Although these geometries did modify the flow field within the enclosure,

none improved the stratification in a way that improved the charging time. In fact, in several cases, the heat transfer was diminished. The prevailing trend was that any interference with ascending plume resulted in the plume flow recirculating down and back through the coil boundary layer. This immediate recirculation of the plume fluid is not desirable because this keeps warmer water flowing around the coil and thereby decreases the heat transfer driving force.

The effect of vertical shrouds on the heat transfer from a coil was examined for three shroud lengths. It was found that all three configurations improved the charging rate of the enclosure fluid. The longest vertical shroud is most effective at decreasing the charging time.

5.2 Conclusions of the Experimental Analysis

An accurate experimental technique has been developed to examine the transient heat transfer from a coil within a cylinder filled with fluid. The experiments show good agreement to Reindl's (1992) numerical results. The time duration of both the conduction regime and the quasi-steady regime are in excellent agreement. The main difference between the experimental results and the numerical results is the value of the Nusselt number during the quasi-steady period. The experimental results have a quasi-steady Nusselt number of 18.0 while the numerical results have a value of 15.5 which is not within the experimental error tolerances although both are within the range of literature values reported by Morgan (1975). This difference may also be due to the three dimension dependence of the convective plume that is not represented in the numerical study.

The ratio of coil height within the enclosure to the total enclosure height (R) was studied experimentally for values of 0.7, 0.4, 0.3, 0.2, 0.1, and 0.029 (bottom). The

optimum position was found to be at R of 0.029 (bottom). The highest position, R = 0.7, has the shortest quasi-steady period and charges the tank most slowly. These results indicate that the presence of the floor of the enclosure is not a major factor in the transient natural convection from the coil. In comparison to the numerical results, it can be concluded that the presence of the floor has a magnified affect on the heat transfer if the walls are at a short distance from the coil.

The effectiveness of the coil heat exchanger was determined experimentally. The effectiveness increases linearly with an increasing temperature difference from a 4 degree difference to the maximum difference of 14 degrees (at R = 0.5). At a small temperature difference, there is a large error in the results. The effect of flow rate is supported by the work of Farrington (1986).

Effectiveness results were obtained for the range of coil height ratios (R). As the coil is moved lower within the tank, the effectiveness becomes constant with respect to the temperature difference.

5.3 Recommendations for Further Numerical Studies

The fluid dynamics package, FLUENT, is excellent for making a preliminary, qualitative investigation of possible geometric modifications prior to experimental construction. This method can save a great deal of time, effort, and money in experiments. This practice should be continued in future enclosure studies.

The mesh used in this numerical study was rough and in future studies, a finer mesh should be used. This will require more computation time and the use of a larger, faster computer would be advisable. Additionally, a new version of FLUENT (Version 4) has recently been installed at the University of Wisconsin Computer Aided Engineering Center which incorporates a body fitted coordinates system that allows simpler grid

creation especially for curved objects and should be considered.

5.4 Recommendations for Further Experimental Studies

There are two main avenues for future research that would extend and expand this research. First, the relative geometry of the coil and enclosure can be varied. Second, the most promising flow impediments that were examined numerically in this study can be examined experimentally.

It still needs to be determined how a larger coil would behave in the same enclosure, and the coil diameter and toroid radius should be varied. Varying the coil diameter would vary the Rayleigh number. The transient heat transfer should be examined at different Rayleigh numbers for further comparison to numerical results.

The toroid radius should be varied to examine the effect of the enclosure side walls on the convective flow from the coil to answer the questions: How close to the walls should the coil be? Is it similar to the height optimization, in that the coil has an optimum location next to the wall?

Several enclosure sizes should be examined see if scaling up the geometry affects the transient heat transfer response. In the present study, considerable research was done into finding larger Duran or fused quartz enclosures. A cylinder larger than the present size would have to be specially produced and would be extremely expensive (several thousand dollars). Larger enclosures could be constructed of Invar which is a nickel-iron alloy with a very low thermal expansion coefficient. Additional advantages to Invar is that it can be machined in-house and would be easy to seal by welding with would help avoid some of the leaking problems that have plagued this experiment. The disadvantages of using Invar include possibly greater thermal conduction within the enclosure that could affect the thermal stratification within the enclosure and, because the Invar is opaque, the

inability to conduct flow visualization experiments.

Several geometric modifications to enhance natural convection should be studied experimentally. The most promising is the use of vertical shrouds around the coil. The vertical height of the shroud should be varied as well as examining the necessary spacing between the vertical shroud and the enclosure to determine how short the shroud can be before it no longer assists the heat transfer? Since most thermal storage tanks have only a small access hole through which the heat exchanger must be inserted, a design of a vertical shroud that can be installed through this hole could be of great significance. Modifications to the shape of the coil could be attempted including fins.

An experimental investigation using a simple mesh would be interesting, relatively simple to set up, and could be compared to numerical results.

A helix type heat exchanger would be interesting to examine. With the hot water entering the coil at the top of the helix and spiraling down to the exit additional heat transfer might occur and the thermal stratification could be enhanced.

BIBLIOGRAPHY

Churchill, S. W., Chu, H. H. S., "Correlating Equations for Laminar and Turbulent Free Convection from a Horizontal Cylinder", *International Journal of Heat and Mass Transfer*, **18**, pp. 1049 - 1053, (1975)

Fand, R. M., Morris, E. W., Lum, M., "Natural Convection Heat Transfer from Horizontal Cylinders to Air, Water, and Silicone Oils for Rayleigh Numbers Between 3 x 10^2 and 2 x 10^7", *International Journal of Heat and Mass Transfer*, **20**, pp. 1173 - 1184, (1977)

Farrington, R. B., Bingham, C.E., "Testing and Analysis of Immersed Heat Exchangers", *SERI Report #TR-253-2866*, August (1986)

Feiereisen, T. J., "An Experimental Study of Immersed Coil Heat Exchangers", Masters Thesis, University of Wisconsin - Madison, (1982)

Incropera, F.P., DeWitt, D.P., *Introduction to Heat Transfer* , pp. A22, (1990)

Morgan, V. T., "The Overall Convective Heat Transfer from Smooth Circular Cylinders", *Advances in Heat Transfer*, **11**, pp. 199-263, (1975)

Keenan, J.H., Keyes, F.G., Hill, P.G., and Moore, J.G., Thermodynamic Properties of Water Including Vapor, Liquid, and Solid Phases, John Wiley & Sons, (1978)

Kline S. J. and McClintock F. A., "Describing Uncertainties in Single-Sample Experiments", Mechanical Engineering, 75, pp. 3-8, (1953)

Patterson, J., Imberger, J., "Unsteady Natural Convection in a Rectangular Cavity", *Journal of Fluid Mechanics*, **100**, pp. 65 - 86, (1980)

Reindl, D. T., "Source Driven Transient Natural Convection in Enclosures", PhD Thesis, University of Wisconsin - Madison, (1992)

Sparrow, E. M., Charmchi, M., "Natural Convection Experiments in an Enclosure Between Eccentric or Concentric Vertical Cylinders of Different Height and Diameter", *International Journal of Heat and Mass Transfer*, **26**, pp. 133 - 143, (1983)

Sparrow, E. M., Pfeil D. R., "Enhancement of Natural Convection Heat Transfer from a Horizontal Cylinder Due to Vertical Shrouding Surfaces", *Journal of Heat Transfer, Transactions of the ASME*, **106**, pp. 124 - 130, (1984)